MANEUVERING AND CONTROL OF MARINE VEHICLES

Michael S. Triantafyllou
Franz S. Hover

Department of Ocean Engineering
Massachusetts Institute of Technology
Cambridge, Massachusetts USA

These notes were developed in the instruction of the MIT graduate subject 13.49: *Maneuvering and Control of Surface and Underwater Vehicles*. We plan many enhancements; your comments are welcome!

Maneuvering and Control of Marine Vehicles
Latest Revision: January 11, 2002

Contents

1 MATH FACTS

1.1 Vectors

1.1.1 Definition

We use the overhead arrow to denote a column vector, i.e., a *number with a direction*. For example, in three-space, we write

$$\vec{a} = \begin{Bmatrix} 2 \\ 1 \\ 7 \end{Bmatrix}.$$

The elements of a vector have a graphical interpretation, which is particularly easy to see in two or three dimensions.

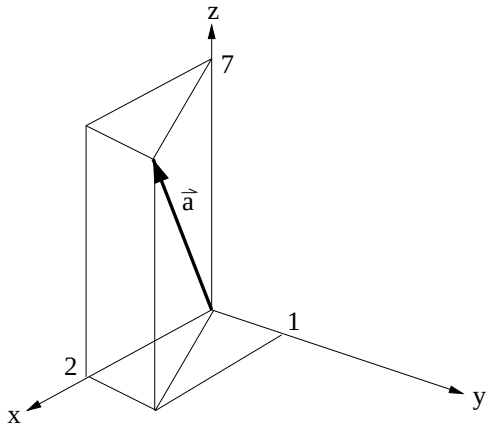

1. Vector addition is pointwise.

$$\begin{array}{rcl} & \vec{a} + \vec{b} & = \quad \vec{c} \\ \begin{Bmatrix} 2 \\ 1 \\ 7 \end{Bmatrix} + \begin{Bmatrix} 3 \\ 3 \\ 2 \end{Bmatrix} & = & \begin{Bmatrix} 5 \\ 4 \\ 9 \end{Bmatrix}. \end{array}$$

Graphically, addition is stringing the vectors together head to tail.

2. Scalar multiplication is pointwise.

$$-2 \times \left\{ \begin{array}{c} 2 \\ 1 \\ 7 \end{array} \right\} = \left\{ \begin{array}{c} -4 \\ -2 \\ -14 \end{array} \right\}.$$

1.1.2 Vector Magnitude

The total length of a vector of dimension m, its Euclidean norm, is given by

$$||\vec{x}|| = \sqrt{\sum_{i=1}^{m} x_i^2};$$

this scalar is commonly used to normalize a vector to length one.

1.1.3 Vector Dot Product

The dot product of two vectors is the sum of the products of the elements:

$$\vec{x} \cdot \vec{y} = \vec{x}^T \vec{y} = \sum_{i=1}^{m} x_i y_i.$$

The dot product also satisfies

$$\vec{x} \cdot \vec{y} = ||\vec{x}||||\vec{y}|| \cos\theta,$$

where θ is the angle between the vectors.

1.1.4 Vector Cross Product

The cross product of two three-dimensional vectors is another vector, $\vec{x} \times \vec{y} = \vec{z}$, whose

1. direction is normal to the plane formed by the two vectors,
2. direction is given by the right-hand rule, rotating from $\vec{x}$ to $\vec{y}$,

3. magnitude is the area of the parallelogram formed by the two vectors – the cross product of two parallel vectors is zero – and

4. (signed) magnitude is equal to $||\vec{x}||||\vec{y}||\sin\theta$, where θ is the angle between the two vectors, measured from $\vec{x}$ to $\vec{y}$.

The schoolbook formula is

$$\vec{x} \times \vec{y} \quad = \left\{ \begin{array}{l} x_2 y_3 - x_3 y_2 \\ x_3 y_1 - x_1 y_3 \\ x_1 y_2 - x_2 y_1 \end{array} \right\}.$$

1.2 Matrices

1.2.1 Definition

A matrix, or array, is equivalent to a set of row vectors, arranged side by side, say

$$A = [\vec{a} \;\; \vec{b}] = \left[\begin{array}{cc} 2 & 3 \\ 1 & 3 \\ 7 & 2 \end{array} \right].$$

This matrix has three rows ($m = 3$) and two columns ($n = 2$); a vector is a special case of a matrix with one column. Matrices, like vectors, permit pointwise addition and scalar multiplication. We usually use an upper-case symbol to denote a matrix.

1.2.2 Multiplying a Vector by a Matrix

If A_{ij} denotes the element of matrix A in the i'th row and the j'th column, then the multiplication $\vec{c} = A\vec{v}$ is constructed as:

$$c_i = A_{i1} v_1 + A_{i2} v_2 + \cdots + A_{in} v_n = \sum_{j=1}^{n} A_{ij} v_j,$$

where n is the number of columns in A. $\vec{c}$ will have as many columns as A has rows (m). Note that this multiplication is well-defined only if $\vec{v}$ has

as many rows as A has columns; they have consistent *inner dimension* n. The product $\vec{v}A$ would be well-posed only if A had one row, and the proper number of columns. There is another important interpretation of this vector multiplication: Let the subscript : indicate all rows, so that each $A_{:j}$ is the j'th column vector. Then

$$\vec{c} = A\vec{v} = A_{:1}v_1 + A_{:2}v_2 + \cdots + A_{:n}v_n.$$

We are multiplying column vectors of A by the scalar elements of $\vec{v}$.

1.2.3 Multiplying a Matrix by a Matrix

The multiplication $C = AB$ is equivalent to a side-by-side arrangement of column vectors $C_{:j} = AB_{:j}$, so that

$$C = AB = [AB_{:1} \;\; AB_{:2} \;\; \cdots \;\; AB_{:k}],$$

where k is the number of columns in matrix B. The same inner dimension condition applies as noted above: the number of columns in A must equal the number of rows in B. Matrix multiplication is:

1. Associative. $(AB)C = A(BC)$.
2. Distributive. $A(B + C) = AB + AC$, $(B + C)A = BA + CA$.
3. NOT Commutative. $AB \neq BA$, except in special cases.

1.2.4 Common Matrices

Identity . The identity matrix is usually denoted I, and comprises a square matrix with ones on the diagonal, and zeros elsewhere, e.g.,

$$I_{3\times 3} = \begin{bmatrix} 1 & 0 & 0 \\ 0 & 1 & 0 \\ 0 & 0 & 1 \end{bmatrix}.$$

The identity always satisfies $AI_{n\times n} = I_{m\times m}A = A$.

Diagonal Matrices . A diagonal matrix is square, and has all zeros off the diagonal. For instance, the following is a diagonal matrix:

$$A = \begin{bmatrix} 4 & 0 & 0 \\ 0 & -2 & 0 \\ 0 & 0 & 3 \end{bmatrix}.$$

The product of a diagonal matrix with another diagonal matrix is diagonal, and in this case the operation is commutative.

1.2.5 Transpose

The transpose of a vector or matrix, indicated by a T superscript results from simply swapping the row-column indices of each entry; it is equivalent to "flipping" the vector or matrix around the diagonal line. For example,

$$\vec{a} = \begin{Bmatrix} 1 \\ 2 \\ 3 \end{Bmatrix} \longrightarrow \vec{a}^{\,T} = \quad \{1 \;\; 2 \;\; 3\}$$

$$A = \begin{bmatrix} 1 & 2 \\ 4 & 5 \\ 8 & 9 \end{bmatrix} \longrightarrow A^T = \begin{bmatrix} 1 & 4 & 8 \\ 2 & 5 & 9 \end{bmatrix}.$$

A very useful property of the transpose is

$$(AB)^T = B^T A^T.$$

1.2.6 Determinant

The determinant of a square matrix A is a scalar equal to *the volume* of the parallelepiped enclosed by the constituent vectors. The two-dimensional case is particularly easy to remember, and illustrates the principle of volume:

$$\begin{aligned} det(A) &= A_{11}A_{22} - A_{21}A_{12} \\ det\left(\begin{bmatrix} 1 & -1 \\ 1 & 1 \end{bmatrix}\right) &= 1 + 1 = 2. \end{aligned}$$

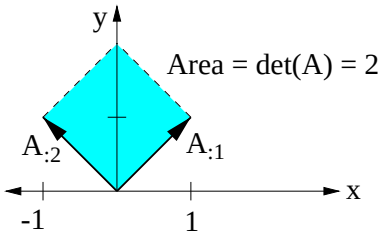

In higher dimensions, the determinant is more complicated to compute. The general formula allows one to pick a row k, perhaps the one containing the most zeros, and apply

$$det(A) = \sum_{j=1}^{j=n} A_{kj}(-1)^{k+j}\Delta_{kj},$$

where Δ_{kj} is the determinant of the sub-matrix formed by neglecting the k'th row and the j'th column. The formula is symmetric, in the sense that one could also target the k'th column:

$$det(A) = \sum_{j=1}^{j=n} A_{jk}(-1)^{k+j}\Delta_{jk}.$$

If the determinant of a matrix is zero, then the matrix is said to be singular – there is no volume, and this results from the fact that the constituent vectors do not span the matrix dimension. For instance, in two dimensions, a singular matrix has the vectors colinear; in three dimensions, a singular matrix has all its vectors lying in a (two-dimensional) plane. Note also that $det(A) = det(A^T)$. If $det(A) \neq 0$, then the matrix is said to be nonsingular.

1.2.7 Inverse

The inverse of a square matrix A, denoted A^{-1}, satisfies $AA^{-1} = A^{-1}A = I$. Its computation requires the determinant above, and the following definition of the $n \times n$ *adjoint* matrix:

$$adj(A) = \begin{bmatrix} (-1)^{1+1}\Delta_{11} & \cdots & (-1)^{1+n}\Delta_{1n} \\ \cdots & \cdots & \cdots \\ (-1)^{n+1}\Delta_{n1} & \cdots & (-1)^{n+n}\Delta_{nn}. \end{bmatrix}^T.$$

Once this computation is made, the inverse follows from

$$A^{-1} = \frac{adj(A)}{det(A)}.$$

If A is singular, i.e., $det(A) = 0$, then the inverse does not exist. The inverse finds common application in solving systems of linear equations such as

$$A\vec{x} = \vec{b} \longrightarrow \vec{x} = A^{-1}\vec{b}.$$

1.2.8 Trace

The trace of a matrix is simply the sum of the diagonals:

$$tr(A) = \sum_{i=1}^{n} A_{ii}.$$

1.2.9 Eigenvalues and Eigenvectors

A typical eigenvalue problem is stated as

$$A\vec{x} = \lambda\vec{x},$$

where A is an $n \times n$ matrix, $\vec{x}$ is a column vector with n elements, and λ is a scalar. We ask for what nonzero vectors $\vec{x}$ (right eigenvectors), and scalars λ (eigenvalues) will the equation be satisfied. Since the above is equivalent to $(A - \lambda I)\vec{x} = \vec{0}$, it is clear that $det(A - \lambda I) = 0$. This observation leads to the solutions for λ; here is an example for the two-dimensional case:

$$\begin{aligned}
A &= \begin{bmatrix} 4 & -5 \\ 2 & -3 \end{bmatrix} \longrightarrow \\
A - \lambda I &= \begin{bmatrix} 4-\lambda & -5 \\ 2 & -3-\lambda \end{bmatrix} \longrightarrow \\
det(A - \lambda I) &= (4-\lambda)(-3-\lambda) + 10 \\
&= \lambda^2 - \lambda - 2 \\
&= (\lambda + 1)(\lambda - 2).
\end{aligned}$$

Thus, A has two eigenvalues, $\lambda_1 = -1$ and $\lambda_2 = 2$. Each is associated with a *right eigenvector* $\vec{x}$. In this example,

$$\begin{aligned} (A - \lambda_1 I)\vec{x}_1 &= \vec{0} \longrightarrow \\ \begin{bmatrix} 5 & -5 \\ 2 & -2 \end{bmatrix} \vec{x}_1 &= \vec{0} \longrightarrow \\ \vec{x}_1 &= \left\{\sqrt{2}/2, \ \sqrt{2}/2\right\}^T . \end{aligned}$$

$$\begin{aligned} (A - \lambda_2 I)\vec{x}_2 &= \vec{0} \longrightarrow \\ \begin{bmatrix} 2 & -5 \\ 2 & -5 \end{bmatrix} \vec{x}_2 &= \vec{0} \longrightarrow \\ \vec{x}_2 &= \left\{5\sqrt{29}/29, \ 2\sqrt{29}/29\right\}^T . \end{aligned}$$

Eigenvectors have arbitrary magnitude and sign; they are often normalized to have unity magnitude, and positive first element (as above). A set of n eigenvectors is always linearly independent. The condition that $rank(A - \lambda_i I) = rank(A) - 1$ indicates that there is only one eigenvector for the eigenvalue λ_i. If the left-hand side is less than this, then there are multiple unique eigenvectors that go with λ_i.

The above discussion relates only the right eigenvectors, generated from the equation $A\vec{x} = \lambda\vec{x}$. Left eigenvectors, also useful for many problems, pertain to the transpose of A: $A^T\vec{y} = \lambda\vec{y}$. A and A^T share the same eigenvalues λ, since they share the same determinant. Example:

$$\begin{aligned} (A^T - \lambda_1 I)\vec{y}_1 &= \vec{0} \longrightarrow \\ \begin{bmatrix} 5 & 2 \\ -5 & -2 \end{bmatrix} \vec{y}_1 &= \vec{0} \longrightarrow \\ \vec{y}_1 &= \left\{2\sqrt{29}/29, \ -5\sqrt{29}/29\right\}^T . \end{aligned}$$

$$\begin{aligned} (A^T - \lambda_2 I)\vec{y}_2 &= \vec{0} \longrightarrow \\ \begin{bmatrix} 2 & 2 \\ -5 & -5 \end{bmatrix} \vec{y}_2 &= \vec{0} \longrightarrow \\ \vec{y}_2 &= \left\{\sqrt{2}/2, \ -\sqrt{2}/2\right\}^T . \end{aligned}$$

1.2.10 Modal Decomposition

The right and left eigenvectors of a particular eigenvalue have unity dot product, that is $\vec{x}_i^T \vec{y}_i = 1$, with the normalization noted above. The dot product of a left eigenvector with the right eigenvector of *a different eigenvalue* is zero. Thus, if

$$\begin{aligned} X &= [\vec{x}_1 \cdots \vec{x}_n], \text{ and} \\ Y &= [\vec{y}_1 \cdots \vec{y}_n], \end{aligned}$$

then we have

$$\begin{aligned} Y^T X &= I, \text{ or} \\ Y^T &= X^{-1}. \end{aligned}$$

Next, construct a diagonal matrix of eigenvalues:

$$\Lambda = \begin{bmatrix} \lambda_1 & & 0 \\ & \cdot & \\ 0 & & \lambda_n \end{bmatrix};$$

it follows that

$$\begin{aligned} AV &= V\Lambda \longrightarrow \\ A &= V\Lambda W^T \\ &= \sum_{i=1}^{n} \lambda_i \vec{v}_i \vec{w}_i^T. \end{aligned}$$

Hence A can be written as a sum of modal components.[1]

1.2.11 Singular Value

Let $G(s)$ be an $m \times n$, possibly complex matrix. The singular value decomposition (SVD) computes three matrices satisfying

[1] By carrying out successive multiplications, it can be shown that A^k has its eigenvalues at λ_i^k, and keeps the same eigenvectors as A.

$$G = U\Sigma V^*,$$

where U is $m \times m$, Σ is $m \times n$, and V is $n \times n$. The star notation indicates a complex-conjugate transpose. The matrix Σ is diagonal, with the form

$$\Sigma = \begin{bmatrix} \sigma_1 & 0 & 0 & 0 \\ 0 & \cdot & 0 & 0 \\ 0 & 0 & \sigma_p & 0 \\ 0 & 0 & 0 & 0 \end{bmatrix},$$

where $p = min(m, n)$. Each nonzero entry on the diagonal is a real, positive singular value, ordered such that $\sigma_1 > \sigma_2 > \cdots \sigma_p$. The notation is common that $\sigma_1 = \overline{\sigma}$, the maximum singular value, and $\sigma_p = \underline{\sigma}$, the minimum singular value. The auxiliary matrices U and V are unitary, i.e., they satisfy $X^* = X^{-1}$. Like eigenvalues, the singular values of G are related to projections. σ_i represents the Euclidean size of the matrix G along the i'th singular vector:

$$\begin{aligned} \overline{\sigma} &= max_{||x||=1}||Gx|| \\ \underline{\sigma} &= min_{||x||=1}||Gx||. \end{aligned}$$

Other properties of the singular value include:

- $\overline{\sigma}(AB) \leq \overline{\sigma}(A)\overline{\sigma}(B)$.
- $\overline{\sigma}(A) = \sqrt{\lambda_{max}(A^*A)}$.
- $\underline{\sigma}(A) = \sqrt{\lambda_{min}(A^*A)}$.
- $\underline{\sigma}(A) = 1/\overline{\sigma}(A^{-1})$.
- $\overline{\sigma}(A) = 1/\underline{\sigma}(A^{-1})$.

1.3 Laplace Transform

1.3.1 Definition

The Laplace transform converts time-domain signals into a frequency-domain equivalent. The signal $y(t)$ has transform $Y(s)$ defined as follows:

$$Y(s) = L(y(t)) = \int_0^\infty y(\tau)e^{-s\tau}d\tau,$$

where s is an unspecified complex number; $Y(s)$ is considered to be complex as a result. Note that the Laplace transform is linear, and so it is is distributive: $L(x(t) + y(t)) = L(x(t)) + L(y(t))$ will hold throughout. The following table gives a list of some useful transform pairs and other properties, for reference.

The last two properties are of special importance: for control system design, the differentiation of a signal is equivalent to multiplication of its Laplace transform by s; integration of a signal is equivalent to division by s. The other terms that arise will cancel if $y(0) = 0$, or if $y(0)$ is finite, so they are usually ignored.

1.3.2 Convergence

We note first that the value of s affects the convergence of the integral. For instance, if $y(t) = e^t$, then the integral converges only for $Re(s) > 1$, since the integrand is e^{1-s} in this case. Convergence issues are not a problem for evaluation of the Laplace transform, however, because of *analytic continuation*. This result from complex analysis holds that if two complex functions are equal on some arc (or line) in the complex plane, then they are equivalent everywhere. This fact allows us to always pick a value of s for which the integral above converges, and then by extension infer the existence of the general transform.

1.3.3 Convolution Theorem

One of the main points of the Laplace transform is the ease of dealing with dynamic systems. As with the Fourier transform, the convolution of two signals in the time domain corresponds with the multiplication of signals in the frequency domain. Consider a system whose impulse response is $g(t)$, being

$$
\begin{array}{rrcl}
 & y(t) & \longleftrightarrow & Y(s) \\
\text{(Impulse)} & \delta(t) & \longleftrightarrow & 1 \\
\text{(Unit Step)} & 1(t) & \longleftrightarrow & \dfrac{1}{s} \\
\text{(Unit Ramp)} & t & \longleftrightarrow & \dfrac{1}{s^2} \\
 & e^{-\alpha t} & \longleftrightarrow & \dfrac{1}{s+\alpha} \\
 & \sin \omega t & \longleftrightarrow & \dfrac{\omega}{s^2+\omega^2} \\
 & \cos \omega t & \longleftrightarrow & \dfrac{s}{s^2+\omega^2} \\
 & e^{-\alpha t} \sin \omega t & \longleftrightarrow & \dfrac{\omega}{(s+\alpha)^2+\omega^2} \\
 & e^{-\alpha t} \cos \omega t & \longleftrightarrow & \dfrac{s+\alpha}{(s+\alpha)^2+\omega^2} \\
 & \dfrac{1}{b-a}(e^{-at}-e^{-bt}) & \longleftrightarrow & \dfrac{1}{(s+a)(s+b)} \\
 & \dfrac{1}{ab}\left[1+\dfrac{1}{a-b}(be^{-at}-ae^{-bt})\right] & \longleftrightarrow & \dfrac{1}{s(s+a)(s+b)} \\
 & \dfrac{\omega_n}{\sqrt{1-\zeta^2}}\, e^{-\zeta\omega_n t} \sin \omega_n \sqrt{1-\zeta^2}\, t & \longleftrightarrow & \dfrac{\omega_n^2}{s^2+2\zeta\omega_n s+\omega_n^2} \\
 & 1-\dfrac{1}{\sqrt{1-\zeta^2}}\, e^{-\zeta\omega_n t} \sin\left(\omega_n\sqrt{1-\zeta^2}\, t+\phi\right) & \longleftrightarrow & \dfrac{\omega_n^2}{s(s^2+2\zeta\omega_n s+\omega_n^2)} \\
 & \left(\phi = \tan^{-1}\dfrac{\sqrt{1-\zeta^2}}{\zeta}\right) & & \\
\text{(Pure Delay)} & y(t-\tau)1(t-\tau) & \longleftrightarrow & Y(s)e^{-s\tau} \\
\text{(Time Derivative)} & \dfrac{dy(t)}{dt} & \longleftrightarrow & sY(s)-y(0) \\
\text{(Time Integral)} & \displaystyle\int_0^t y(\tau)d\tau & \longleftrightarrow & \dfrac{Y(s)}{s}+\dfrac{\int_{0-}^{0+} y(t)dt}{s}
\end{array}
$$

driven by an input signal $x(t)$; the output is $y(t) = g(t) * x(t)$. The *Convolution Theorem* is

$$y(t) = \int_0^t g(t-\tau)x(\tau)d\tau \Longleftrightarrow Y(s) = G(s)X(s).$$

Here's the proof given by Siebert:

$$\begin{aligned}
Y(s) &= \int_0^\infty y(t)e^{-st}dt \\
&= \int_0^\infty \left[\int_0^t g(t-\tau)\ x(\tau)\ d\tau\right] e^{-st}\ dt \\
&= \int_0^\infty \left[\int_0^\infty g(t-\tau)\ 1(t-\tau)\ x(\tau)\ d\tau\right] e^{-st}dt \\
&= \int_0^\infty x(\tau)\left[\int_0^\infty g(t-\tau)\ 1(t-\tau)\ e^{-st}\ dt\right] d\tau \\
&= \int_0^\infty x(\tau)\ G(s)e^{-s\tau}\ d\tau \\
&= G(s)X(s)
\end{aligned}$$

When $g(t)$ is the impulse response of a dynamic system, then $y(t)$ represents the output of this system when it is driven by the external signal $x(t)$.

1.3.4 Solution of Differential Equations by Laplace Transform

The Convolution Theorem allows one to solve (linear time-invariant) differential equations in the following way:

1. Transform the system impulse response $g(t)$ into $G(s)$, and the input signal $x(t)$ into $X(s)$, using the transform pairs.
2. Perform the multiplication in the Laplace domain to find $Y(s)$.
3. Ignoring the effects of pure time delays, break $Y(s)$ into partial fractions with no powers of s greater than 2 in the denominator.
4. Generate the time-domain response from the simple transform pairs. Apply time delay as necessary.

Specific examples of this procedure are given in a later section on transfer functions.

2 KINEMATICS OF MOVING FRAMES

2.1 Rotation of Reference Frames

We say that a vector expressed in the inertial frame has coordinates $\vec{x}$, and in a body-reference frame $\vec{x}_b$. For the moment, we assume that the origins of these frames are coincident, but that the body frame has a different angular orientation. The angular orientation has several well-known descriptions, including the Euler angles and the Euler parameters (quaternions). The former method involves successive rotations about the principle axes, and has a solid link with the intuitive notions of roll, pitch, and yaw. Quaternions present a more elegant and robust method, but with more abstraction. We will develop the equations of motion using Euler angles.

Tape three pencils together to form a right-handed three-dimensional coordinate system. Successively rotating the system about three of *its own* principle axes, it is easy to see that any possible orientation can be achieved. For example, consider the sequence of [yaw, pitch, roll]: starting from an orientation identical to some inertial frame, rotate the movable system about its yaw axis, then about the *new* pitch axis, then about the *newer still* roll axis. Needless to say, there are many valid Euler angle rotation sets possible to reach a given orientation; some of them might use the same axis twice.

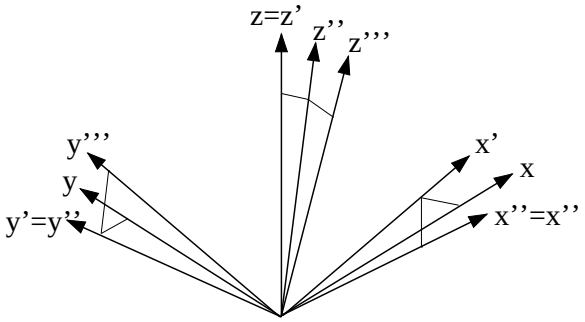

Figure 1: Successive application of three Euler angles transforms the original coordinate frame into an arbitrary orientation.

A first question is: what is the coordinate of a point fixed in inertial space, referenced to a rotated *body* frame? The transformation takes the form of a 3×3 matrix, which we now derive through successive rotations of the three

Euler angles. Before the first rotation, the body-referenced coordinate matches that of the inertial frame: $\vec{x}_b^{\,0} = \vec{x}$. Now rotate the movable frame yaw axis (z) through an angle ϕ. We have

$$\vec{x}_b^{\,1} = \begin{bmatrix} \cos\phi & \sin\phi & 0 \\ -\sin\phi & \cos\phi & 0 \\ 0 & 0 & 1 \end{bmatrix} \vec{x}_b^{\,0} = R(\phi)\vec{x}_b^{\,0}. \tag{1}$$

Rotation about the z-axis does not change the z-coordinate of the point; the other axes are modified according to basic trigonometry. Now apply the second rotation, pitch about the *new* y-axis by the angle θ:

$$\vec{x}_b^{\,2} = \begin{bmatrix} \cos\theta & 0 & -\sin\theta \\ 0 & 1 & 0 \\ \sin\theta & 0 & \cos\theta \end{bmatrix} \vec{x}_b^{\,1} = R(\theta)\vec{x}_b^{\,1}. \tag{2}$$

Finally, rotate the body system an angle ψ about its *newest* x-axis:

$$\vec{x}_b^{\,3} = \begin{bmatrix} 1 & 0 & 0 \\ 0 & \cos\psi & \sin\psi 0 \\ 0 & -\sin\psi & \cos\psi \end{bmatrix} \vec{x}_b^{\,2} = R(\psi)\vec{x}_b^{\,2}. \tag{3}$$

This represents the location of the original point, in the fully-transformed body-reference frame, i.e., $\vec{x}_b^{\,3}$. We will use the notation $\vec{x}_b$ instead of $\vec{x}_b^{\,3}$ from here on. The three independent rotations can be cascaded through matrix multiplication (order matters!):

$$\begin{aligned} \vec{x}_b &= R(\psi)R(\theta)R(\phi)\vec{x} \\ &= \begin{bmatrix} c\theta c\phi & c\theta s\phi & -s\theta \\ -c\psi s\psi + s\psi s\theta c\phi & c\psi c\phi + s\psi s\theta s\phi & s\psi c\theta \\ s\psi s\phi + c\psi s\theta c\phi & -s\psi c\phi + c\psi s\theta s\psi & c\psi c\theta \end{bmatrix} \vec{x} \\ &= R(\phi,\theta,\psi)\vec{x}. \end{aligned} \tag{4}$$

All of the transformation matrices, including $R(\phi,\theta,\psi)$, are orthonormal: their inverse is equivalent to their transpose. Additionally, we should note that the rotation matrix R is universal to *all* representations of orientation, including quaternions. The roles of the trigonometric functions, as written, are specific to Euler angles, and to the order in which we performed the rotations.
In the case that the movable (body) reference frame has a different origin than the inertial frame, we have

$$\vec{x} = \vec{x}_0 + R^T \vec{x}_b, \tag{5}$$

where $\vec{x}_0$ is the location of the moving origin, expressed in inertial coordinates.

2.2 Differential Rotations

Now consider small rotations from one frame to another; using the small angle assumption to ignore higher-order terms gives

$$\begin{aligned} R &\simeq \begin{bmatrix} 1 & \delta\phi & -\delta\theta \\ -\delta\phi & 1 & \delta\psi \\ \delta\theta & -\delta\psi & 1 \end{bmatrix} \\ &= \begin{bmatrix} 0 & \delta\phi & -\delta\theta \\ -\delta\phi & 0 & \delta\psi \\ \delta\theta & -\delta\psi & 0 \end{bmatrix} + I_{3\times 3}. \end{aligned} \tag{6}$$

R comprises the identity plus a part equal to the (negative) cross-product operator $[-\delta\vec{E}\times]$, where $\delta\vec{E} = [\delta\psi, \delta\theta, \delta\phi]$, the vector of Euler angles ordered with the axes $[x, y, z]$. Small rotations are completely decoupled; the order of the small rotations does not matter. Since $R^{-1} = R^T$, we have also $R^{-1} = I_{3\times 3} + \delta\vec{E}\times$;

$$\vec{x}_b = \vec{x} - \delta\vec{E} \times \vec{x} \tag{7}$$

$$\vec{x} = \vec{x}_b + \delta\vec{E} \times \vec{x}_b. \tag{8}$$

We now fix the point of interest on the *body*, instead of in inertial space, calling its location in the body frame $\vec{r}$ (radius). The differential rotations occur over a time step δt, so that we can write the location of the point before and after the rotation, with respect to the first frame as follows:

$$\begin{aligned} \vec{x}(t) &= \vec{r} \\ \vec{x}(t+\delta t) &= R^T\vec{r} = \vec{r} + \delta\vec{E} \times \vec{r}. \end{aligned} \tag{9}$$

Dividing by the differential time step gives

$$\begin{aligned} \frac{\delta\vec{x}}{\delta t} &= \frac{\delta\vec{E}}{\delta t}\times\vec{r} \\ &= \omega\times\vec{r}, \end{aligned} \tag{10}$$

where the *rotation rate* vector $\omega \simeq d\vec{E}/dt$ because the Euler angles for this infinitesimal rotation are small and decoupled. This same cross-product relationship can be derived in the second frame as well:

$$\begin{aligned} \vec{x}_b(t) &= R\vec{r} = \vec{r} - \delta\vec{E}\times\vec{r} \\ \vec{x}_b(t+\delta t) &= \vec{r}. \end{aligned} \tag{11}$$

such that

$$\begin{aligned} \frac{\delta\vec{x}_b}{\delta t} &= \frac{\delta\vec{E}}{\delta t}\times\vec{r} \\ &= \omega\times\vec{r}, \end{aligned} \tag{12}$$

On a rotating body whose origin point is fixed, the time rate of change of a constant radius vector is the cross-product of the rotation rate vector $\vec{\omega}$ and the radius vector itself. The resultant derivative is in the moving body frame. In the case that the radius vector changes with respect to the body frame, we need an additional term:

$$\frac{d\vec{x}_b}{dt} = \omega\times\vec{r} + \frac{\partial\vec{r}}{\partial t}. \tag{13}$$

Finally, allowing the origin to move as well gives

$$\frac{d\vec{x}_b}{dt} = \omega\times\vec{r} + \frac{\partial\vec{r}}{\partial t} + \frac{d\vec{x}_o}{dt}. \tag{14}$$

This result is often written in terms of body-referenced velocity $\vec{v}$:

$$\vec{v} = \omega\times\vec{r} + \frac{\partial\vec{r}}{\partial t} + \vec{v}_o, \tag{15}$$

where $\vec{v}_o$ is the body-referenced velocity of the origin. The total velocity of the particle is equal to the velocity of the reference frame origin, plus a component

due to rotation of this frame. The velocity equation can be generalized to *any* body-referenced vector $\vec{f}$:

$$\frac{d\vec{f}}{dt} = \frac{\partial f}{\partial t} + \vec{\omega} \times \vec{f}. \tag{16}$$

2.3 Rate of Change of Euler Angles

Only for the case of infinitesimal Euler angles is it true that the time rate of change of the Euler angles equals the body-referenced rotation rate. For example, with the sequence [yaw,pitch,roll], the Euler yaw angle (applied first) is definitely not about the final body yaw axis; the pitch and roll rotations moved the axis. An important part of any simulation is the evolution of the Euler angles. Since the physics determine rotation rate $\vec{\omega}$, we seek a mapping $\vec{\omega} \rightarrow d\vec{E}/dt$.

The idea is to consider small changes in each Euler angle, and determine the effects on the rotation vector. The first Euler angle undergoes two additional rotations, the second angle one rotation, and the final Euler angle no additional rotations:

$$\begin{aligned} \vec{\omega} &= R(\psi)R(\theta) \left\{ \begin{array}{c} 0 \\ 0 \\ \frac{d\phi}{dt} \end{array} \right\} + R(\psi) \left\{ \begin{array}{c} 0 \\ \frac{d\theta}{dt} \\ 0 \end{array} \right\} + \left\{ \begin{array}{c} \frac{d\psi}{dt} \\ 0 \\ 0 \end{array} \right\} \\ &= \left[\begin{array}{ccc} 1 & 0 & -\sin\theta \\ 0 & \cos\psi & \sin\psi\cos\theta \\ 0 & -\sin\psi & \cos\psi\cos\theta \end{array} \right] \left\{ \begin{array}{c} \frac{d\psi}{dt} \\ \frac{d\theta}{dt} \\ \frac{d\phi}{dt} \end{array} \right\}. \end{aligned} \tag{17}$$

Taking the inverse gives

$$\begin{aligned} \frac{d\vec{E}}{dt} &= \left[\begin{array}{ccc} 1 & \sin\psi\tan\theta & \cos\psi\tan\theta \\ 0 & \cos\psi & -\sin\psi \\ 0 & \sin\psi/\cos\theta & \cos\psi/\cos\theta \end{array} \right] \vec{\omega} \\ &= \Gamma(\vec{E})\vec{\omega}. \end{aligned} \tag{18}$$

Singularities exist in Γ at $\theta = \{\pi/2, 3\pi/2\}$, because of the division by $\cos\theta$, and hence this otherwise useful equation for propagating the angular orientation of a body fails when the vehicle rotates about the intermediate y-axis by ninety

degrees. In applications where this is a real possibility, for example in orbiting satellites and robotic arms, quaternions provide a seamless mapping. For most ocean vessels, the singularity is acceptable, as long as it is not on the yaw axis!

2.4 Dead Reckoning

The measurement of heading and longitudinal speed gives rise to one of the oldest methods of navigation: dead reckoning. Quite simply, if the estimated longitudinal speed over ground is U, and the estimated heading is ϕ, ignoring the lateral velocity leads to the evolution of Cartesian coordinates:

$$\begin{aligned} \dot{x} &= U \cos \phi \\ \dot{y} &= U \sin \phi. \end{aligned}$$

Needless to say, currents and vehicle sideslip will cause this to be in error. Nonetheless, some of the most remarkable feats of navigation in history have depended on dead reckoning.

3 VESSEL INERTIAL DYNAMICS

We consider the rigid body dynamics with a coordinate system affixed on the body. A common frame for ships, submarines, and other marine vehicles has the body-referenced x-axis forward, y-axis to port (left), and z-axis up. This will be the sense of our body-referenced coordinate system here.

3.1 Momentum of a Particle

Since the body moves with respect to an inertial frame, dynamics expressed in the body-referenced frame need extra attention. First, linear momentum for a particle obeys the equality

$$\vec{F} = \frac{d}{dt}\left(m\vec{v}\right) \tag{19}$$

A rigid body consists of a large number of these small particles, which can be indexed. The summations we use below can be generalized to integrals quite easily. We have

$$\vec{F_i} + \vec{R_i} = \frac{d}{dt}\left(m_i\vec{v_i}\right), \tag{20}$$

where $\vec{F_i}$ is the external force acting on the particle and $\vec{R_i}$ is the net force exerted by all the other surrounding particles (internal forces). Since the collection of particles is not driven apart by the internal forces, we must have equal and opposite internal forces such that

$$\sum_{i=1}^{N} \vec{R_i} = 0. \tag{21}$$

Then summing up all the particle momentum equations gives

$$\sum_{i=1}^{N} \vec{F_i} = \sum_{i=1}^{N} \frac{d}{dt}\left(m_i\vec{v_i}\right). \tag{22}$$

Note that the particle velocities are *not* independent, because the particles are rigidly attached.

Now consider a body reference frame, with origin $\mathbf{0}$, in which the particle i resides at body-referenced radius vector $\vec{r}$; the body translates and rotates, and we now consider how the momentum equation depends on this motion.

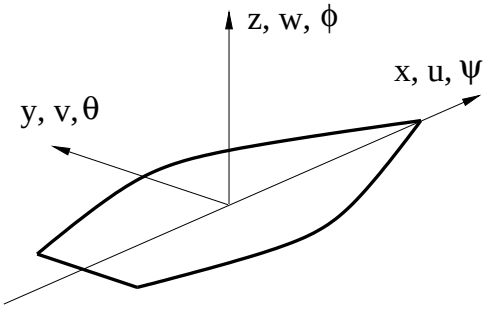

Figure 2: Convention for the body-referenced coordinate system on a vessel: x is forward, y is sway to the left, and z is heave upwards. Looking forward from the vessel bridge, roll about the x axis is positive counterclockwise, pitch about the y-axis is positive bow-down, and yaw about the z-axis is positive turning left.

3.2 Linear Momentum in a Moving Frame

The expression for total velocity may be inserted into the summed linear momentum equation to give

$$\begin{aligned} \sum_{i=1}^{N} \vec{F}_i &= \sum_{i=1}^{N} \frac{d}{dt}(m_i(\vec{v}_o + \vec{\omega} \times \vec{r}_i)) \\ &= m\frac{\partial \vec{v}_o}{\partial t} + \frac{d}{dt}\left[\vec{\omega} \times \sum_{i=1}^{N} m_i \vec{r}_i\right], \end{aligned} \tag{23}$$

where $m = \sum_{i=1}^{N} m_i$, and $\vec{v}_i = \vec{v}_o + \vec{\omega} \times \vec{r}_i$. Further defining the center of gravity vector $\vec{r}_G$ such that

$$m\vec{r}_G = \sum_{i=1}^{N} m_i \vec{r}_i, \tag{24}$$

we have

$$\sum_{i=1}^{N} \vec{F}_i = m\frac{\partial \vec{v}_o}{\partial t} + m\frac{d}{dt}(\vec{\omega} \times \vec{r}_G). \tag{25}$$

Using the expansion for total derivative again, the complete vector equation in body coordinates is

$$\vec{F} = \sum_{i=1} N = m\left(\frac{\partial \vec{v}_o}{\partial t} + \vec{\omega} \times \vec{v}_o + \frac{d\vec{\omega}}{dt} \times \vec{r}_G + \vec{\omega} \times (\vec{\omega} \times \vec{r}_G)\right). \qquad (26)$$

Now we list some conventions that will be used from here on:

$$\begin{aligned} \vec{v}_o &= \{u, v, w\} \text{ (body-referenced velocity)} \\ \vec{r}_G &= \{x_G, y_G, z_g\} \text{ (body-referenced location of center of mass)} \\ \vec{\omega} &= \{p, q, r\} \text{ (rotation vector, in body coordinates)} \\ \vec{F} &= \{X, Y, Z\} \text{ (external force, body coordinates).} \end{aligned}$$

The last term in the previous equation simplifies using the vector triple product identity

$$\vec{\omega} \times (\vec{\omega} \times \vec{r}_G) = (\vec{\omega} \cdot \vec{r}_G)\vec{\omega} - (\vec{\omega} \cdot \vec{\omega})\vec{r}_G,$$

and the resulting three linear momentum equations are

$$\begin{aligned} X &= m\left[\frac{\partial u}{\partial t} + qw - rv + \frac{dq}{dt}z_G - \frac{dr}{dt}y_G + (qy_G + rz_G)p - (q^2 + r^2)x_G\right] \qquad (27) \\ Y &= m\left[\frac{\partial v}{\partial t} + ru - pw + \frac{dr}{dt}x_G - \frac{dp}{dt}z_G + (rz_G + px_G)q - (r^2 + p^2)y_G\right] \\ Z &= m\left[\frac{\partial w}{\partial t} + pv - qu + \frac{dp}{dt}y_G - \frac{dq}{dt}x_G + (px_G + qy_G)r - (p^2 + q^2)z_G\right]. \end{aligned}$$

Note that about half of the terms here are due to the mass center being in a different location than the reference frame origin, i.e., $\vec{r}_G \neq \vec{0}$.

3.3 Example: Mass on a String

Consider a mass on a string, being swung around around in a circle at speed U, with radius r. The centrifugal force can be computed in at least three different ways. The vector equation at the start is

$$\vec{F} = m\left(\frac{\partial \vec{v}_o}{\partial t} + \vec{\omega} \times \vec{v}_o + \frac{d\vec{\omega}}{dt} \times \vec{r}_G + \vec{\omega} \times (\vec{\omega} \times \vec{r}_G)\right).$$

3.3.1 Moving Frame Affixed to Mass

Affixing a reference frame *on* the mass, with the local x oriented forward and y inward towards the circle center, gives

$$\begin{aligned}
\vec{v}_o &= \{U, 0, 0\}^T \\
\vec{\omega} &= \{0, 0, U/r\}^T \\
\vec{r}_G &= \{0, 0, 0\}^T \\
\frac{\partial \vec{v}_o}{\partial t} &= \{0, 0, 0\}^T \\
\frac{\partial \vec{\omega}}{\partial t} &= \{0, 0, 0\}^T,
\end{aligned}$$

such that

$$\vec{F} = m\vec{\omega} \times \vec{v}_o = m\{0, U^2/r, 0\}^T.$$

The force of the string pulls in on the mass to create the circular motion.

3.3.2 Rotating Frame Attached to Pivot Point

Affixing the moving reference frame to the pivot point of the string, with the same orientation as above but allowing it to rotate with the string, we have

$$\begin{aligned}
\vec{v}_o &= \{0, 0, 0\}^T \\
\vec{\omega} &= \{0, 0, U/r\}^T \\
\vec{r}_G &= \{0, r, 0\}^T \\
\frac{\partial \vec{v}_o}{\partial t} &= \{0, 0, 0\}^T \\
\frac{\partial \vec{\omega}}{\partial t} &= \{0, 0, 0\}^T,
\end{aligned}$$

giving the same result:

$$\vec{F} = m\vec{\omega} \times (\vec{\omega} \times \vec{r}_G) = m\{0, U^2/r, 0\}^T.$$

3.3.3 Stationary Frame

A frame fixed in inertial space, and momentarily coincident with the frame on the mass (3.3.1), can also be used for the calculation. In this case, as the string travels through a small arc $\delta\psi$, vector subtraction gives

$$\delta\vec{v} \;=\; \{0, U\sin\delta\psi, 0\}^T \simeq \{0, U\delta\psi, 0\}^T.$$

Since $\dot{\psi} = U/r$, it follows easily that in the fixed frame $d\vec{v}/dt = \{0, U^2/r, 0\}^T$, as before.

3.4 Angular Momentum

For angular momentum, the summed particle equation is

$$\sum_{i=1}^{N}(\vec{M}_i + \vec{r}_i \times \vec{F}_i) = \sum_{i=1}^{N} \vec{r}_i \times \frac{d}{dt}(m_i\vec{v}_i), \tag{28}$$

where $\vec{M}_i$ is an external moment on the particle i. Similar to the case for linear momentum, summed internal moments cancel. We have

$$\begin{aligned}\sum_{i=1}^{N}(\vec{M}_i + \vec{r}_i \times \vec{F}_i) \;&=\; \sum_{i=1}^{N} m_i\vec{r}_i \times \left[\frac{\partial\vec{v}_o}{\partial t} + \vec{\omega}\times\vec{v}_o\right] + \sum_{i=1}^{N} m_i\vec{r}_i \times \left(\frac{\partial\vec{\omega}}{\partial t}\times\vec{r}_i\right) + \\ &\quad \sum_{i=1}^{N} m_i\vec{r}_i \times (\vec{\omega}\times(\vec{\omega}\times\vec{r}_i)).\end{aligned}$$

The summation in the first term of the right-hand side is recognized simply as $m\vec{r}_G$, and the first term becomes

$$m\vec{r}_G \times \left[\frac{\partial\vec{v}_o}{\partial t} + \vec{\omega}\times\vec{v}_o\right]. \tag{29}$$

The second term expands as (using the triple product)

$$\begin{aligned}\sum_{i=1}^{N} m_i\vec{r}_i \times \left(\frac{\partial\vec{\omega}}{\partial t}\times\vec{r}_i\right) \;&=\; \sum_{i=1}^{N} m_i\left((\vec{r}_i\cdot\vec{r}_i)\frac{\partial\vec{\omega}}{\partial t} - \left(\frac{\partial\vec{\omega}}{\partial t}\cdot\vec{r}_i\right)\vec{r}_i\right) \qquad (30)\\ &=\; \left\{\begin{array}{l}\sum_{i=1}^{N} m_i\left((y_i^2+z_i^2)\dot{p} - (y_i\dot{q} + z_i\dot{r})x_i\right)\\ \sum_{i=1}^{N} m_i\left((x_i^2+z_i^2)\dot{q} - (x_i\dot{p} + z_i\dot{r})y_i\right)\\ \sum_{i=1}^{N} m_i\left((x_i^2+y_i^2)\dot{r} - (x_i\dot{p} + y_i\dot{q})z_i\right)\end{array}\right\}.\end{aligned}$$

Employing the definitions of moments of inertia,

$$
\begin{aligned}
I &= \begin{bmatrix} I_{xx} & I_{xy} & I_{xz} \\ I_{yx} & I_{yy} & I_{yz} \\ I_{zx} & I_{zy} & I_{zz} \end{bmatrix} \qquad \text{(inertia matrix)} \\
I_{xx} &= \sum_{i=1}^{N} m_i (y_i^2 + z_i^2) \\
I_{yy} &= \sum_{i=1}^{N} m_i (x_i^2 + z_i^2) \\
I_{zz} &= \sum_{i=1}^{N} m_i (x_i^2 + y_i^2) \\
I_{xy} &= I_{yx} = -\sum_{i=1}^{N} m_i x_i y_i \qquad \text{(cross-inertia)} \\
I_{xz} &= I_{zx} = -\sum_{i=1}^{N} m_i x_i z_i \\
I_{yz} &= I_{zy} = -\sum_{i=1}^{N} m_i y_i z_i,
\end{aligned}
$$

the second term of the angular momentum right-hand side collapses neatly into $I\partial\vec{\omega}/\partial t$. The third term can be worked out along the same lines, but offers no similar condensation:

$$
\begin{aligned}
\sum_{i=1}^{N} m_i \vec{r}_i \times ((\vec{\omega}\cdot\vec{r}_i)\vec{\omega} - (\vec{\omega}\cdot\vec{\omega})\vec{r}_i) &= \sum_{i=1}^{N} m_i \vec{r}_i \times \vec{\omega}(\vec{\omega}\cdot\vec{r}_i) \qquad (31) \\
&= \begin{Bmatrix} \sum_{i=1}^{N} m_i (y_i r - z_i q)(x_i p + y_i q + z_i r) \\ \sum_{i=1}^{N} m_i (z_i p - x_i r)(x_i p + y_i q + z_i r) \\ \sum_{i=1}^{N} m_i (x_i q - y_i p)(x_i p + y_i q + z_i r) \end{Bmatrix} \\
&= \begin{Bmatrix} I_{yz}(q^2 - r^2) + I_{xz} pq - I_{xy} pr \\ I_{xz}(r^2 - p^2) + I_{xy} rq - I_{yz} pq \\ I_{xy}(p^2 - q^2) + I_{yz} pr - I_{xz} qr \end{Bmatrix} + \\
&\quad \begin{Bmatrix} (I_{zz} - I_{yy}) rq \\ (I_{xx} - I_{zz}) rp \\ (I_{yy} - I_{xx}) qp \end{Bmatrix}.
\end{aligned}
$$

Letting $\vec{M} = \{K, M, N\}$ be the total moment acting on the body, i.e., the left side of Equation 28, the complete moment equations are

$$\begin{aligned} K &= I_{xx}\dot{p} + I_{xy}\dot{q} + I_{xz}\dot{r} + \\ &\quad (I_{zz} - I_{yy})rq + I_{yz}(q^2 - r^2) + I_{xz}pq - I_{xy}pr + \\ &\quad m\left[y_G(\dot{w} + pv - qu) - z_G(\dot{v} + ru - pw)\right] \end{aligned} \tag{32}$$

$$\begin{aligned} M &= I_{yx}\dot{p} + I_{yy}\dot{q} + I_{yz}\dot{r} + \\ &\quad (I_{xx} - I_{zz})pr + I_{xz}(r^2 - p^2) + I_{xy}qr - I_{yz}qp + \\ &\quad m\left[z_G(\dot{u} + qw - rv) - x_G(\dot{w} + pv - qu)\right] \end{aligned}$$

$$\begin{aligned} N &= I_{zx}\dot{p} + I_{zy}\dot{q} + I_{zz}\dot{r} + \\ &\quad (I_{yy} - I_{xx})pq + I_{xy}(p^2 - q^2) + I_{yz}pr - I_{xz}qr + \\ &\quad m\left[x_G(\dot{v} + ru - pw) - y_G(\dot{u} + qw - rv)\right]. \end{aligned}$$

3.5 Example: Spinning Book

Consider a homogeneous rectangular block with $I_{xx} < I_{yy} < I_{zz}$ and all off-diagonal moments of inertia are zero. The linearized angular momentum equations, with no external forces or moments, are

$$\begin{aligned} I_{xx}\frac{dp}{dt} + (I_{zz} - I_{yy})rq &= 0 \\ I_{yy}\frac{dq}{dt} + (I_{xx} - I_{zz})pr &= 0 \\ I_{zz}\frac{dr}{dt} + (I_{yy} - I_{xx})qp &= 0. \end{aligned}$$

We consider in turn the stability of rotations about each of the main axes, with constant angular rate Ω. The interesting result is that rotations about the x and z axes are unstable, while rotation about the y axis is not.

3.5.1 x-axis

In the case of the x-axis, $p = \Omega + \delta p$, $q = \delta q$, and $r = \delta r$, where the δ prefix indicates a small value compared to Ω. The first equation above is uncoupled

from the others, and indicates no change in δp, since the small term $\delta q \delta r$ can be ignored. Differentiate the second equation to obtain

$$I_{yy}\frac{\partial^2 \delta q}{\partial t^2} + (I_{xx} - I_{zz})\Omega\frac{\partial \delta r}{\partial t} = 0$$

Substitution of this result into the third equation yields

$$I_{yy}I_{zz}\frac{\partial^2 \delta q}{\partial t^2} + (I_{xx} - I_{zz})(I_{xx} - I_{yy})\Omega^2 \delta q = 0.$$

A simpler expression is $\delta\ddot{q} + \alpha\delta q = 0$, which has response $\delta q(t) = \delta q(0)e^{\sqrt{-\alpha}t}$, when $\delta\dot{q}(0) = 0$. For spin about the x-axis, both coefficients of the differential equation are positive, and hence $\alpha > 0$. The imaginary exponent indicates that the solution is of the form $\delta q(t) = \delta q(0) cos\sqrt{\alpha}t$, that is, it oscillates but does not grow. Since the perturbation δr is coupled, it too oscillates.

3.5.2 y-axis

Now suppose $q = \Omega + \delta q$: differentiate the first equation and substitute into the third equation to obtain

$$I_{zz}I_{xx}\frac{\partial^2 \delta p}{\partial t^2} + (I_{yy} - I_{xx})(I_{yy} - I_{zz})\Omega^2 \delta p = 0.$$

Here the second coefficient has negative sign, and therefore $\alpha < 0$. The exponent is real now, and the solution grows without bound, following $\delta p(t) = \delta p(0)e^{\sqrt{-\alpha}t}$.

3.5.3 z-axis

Finally, let $r = \Omega + \delta r$: differentiate the first equation and substitute into the second equation to obtain

$$I_{yy}I_{xx}\frac{\partial^2 \delta p}{\partial t^2} + (I_{xx} - I_{zz})(I_{yy} - I_{zz})\Omega^2 \delta p = 0.$$

The coefficients are positive, so bounded oscillations occur.

3.6 Parallel Axis Theorem

Often, the mass center of an body is at a different location than a more convenient measurement point, the geometric center of a vessel for example. The parallel axis theorem allows one to translate the mass moments of inertia referenced to the mass center into another frame with parallel orientation, and vice versa. Sometimes a translation of coordinates to the mass center will make the cross-inertial terms I_{xy}, I_{yz}, I_{xz} small enough that they can be ignored; in this case $\vec{r}_G = \vec{0}$ also, so that the equations of motion are significantly reduced, as in the spinning book example.
The formulas are:

$$\begin{aligned} I_{xx} &= \bar{I}_{xx} + m(\delta y^2 + \delta z^2) \\ I_{yy} &= \bar{I}_{yy} + m(\delta x^2 + \delta z^2) \\ I_{zz} &= \bar{I}_{zz} + m(\delta x^2 + \delta y^2) \\ I_{yz} &= \bar{I}_{yz} - m\delta y \delta z \\ I_{xz} &= \bar{I}_{xz} - m\delta x \delta z \\ I_{xy} &= \bar{I}_{xy} - m\delta x \delta y, \end{aligned} \tag{33}$$

where $\bar{I}$ represents an MMOI in the axes of the mass center, and δx, for example, is the translation of the x-axis to the new frame. Note that translation of MMOI using the parallel axis theorem *must* be either to or from a frame resting exactly at the center of gravity.

3.7 Basis for Simulation

Except for external forces and moments $\vec{F}$ and $\vec{M}$, we now have the necessary terms for writing a full nonlinear simulation of a rigid body, in body coordinates. There are twelve states, comprising the following components:

- $\vec{v}_o$, the vector of body-referenced velocities.
- $\vec{\omega}$, body rotation rate vector.
- $\vec{x}$, location of the body origin, in *inertial* space.
- $\vec{E}$, Euler angle vector.

The derivatives of body-referenced velocity and rotation rate come from Equations 27 and 32, with some coupling which generally requires a 6×6 matrix inverse. The Cartesian position propagates according to

$$\dot{\vec{x}} = R^T(\vec{E})\vec{v}_o, \tag{34}$$

while the Euler angles follow:

$$\dot{\vec{E}} = \Gamma(\vec{E})\vec{\omega}. \tag{35}$$

4 HYDRODYNAMICS: INTRODUCTION

The forces and moments on a vessel are complicated functions of many factors, including water density, viscosity, surface tension, pressure, vapor pressure, and motions of the body. The most important factors for large ocean vehicles are density and motion, and we can make simplifications to parameterize the most prominent relationships. This section pertains to the use of *hydrodynamic coefficients* for predicting hydrodynamic response.

4.1 Taylor Series and Hydrodynamic Coefficients

Recall the Taylor expansion of a function:

$$f(x) = f(x_o) + \frac{\partial f(x_o)}{\partial x}(x - x_o) + \frac{1}{2!}\frac{\partial^2 f(x_o)}{\partial x^2}(x - x_o)^2 + \cdots. \tag{36}$$

We introduce the notation

$$\begin{aligned} f_x &= \frac{\partial f(x_o)}{\partial x} \\ f_x x &= \frac{1}{2!}\frac{\partial^2 f(x_o)}{\partial x^2}, \end{aligned}$$

and so on, so that a two-variable Taylor expansion would have the form

$$\begin{aligned} f(x,y) &= f(x_o, y_o) + & (37) \\ & \quad f_x(x - x_o) + f_y(y - y_o) + \\ & \quad f_{xx}(x - x_o)^2 + f_{yy}(y - y_o)^2 + f_{xy}(x - x_o)(y - y_o) + \\ & \quad f_{xxx}(x - x_o)^3 + \cdots. & (38) \end{aligned}$$

Note that all of the factorials are included in the coefficients. This notation covers some instances where the formal Taylor series is meaningless, but the notation is still clear. As one example, fluid drag is often written as

$$F = \frac{1}{2}\rho C_d A u|u| = F_{u|u|} u|u|.$$

4.2 Surface Vessel Linear Model

We now discuss some of the hydrodynamic parameters which govern a ship maneuvering in the horizontal plane. The body x-axis is forward and the y-axis is to port, so positive r has the boat turning left. We will consider motions only in the horizontal plane, which means $\theta = \psi = p = q = w = 0$. Since the vessel is symmetric about the $x - z$ plane, $y_G = 0$; z_G is inconsequential. We then have at the outset

$$\begin{aligned} X &= m\left(\frac{\partial u}{\partial t} - rv - x_G r^2\right) \\ Y &= m\left(\frac{\partial v}{\partial t} + ru + x_G \frac{\partial r}{\partial t}\right) \\ N &= I_{zz}\frac{\partial r}{\partial t} + mx_G\left(\frac{\partial v}{\partial t} + ru\right). \end{aligned} \tag{39}$$

Letting $u = U + u$, where $U >> u$, and eliminating higher-order terms, this set is

$$\begin{aligned} X &= m\frac{\partial u}{\partial t} \\ Y &= m\left(\frac{\partial v}{\partial t} + rU + x_G \frac{\partial r}{\partial t}\right) \\ N &= I_{zz}\frac{\partial r}{\partial t} + mx_G\left(\frac{\partial v}{\partial t} + rU\right). \end{aligned} \tag{40}$$

A number of coefficients can be discounted. First, in a homogeneous sea, with no current, wave, or wind effects, $\{X_x, X_y, X_\phi, Y_x, Y_y, Y_\phi, N_x, N_y, N_\phi\}$ are all zero. We assume that no hydrodynamic forces depend on the position of the vessel.[2] Second, consider X_v: since this longitudinal force would have the same sign regardless of the sign of v (because of side-to-side hull symmetry), it must have zero slope with v at the origin. Thus $X_v = 0$. The same argument shows that $\{X_r, X_{\dot{v}}, X_{\dot{r}}, Y_u, Y_{\dot{u}}, N_u, N_{\dot{u}}\} = 0$. Finally, since fluid particle acceleration relates linearly with pressure or force, we do not consider nonlinear acceleration

[2]Note that the linearized heave/pitch dynamics of a submarine do depend on the pitch angle; this topic will be discussed later.

terms, or higher time derivatives. It should be noted that some nonlinear terms related to those we have eliminated above are *not* zero. For instance, $Y_{uu} = 0$ because of hull symmetry, but in general $X_{vv} = 0$ only if the vessel is bow-stern symmetric.
We have so far, considering only the linear hydrodynamic terms,

$$\begin{aligned}
(m - X_{\dot{u}})\dot{u} &= X_u u + X' && (41)\\
(m - Y_{\dot{v}})\dot{v} + (mx_G - Y_{\dot{r}})\dot{r} &= Y_v v + (Y_r - mU)r + Y' && (42)\\
(mx_G - N_{\dot{v}})\dot{v} + (I_{zz} - N_{\dot{r}})\dot{r} &= N_v v - (N_r - mx_G U)r + N'. && (43)
\end{aligned}$$

The right side here carries also the imposed forces from a thruster(s) and rudder(s) $\{X', Y', N'\}$. Note that the surge equation is *decoupled* from the sway and yaw, but that sway and yaw themselves are coupled, and therefore are of immediate interest. With the state vector $\vec{s} = \{v, r\}$ and external force/moment vector $\vec{F} = \{Y', N'\}$, a state-space representation of the sway/yaw system is

$$\begin{aligned}
\begin{bmatrix} m - Y_{\dot{v}} & mx_G - Y_{\dot{r}} \\ mx_G - N_{\dot{v}} & I_{zz} - N_{\dot{r}} \end{bmatrix} \frac{d\vec{s}}{dt} &= \begin{bmatrix} Y_v & Y_r - mU \\ N_v & N_r - mx_G U \end{bmatrix} \vec{s} + \vec{F}, \text{ or} && (44)\\
M\dot{\vec{s}} &= P\vec{s} + \vec{F} \\
\dot{\vec{s}} &= M^{-1}P\vec{s} + M^{-1}\vec{F} \\
\dot{\vec{s}} &= A\vec{s} + B\vec{F}. && (45)
\end{aligned}$$

The matrix M is a mass or inertia matrix, which is always invertible. The last form of the equation is a standard one wherein A represents the internal dynamics of the system, and B is a gain matrix for the control and disturbance inputs.

4.3 Stability of the Sway/Yaw System

Consider the homogeneous system $\dot{\vec{s}} = A\vec{s}$:

$$\begin{aligned}
\dot{s}_1 &= A_{11}s_1 + A_{12}s_2 \\
\dot{s}_2 &= A_{21}s_1 + A_{22}s_2.
\end{aligned}$$

We can rewrite the second equation as

$$s_2 = \left(\frac{d(\cdot)}{dt} - A_{22} \right)^{-1} A_{21} s_1 \tag{46}$$

and substitute into the first equation to give

$$\ddot{s}_1 + (-A_{11} - A_{22})\dot{s}_1 + (A_{11}A_{22} - A_{12}A_{21})s_1 = 0. \tag{47}$$

Note that these operations are allowed because the derivative operator is linear; in the language of the Laplace transform, we would simply use s. A necessary and sufficient condition for stability of this ODE system is that each coefficient must be greater than zero:

$$\begin{aligned} -A_{11} - A_{22} &> 0 \\ A_{11}A_{22} - -A_{12}A_{21} &> 0 \end{aligned} \tag{48}$$

The components of A for the sway/yaw problem are

$$\begin{aligned} A_{11} &= \frac{(I_{zz} - N_{\dot{r}})Y_v + (Y_{\dot{r}} - mx_G)N_v}{(m - Y_{\dot{v}})(I_{zz} - N_{\dot{r}}) - (mx_G - Y_{\dot{r}})(mx_G - N_{\dot{v}})} \\ A_{12} &= \frac{-(I_{zz} - N_{\dot{r}})(mU - Y_r) - (Y_{\dot{r}} - mx_G)(mx_G U - N_r)}{(m - Y_{\dot{v}})(I_{zz} - N_{\dot{r}}) - (mx_G - Y_{\dot{r}})(mx_G - N_{\dot{v}})} \\ A_{21} &= \frac{(N_{\dot{v}} - mx_G)Y_v + (m - Y_{\dot{v}})N_v}{(m - Y_{\dot{v}})(I_{zz} - N_{\dot{r}}) - (mx_G - Y_{\dot{r}})(mx_G - N_{\dot{v}})} \\ A_{22} &= \frac{-(N_{\dot{v}} - mx_G)(mU - Y_r) - (m - Y_{\dot{v}})(mx_G U - N_r)}{(m - Y_{\dot{v}})(I_{zz} - N_{\dot{r}}) - (mx_G - Y_{\dot{r}})(mx_G - N_{\dot{v}})}. \end{aligned} \tag{49}$$

The denominators are identical, and can be simplified. First, let $x_G \simeq 0$; valid for many vessels with the origin is at the geometric center. If the origin is at the center of mass, $x_G = 0$. Next, if the vessel is reasonably balanced with regard to forward and aft areas with respect to the origin, the terms $\{N_{\dot{v}}, Y_{\dot{r}}, N_v, Y_r\}$ take very small values in comparison with the others. To wit, the added mass term $-Y_{\dot{v}}$ is of the order of the vessel's material mass m, and similarly $N_{\dot{r}} \simeq -I_{zz}$. Both $Y_{\dot{v}}$ and $N_{\dot{r}}$ take large negative values. Linear drag and rotational drag are significant also; these are the terms Y_v and N_r,

both large and negative. The denominator for A's components reduces to $(m - Y_{\dot{v}})(I_{zz} - N_{\dot{r}})$, and

$$\begin{aligned} A_{11} &= \tfrac{Y_v}{m - Y_{\dot{v}}} < 0 \\ A_{22} &= \tfrac{N_r}{I_{zz} - N_{\dot{r}}} < 0. \end{aligned}$$

Hence the first condition for stability is met: $-A_{11} - A_{22} > 0$. For the second condition, since the denominators of the A_{ij} are identical, we have only to look at the numerators. For stability, we require

$$\begin{aligned} (I_{zz} - N_{\dot{r}})Y_v(m - Y_{\dot{v}})N_r \\ - \left[N_{\dot{v}}Y_v + (m - Y_{\dot{v}})N_v\right]\left[-(I_{zz} - N_{\dot{r}})(mU - Y_r) + Y_{\dot{r}}N_r\right] > 0. \end{aligned} \tag{50}$$

The first term is the product of two large negative and two large positive numbers. The second part of the second term contains mU, which has a large positive value, generally making stability critical on the (usually negative) N_v. When only the largest terms are considered for a vessel, a simpler form is common:

$$C = Y_v N_r + N_v(mU - Y_r) > 0. \tag{51}$$

C is called the vessels *stability parameter*. The terms of C compete, and yaw/sway stability depends closely on the magnitude and sign of N_v. Adding more surface area aft drives N_v more positive, increasing stability as expected. Stability can also be improved by moving the center of gravity forward. Nonzero x_G shows up as follows:

$$C = Y_v(N_r - mx_G U) + N_v(mU - Y_r) > 0. \tag{52}$$

Since N_r and Y_v are both negative, positive x_G increases the (positive) influence of C's first term.

4.4 Basic Rudder Action in the Sway/Yaw Model

Rudders are devices which develop large lift forces due to an angle of attack with respect to the oncoming fluid. As in our discussion of lift on the body, the form is as follows: $L = \frac{1}{2}\rho A U^2 C_l(\alpha)$, where α is the angle of attack. The

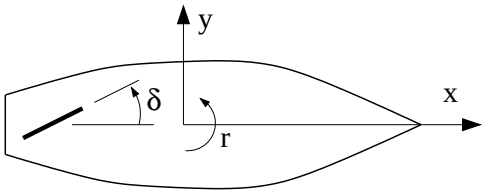

Figure 3: Convention for positive rudder angle in the vessel reference system.

lift coefficient C_l is normally linear with α near $\alpha = 0$, but the rudder stalls when the angle of attack reaches a critical value, and thereafter develops much less lift. We will assume that α is small enough that the linear relationship applies:

$$C_l(\alpha) = \left.\frac{\partial C_l}{\partial \alpha}\right|_{\alpha=0} \alpha. \tag{53}$$

Since the rudder develops force (and a small moment) far away from the body origin, say a distance l aft, the moment equation is quite simple. We have

$$Y_\alpha = \frac{1}{2}\rho A \left.\frac{\partial C_l}{\partial \alpha}\right|_{\alpha=0} U^2 \tag{54}$$

$$N_\alpha = -\frac{1}{2}\rho A \left.\frac{\partial C_l}{\partial \alpha}\right|_{\alpha=0} lU^2. \tag{55}$$

Note the difference between the rudder angle expressed in the body frame, δ, and the total angle of attack α. Angle of attack is influenced by δ, as well as v/U and lr. Thus, in tank testing with $v = 0$, $\delta = \alpha$ and $N_\delta = N_\alpha$, etc., but in real conditions, other hydrodynamic derivatives are augmented to capture the necessary effects, for example N_v and N_r. Generally speaking, the hydrodynamic characteristics of the vessel depend strongly on the rudder, even when $\delta = 0$. In this case the rudder still opposes yaw and sway perturbations and acts to stabilize the vessel.

A positive rudder deflection (defined to have the same sense as the yaw angle) causes a negative yaw perturbation, and a very small positive sway perturbation.

4.4.1 Adding Yaw Damping through Feedback

The stability coefficient C resulting from the addition of a control law $\delta = k_r r$, where $k_r > 0$ is a feedback gain, is

$$C = Y_v(N_r - mx_G U + k_r N_\delta) + N_v(mU - Y_r - k_r Y_\delta). \tag{56}$$

Y_δ is small positive, but N_δ is large and negative. Hence C becomes more positive, since Y_v is negative.

Control system limitations and the stalling of rudders make obvious the fact that even a very large control gain k_r cannot completely solve stability problems of a poorly-designed vessel with an inadequate rudder. On the other hand, a vessel which is overly stable ($C >> 0$ with no rudder action) is unmaneuverable. A properly-balanced vessel just achieves stability with zero rudder action, so that a reasonable amount of control will provide good maneuvering capabilities.

4.4.2 Heading Control in the Sway/Yaw Model

Considering just the yaw equation of motion, i.e., $v = 0$, with a rudder, we have

$$(I_{zz} - N_{\dot{r}})\ddot{\phi} + (mx_G U - N_r)\dot{\phi} = N_\delta \delta. \tag{57}$$

Employing the control law $\delta = k_\phi \phi$, the system equation becomes a homogeneous, second-order ODE:

$$(I_{zz} - N_{\dot{r}})\ddot{\phi} + (mx_G U - N_r)\dot{\phi} - N_\delta k_\phi \phi = 0. \tag{58}$$

Since all coefficients are positive (recall $N_\delta < 0$), the equation gives a stable θ response, settling under second-order dynamics to $\theta(\infty) = 0$. The control law $\delta = k_\phi(\phi - \phi_{desired}) + k_r r$ is the basis for heading autopilots, which are used to track $\phi_{desired}$. This use of an error signal to drive an actuator is in fact the essence of feedback control. In this case, we require *sensors* to obtain r and ϕ, a *controller* to calculate δ, and an *actuator* to implement the corrective action.

4.5 Response of the Vessel to Step Rudder Input

4.5.1 Phase 1: Accelerations Dominate

When the rudder first moves, acceleration terms dominate, since the velocities are zero. The equation looks like this:

$$\begin{bmatrix} m - Y_{\dot{v}} & mx_G - Y_{\dot{r}} \\ mx_G - N_{\dot{v}} & I_{zz} - N_{\dot{r}} \end{bmatrix} \begin{Bmatrix} \dot{v} \\ \dot{r} \end{Bmatrix} = \begin{Bmatrix} Y_\delta \\ N_\delta \end{Bmatrix} \delta. \tag{59}$$

Since $Y_{\dot{r}}$ and mx_G are comparatively small in the first row, we have

$$\dot{v}(0) = \frac{Y_\delta \delta}{m - Y_{\dot{v}}}, \tag{60}$$

and the vessel moves to the left, the positive v-direction. The initial yaw is in the negative r-direction, since $N_\delta < 0$:

$$\dot{r}(0) = \frac{N_\delta \delta}{I_{zz} - N_{\dot{r}}}. \tag{61}$$

The first phase is followed by a period (**Phase 2**), in which many terms are competing and contributing to the transient response.

4.5.2 Phase 3: Steady State

When the transients have decayed, the vessel is in a steady turning condition, and the accelerations are zero. The system equations reduce to

$$\begin{Bmatrix} v \\ r \end{Bmatrix} = \frac{\delta}{C} \begin{Bmatrix} (mx_G U - N_r)Y_\delta + (Y_r - mU)N_\delta \\ N_v Y_\delta - Y_v N_\delta \end{Bmatrix}. \tag{62}$$

Note that the denominator is the stability parameter. The steady turning rate is thus approximated by

$$r = -\frac{Y_v N_\delta}{C}\delta. \tag{63}$$

With $C > 0$, the steady-state yaw rate is negative. If the vessel is unstable ($C < 0$), it turns in the opposite direction than expected. This turning rate equation can also be used to estimate turning radius R:

$$R = \frac{U}{r} = \frac{UC}{-Y_v N_\delta \delta}. \tag{64}$$

The radius goes up directly with C, indicating that too stable a ship has poor turning performance. We see also that increasing the rudder area increases N_δ, decreasing R as desired. Increasing the deflection δ to reduce R works only to the point of stalling.

4.6 Summary of the Linear Maneuvering Model

We conclude our discussion of the yaw/sway model by noting that

1. The linearized sway/yaw dynamics of a surface vessel are strongly coupled, and they are independent of the longitudinal dynamics.

2. The design parameter C should be slightly greater than zero for easy turning, and " hands-off" stability. The case $C < 0$ should only be considered under active feedback control.

3. The analysis is valid only up to small angles of attack and turning rates. Very tight maneuvering requires the nonlinear inertial components and hydrodynamic terms. Among other effects, the nonlinear equations couple surge to the other motions, and the actual vessel loses forward speed during maneuvering.

4.7 Stability in the Vertical Plane

Stability in the horizontal plane changes very little as a function of speed, because drag and lift effects generally scale with U^2. This fact is *not* true in the vertical plane, for which the dimensional weight/buoyancy forces and moments are invariant with speed. For example, consider the case of heave and pitch, with $x_G = 0$ and no actuation:

$$m\left(\frac{\partial w}{\partial t} - Uq\right) = Z_{\dot{w}}\dot{w} + Z_w w + Z_{\dot{q}}\dot{q} + Z_q q + (B - W) \tag{65}$$

$$I_{yy}\frac{dq}{dt} = M_{\dot{w}}\dot{w} + M_w w + M_{\dot{q}}\dot{q} + M_q q - Bl_b \sin\theta. \tag{66}$$

The last term in each equation is a hydrostatic effect induced by opposing net buoyancy B and weight W. l_b denotes the vertical separation of the center of gravity and the center of buoyancy, creating the so-called righting moment which nearly all underwater vehicles possess. Because buoyancy effects do not

change with speed, the dynamic properties and hence stability of the vehicle may change with speed.

5 SIMILITUDE

5.1 Use of Nondimensional Groups

For a consistent description of physical processes, we require that all terms in an equation must have the same units. On the basis of physical laws, some quantities are dependent on other, independent quantities. We form nondimensional groups out of the dimensional ones in this section, and apply the technique to maneuvering.

The Buckingham π-theorem provides a basis for all nondimensionalization. Let a quantity Q_n be given as a function of a set of $n-1$ other quantities:

$$Q_n = f_Q(Q_1, Q_2, \cdots, Q_{n-1}). \tag{67}$$

There are n variables here, but suppose also that there are only k independent ones; k is equivalent to the number of physical unit types encountered. The theorem asserts that there are $n-k$ dimensionless groups π_i that can be formed, and the functional equivalence is reduced to

$$\pi_{n-k} = f_\pi(\pi_1, \pi_2, \cdots, \pi_{n-k-1}). \tag{68}$$

Example. Suppose we have a block of mass m resting on a frictionless horizontal surface. At time zero, a steady force of magnitude F is applied. We want to know $X(T)$, the distance that the block has moved as of time T. The dimensional function is $X(T) = f_Q(m, F, T)$, so $n = 4$. The (MKS) units are

$$\begin{aligned} [X(\cdot)] &= m \\ [m] &= kg \\ [F] &= kgm/s^2 \\ [T] &= s, \end{aligned}$$

and therefore $k = 3$. There is just one nondimensional group in this relationship; π_1 assumes only a constant (but unknown) value. Simple term-cancellation gives $\pi_1 = X(T)m/FT^2$, not far at all from the known result that $X(T) = FT^2/2m$!

Example. Consider the flow rate Q of water from an open bucket of height h, through a drain nozzle of diameter d. We have

$$Q = f_Q(h, d, \rho, \mu, g),$$

where the water density is ρ, and its absolute viscosity μ; g is the acceleration due to gravity. No other parameters affect the flow rate. We have $n = 6$, and the (MKS) units of these quantities are:

$$\begin{aligned} [Q] &= m^3/s \\ [h] &= m \\ [d] &= m \\ [\rho] &= kg/m^3 \\ [\mu] &= kg/ms \\ [g] &= m/s^2 \end{aligned}$$

There are only three units that appear: [length, time, mass], and thus $k = 3$. Hence, only three non-dimensional groups exist, and one is a unique function of the other two. To arrive at a set of valid groups, we must create three nondimensional quantities, making sure that each of the original (dimensional) quantities is represented. Intuition and additional manipulations come in handy, as we now show.

Three plausible first groups are: $\pi_1 = \rho Q/d\mu$, $\pi_2 = d\rho\sqrt{gh}/\mu$, and $\pi_3 = h/d$. Note that all six quantities appear at least once. Since h and d have the same units, they could easily change places in the first two groups. However, π_1 is recognized as a Reynolds number pertaining to the orifice flow. π_2 is more awkward, but products and fractions of groups are themselves valid groups, and we may construct $\pi_4 = \pi_1/\pi_2 = Q/d^2\sqrt{gh}$ to nondimensionalize Q with a pressure velocity, and then $\pi_5 = \pi_1/\pi_4 = \rho d\sqrt{gh}/\mu$ to establish an orifice Reynolds number independent of Q. We finally have the useful result

$$\pi_4 = f_\pi(\pi_5, \pi_2) \longrightarrow$$
$$\frac{Q}{d^2\sqrt{gh}} = f_\pi\left(\frac{\rho d\sqrt{gh}}{\mu}, \frac{h}{d}\right).$$

The uncertainty about where to use h and d, and the questionable importance of h/d as a group are remnants of the theorem. Intuition is that h/d is im-

material, and the other two terms have a nice physical meaning, e.g., π_5 is a Reynolds number.
The power of the π-theorem is primarily in reducing the number of parameters which must be considered independently to characterize a process. In the flow example, the theorem reduced the number of independent parameters from five to two, with no constraints about the actual physics taking place.

5.2 Common Groups in Marine Engineering

One frequently encounters the following groups in fluid mechanics and marine engineering:

1. Froude number:

$$Fr = \frac{U}{\sqrt{gL}}, \tag{69}$$

   where U is the speed of the vessel, g is the acceleration due to gravity, and L is the waterline length of the vessel. The Froude number appears in problems involving pressure boundary conditions, such as in waves on the ocean surface. Roughly speaking, it relates the vessel speed U to water wave speeds of wavelength L; the phase speed of a surface wave is $V = \sqrt{\lambda g/2\pi}$, where λ is the wavelength.

2. Cavitation number:

$$\delta = \frac{P_\infty - P_v}{\frac{1}{2}\rho U^2}, \tag{70}$$

   where P_∞ represents the ambient total pressure, P_v the vapor pressure of the fluid, and U the propeller inlet velocity. A low cavitation number means that the Bernoulli pressure loss across the lifting surface will cause the fluid to vaporize, causing bubbles, degradation of performance, and possible deterioration of the material.

3. Reynolds number:

$$Re = \frac{Ul}{\mu/\rho}, \tag{71}$$

where U is velocity, μ is absolute viscosity, and ρ is density. Since Re appears in many applications, l represents one of many length scales. Reynolds number is a ratio of fluid inertial pressures to viscous pressures: When Re is high, viscous effects are negligible. Re can be used to characterize pipe flow, bluff body wakes, and flow across a plate, among others.

4. Weber number:

$$W = \frac{\rho U^2 l}{\sigma}, \tag{72}$$

where σ is the surface tension of a fluid. Given that $[\sigma] = N/m$ (MKS), ρU^2 normalizes pressure, and l normalizes length. The Weber number indicates the importance of surface tension.

To appreciate the origins of these terms from a fluid particle's point of view, consider a box having side lengths $[dx, dy, dz]$. Various forces on the box scale as

$$\begin{aligned}
\text{(inertia)} \quad F_i &= \rho \frac{\partial v}{\partial t} dxdydz + \rho v \frac{\partial v}{\partial x} dxdydz \simeq \rho U^2 l^2 \\
\text{(gravity)} \quad F_g &= \rho g dxdydz \simeq \rho g l^3 \\
\text{(pressure)} \quad F_p &= P dxdy \simeq P l^2 \\
\text{(shear)} \quad F_s &= \mu \frac{\partial v}{\partial z} dxdy \simeq \mu U l \\
\text{(surface tension)} \quad F_\sigma &= \sigma dx \simeq \sigma l.
\end{aligned}$$

Thus the groups listed above can be written as

$$\begin{aligned}
Fr = \frac{F_i}{F_g} &\simeq \frac{U^2}{gl} \\
\delta = \frac{F_p}{F_i} &\simeq \frac{P}{\rho U^2} \\
Re = \frac{F_i}{F_s} &\simeq \frac{\rho U l}{\mu} \\
W = \frac{F_i}{F_\sigma} &\simeq \frac{\rho U^2 l}{\sigma}
\end{aligned}$$

When testing models, it is imperative to maintain as many of the nondimensional groups as possible of the full-scale system. This holds for the geometry of the body and the kinematics of the flow, the surface roughness, and the all of the relevant groups governing fluid dynamics. Consider the example of nozzle flow from a bucket. Suppose that we conduct a model test in which Re is abnormally large, i.e., the viscous effects are negligible. Under inviscid conditions, the flow rate is $Q = \pi d^2\sqrt{2gh}/4$. This rate cannot be achieved for lower-Re conditions because of fluid drag in the orifice, however.
In a vessel, we write the functional relationship for drag as a starting point:

$$\begin{aligned} C_r = \frac{D}{\frac{1}{2}\rho A U^2} &= f_Q(\rho, \mu, g, \sigma, U, l) \\ &= f_\pi(Re, Fr, W). \end{aligned}$$

First, since l is large, W is very large, and hence surface tension plays no role. Next, we look at $Re = Ul/\nu$ and $Fr = U/\sqrt{gl}$, both of which are important for surface vessels. Suppose that $l_{ship} = \lambda l_{model}$, so that usually $\lambda >> 1$; additionally, we set $g_{model} = g_{ship}$, i.e., the model and the true vessel operate in the same gravity field.
Froude number similitude requires $U_{model} = U_{ship}/\sqrt{\lambda}$. Then Reynolds number scaling implies directly $\nu_{model} = \nu_{ship}/\lambda^{3/2}$. Unfortunately, few fluids with this property are workable in a large testing tank. As a result, accurate scaling of Re for large vessels to model scale is quite difficult.
For surface vessels, and submarines near the surface, it is a routine procedure to employ turbulence stimulators to achieve flow that would normally occur with ship-scale Re. Above a critical value $Re \simeq 500,000$, C_f is not sensitive to Re. With this achieved, one then tries to match Fr closely.

5.3 Similitude in Maneuvering

The linear equations of motion for the horizontal yaw/sway problem are:

$$\begin{aligned} (m - Y_{\dot{v}})\dot{v} - Y_v v + (mU - Y_r)r + (mx_G - Y_{\dot{r}})\dot{r} &= Y \\ (I_{zz} - N_{\dot{r}})\dot{r} + (mx_G U - Nr)r + (mx_G - N_{\dot{v}})\dot{v} - N_v v &= N. \end{aligned}$$

These equations can be nondimensionalized in a standard way, by using the quantities $[U, L, \rho]$: these three values provide the necessary units of length,

time, and mass, and furthermore are readily accessible to the user. First, we create nondimensional states, denoted with a prime symbol:

$$\begin{aligned} \dot{v}' &= \frac{L}{U^2}\dot{v} \\ v' &= \frac{1}{U}v \\ \dot{r}' &= \frac{L^2}{U^2}\dot{r} \\ r' &= \frac{L}{U}r. \end{aligned} \tag{73}$$

We follow a similar procedure for the constant terms as follows, including a factor of 1/2 with ρ, for consistency with our previous expressions:

$$\begin{aligned} m' &= \frac{m}{\frac{1}{2}\rho L^3} \\ I'_{zz} &= \frac{I_{zz}}{\frac{1}{2}\rho L^5} \\ x'_G &= \frac{x_G}{L} \\ U' &= \frac{U}{U} = 1 \\ Y'_{\dot{v}} &= \frac{Y_{\dot{v}}}{\frac{1}{2}\rho L^3} \\ Y'_v &= \frac{Y_v}{\frac{1}{2}\rho U L^2} \\ Y'_{\dot{r}} &= \frac{Y_{\dot{r}}}{\frac{1}{2}\rho L^4} \\ Y'_r &= \frac{Y_r}{\frac{1}{2}\rho U L^3} \\ Y' &= \frac{Y}{\frac{1}{2}\rho U^2 L^2} \\ N'_{\dot{v}} &= \frac{N_{\dot{v}}}{\frac{1}{2}\rho L^4} \\ N'_v &= \frac{N_v}{\frac{1}{2}\rho U L^3} \end{aligned} \tag{74}$$

$$
\begin{aligned}
N'_{\dot{r}} &= \frac{N_{\dot{r}}}{\frac{1}{2}\rho L^5} \\
N'_{r} &= \frac{N_{r}}{\frac{1}{2}\rho U L^4} \\
N' &= \frac{N}{\frac{1}{2}\rho U^2 L^3}.
\end{aligned}
$$

Note that every force has been normalized with $\frac{1}{2}\rho U^2 L^2$, and every moment with $\frac{1}{2}\rho U^2 L^3$; time has been also nondimensionalized with L/U. Thus we arrive at a completely equivalent set of nondimensional system equations,

$$
\begin{aligned}
(m' - Y'_{\dot{v}})\dot{v}' - Y'_v v' + (m'U' - Y'_r)r' + (m'x'_G - Y'_{\dot{r}})\dot{r}' &= Y' \quad (75) \\
(I'_{zz} - N'_{\dot{r}})\dot{r}' + (m'x'_G U' - N'r')r' + (m'x'_G - N'_{\dot{v}})\dot{v}' - N'_v v' &= N'.
\end{aligned}
$$

Since fluid forces and moments generally scale with U^2, the nondimensionalized description holds for a range of velocities.

5.4 Roll Equation Similitude

Certain nondimensional coefficients may arise which depend explicitly on U, and therefore require special attention. Let us carry out a similar normalization of the simplified roll equation

$$
(I_{xx} - K_{\dot{p}})\dot{p} - K_p p - K_\psi \psi = K. \quad (76)
$$

For a surface vessel, the roll moment K_ψ is based on metacentric stability, and has the form $K_\psi = -\rho g \nabla (GM)$, where ∇ is the displaced fluid volume of the vessel, and GM is the metacentric height. The nondimensional terms are

$$
\begin{aligned}
I'_{xx} &= \frac{I_{xx}}{\frac{1}{2}\rho L^5} \quad (77) \\
K'_{\dot{p}} &= \frac{K_{\dot{p}}}{\frac{1}{2}\rho L^5} \\
K'_{p} &= \frac{K_{p}}{\frac{1}{2}\rho U L^4} \\
K'_{\psi} &= \frac{K_{\psi}}{\frac{1}{2}\rho U^2 L^3}
\end{aligned}
$$

$$\begin{aligned} \dot{p}' &= \frac{L^2}{U^2}\dot{p} \\ p' &= \frac{L}{U}p, \end{aligned}$$

leading to the equivalent system

$$(I'_{xx} - K'_{\dot{p}})\ddot{p}' - K'_p p' - \left(\frac{2gL}{U^2}\right)\nabla'(GM')\phi = K'. \tag{78}$$

Note that the roll angle ϕ was not nondimensionalized. The Froude number has a very strong influence on roll stability, since it appears explicitly in the nondimensional righting moment term, and also has a strong influence on K'_p. In the case of a submarine, the righting moment has the form $K_\psi = -Bh$, where B is the buoyant force, and h is the righting arm. The nondimensional coefficient becomes

$$K'_\psi = -\frac{Bh}{\frac{1}{2}\rho U^2 L^3}.$$

K'_ψ again depends strongly on U, since B and h are fixed; this K'_ψ needs to be maintained in model tests.

6 CAPTIVE MEASUREMENTS

Before making the decision to measure hydrodynamic derivatives, a preliminary search of the literature may turn up useful estimates. For example, test results for many hull-forms have already been published, and the basic lifting surface models are not difficult. The available computational approaches should be considered as well; these are very good for predicting added mass in particular. Finally, modern sensors and computer control systems make possible the estimation of certain coefficients based on open-water tests of a model or a full-scale design.

In model tests, the Froude number $Fr = \frac{U}{\sqrt{gL}}$, which scales the influence of surface waves, must be maintained between model and full-scale surface vessels. Reynolds number $Re = \frac{UL}{\nu}$, which scales the effect of viscosity, need not be matched as long as the scale model attains turbulent flow (supercritical Re). One can use turbulence stimulators near the bow if necessary. Since the control surface(s) and propeller(s) affect the coefficients, they should both be implemented in model testing.

6.1 Towtank

In a towtank, tow the vehicle at different angles of attack, measuring sway force and yaw moment. The slope of the curve at zero angle determines Y_v and N_v respectively; higher-order terms can be generated if the points deviate from a straight line. Rudder derivatives can be computed also by towing with various rudder angles.

6.2 Rotating Arm Device

On a rotating arm device, the vessel is fixed on an arm of length R, rotating at constant rate r: the vessel forward speed is $U = rR$. The idea is to measure the crossbody force and yaw moment as a function of r, giving the coefficients Y_r and N_r. Note that the lateral force also contains the component $(m - Y_{\dot{v}})r^2R$. The coefficients Y_v and N_v can also be obtained by running with a fixed angle of attack. Finally, the measurement is made over one rotation only, so that the vessel does not re-enter its own wake.

6.3 Planar-Motion Mechanism

With a planar motion mechanism, the vessel is towed at constant forward speed U, but is held by two posts, one forward and one aft, which can each impose independent sway motions, therefore producing variable yaw. The model moves in pure sway if $y_a(t) = y_b(t)$, in a pure yaw motion about the mid-length point if $y_a(t) = -y_b(t)$, or in a combination sway and yaw motion. The connection points are a distance l forward and aft from the vessel origin. Usually a sinusoidal motion is imposed:

$$\begin{aligned} y_a(t) &= a\cos\omega t \\ y_b(t) &= b\cos(\omega t + \psi), \end{aligned} \tag{79}$$

and the transverse forces on the posts are measured and approximated as

$$\begin{aligned} Y_a(t) &= F_a\cos(\omega t + \theta_a) \\ Y_b(t) &= F_b\cos(\omega t + \theta_b). \end{aligned} \tag{80}$$

If linearity holds, then

$$\begin{aligned} (m - Y_{\dot v})\dot v - Y_v v + (mU - Y_r)r + (mx_G - Y_{\dot r})\dot r &= Y_a + Y_b \\ (I_{zz} - N_{\dot r})\dot r + (mx_G U - N_r)r + (mx_G - N_{\dot v})\dot v - N_v v &= (Y_b - Y_a)l. \end{aligned} \tag{81}$$

We have $v = (\dot y_a + \dot y_a)/2$ and $r = (\dot y_b - \dot y_a)/2l$. When $a = b$, these become

$$\begin{aligned} v &= -\frac{a\omega}{2}\left(\sin\omega t(1+\cos\psi) + \cos\omega t\sin\psi\right) \\ \dot v &= -\frac{a\omega^2}{2}\left(\cos\omega t(1+\cos\psi) - sin\omega t\sin\psi\right) \\ r &= -\frac{a\omega}{2l}\left(\sin\omega t(\cos\psi - 1) + \cos\omega t\sin\psi\right) \\ \dot r &= -\frac{a\omega^2}{2l}\left(\cos\omega t(\cos\psi - 1) - \sin\omega t\sin\psi\right). \end{aligned} \tag{82}$$

Equating the sine terms and then the cosine terms, we obtain four independent equations:

$$
\begin{aligned}
(m - Y_{\dot{v}}) \left(-\frac{a\omega^2}{2}\right) (1 + \cos\psi) - \\
Y_v \left(-\frac{a\omega}{2}\right) \sin\psi + \\
(mU - Y_r) \left(-\frac{a\omega}{2l}\right) \sin\psi + \\
(mx_G - Y_{\dot{r}}) \left(-\frac{a\omega^2}{2l}\right) (\cos\psi - 1) &= F_a \cos\theta_a + F_b \cos\theta_b
\end{aligned} \tag{83}
$$

$$
\begin{aligned}
(m - Y_{\dot{v}}) \left(-\frac{a\omega^2}{2}\right) (-\sin\psi) - \\
Y_v \left(-\frac{a\omega}{2}\right) (1 + \cos\psi) + \\
(mU - Y_r) \left(-\frac{a\omega}{2l}\right) (\cos\psi - 1) + \\
(mx_G - Y_{\dot{r}}) \left(-\frac{a\omega^2}{2l}\right) (-\sin\psi) &= -F_a \sin\theta_a - F_b \sin\theta_b
\end{aligned} \tag{84}
$$

$$
\begin{aligned}
(I_{zz} - N_{\dot{r}}) \left(-\frac{a\omega^2}{2l}\right) (\cos\psi - 1) + \\
(mx_G U - N_r) \left(-\frac{a\omega}{2l}\right) \sin\psi + \\
(mx_G - N_{\dot{v}}) \left(-\frac{a\omega^2}{2}\right) (1 + \cos\psi) - \\
N_v \left(-\frac{a\omega}{2}\right) \sin\psi &= l(F_b \cos\theta_b - F_a \cos\theta_a)
\end{aligned} \tag{85}
$$

$$
\begin{aligned}
(I_{zz} - N_{\dot{r}}) \left(-\frac{a\omega^2}{2l}\right) (-\sin\psi) + \\
(mx_G U - N_r) \left(-\frac{a\omega}{2l}\right) (\cos\psi - 1) + \\
(mx_G - N_{\dot{v}}) \left(-\frac{a\omega^2}{2}\right) (-\sin\psi) - \\
N_v \left(-\frac{a\omega}{2}\right) (1 + \cos\psi) &= l(-F_b \sin\theta_b + F_a \sin\theta_a)
\end{aligned} \tag{86}
$$

In this set of four equations, we know from the imposed motion the values $[U, \psi, a, \omega]$. From the experiment, we obtain $[F_a, F_b, \theta_a, \theta_b]$, and from the rigid-body model we have $[m, I_{zz}, x_G]$. It turns out that the two cases of $\psi = 0$ (pure sway motion) and $\psi = 180^o$ (pure yaw motion) yield a total of eight independent equations, exactly what is required to find the eight coefficients $[Y_{\dot{v}}, Y_v, Y_{\dot{r}}, Y_r, N_{\dot{v}}, N_v, N_{\dot{r}}, N_r]$. Remarkably, we can write the eight solutions directly: For $\psi = 0$,

$$\begin{aligned}
(m - Y_{\dot{v}})\left(-\frac{a\omega^2}{2}\right)(2) &= F_a \cos\theta_a + F_b \cos\theta_b \\
-Y_v\left(-\frac{a\omega}{2}\right)(2) &= -F_a \sin\theta_a - F_b \sin\theta_b \\
(mx_G - N_{\dot{v}})\left(-\frac{a\omega^2}{2}\right)(2) &= l(F_b \cos\theta_b - F_a \cos\theta_a) \\
-N_v\left(-\frac{a\omega}{2}\right)(2) &= l(-F_b \sin\theta_b + F_a \sin\theta_a),
\end{aligned} \tag{87}$$

to be solved respectively for $[Y_{\dot{v}}, Y_v, N_{\dot{v}}, N_v]$. For $\psi = 180^o$, we have

$$\begin{aligned}
(mx_G - Y_{\dot{r}})\left(-\frac{a\omega^2}{2l}\right)(-2) &= F_a \cos\theta_a + F_b \cos\theta_b \\
(mU - Y_r)\left(-\frac{a\omega}{2l}\right)(-2) &= -F_a \sin\theta_a - F_b \sin\theta_b \\
(I_{zz} - N_{\dot{r}})\left(-\frac{a\omega^2}{2l}\right)(-2) &= l(F_b \cos\theta_b - F_a \cos\theta_a) \\
(mx_G U - N_r)\left(-\frac{a\omega}{2l}\right)(-2) &= l(-F_b \sin\theta_b + F_a \sin\theta_a),
\end{aligned} \tag{88}$$

to be solved for $[Y_{\dot{r}}, Y_r, N_{\dot{r}}, N_r]$. Thus, the eight linear coefficients for a surface vessel maneuvering, for a given speed, can be deduced from two tests with a planar motion mechanism. We note that the nonlinear terms will play a significant role if the motions are too large, and that some curve fitting will be needed in any event. The PMM can be driven with more complex trajectories which will target specific nonlinear terms.

7 STANDARD MANEUVERING TESTS

This section describes some of the typical maneuvering tests which are performed on full-scale vessels, to assess stability and performance.

7.1 Dieudonné Spiral

1. Achieve steady speed and direction for one minute. No changes in speed setting are made after this point.
2. Turn rudder quickly by 15°, and keep it there until steady yaw rate is maintained for one minute.
3. Reduce rudder angle by 5°, and keep it there until steady yaw rate is maintained for one minute.
4. Repeat in decrements of -5°, to -15°.
5. Proceed back up to 15°.

The Dieudonné maneuver has the vessel path following a growing spiral, and then a contracting spiral in the opposite direction. The test reveals if the vessel has a memory effect, manifested as a hysteresis in yaw rate r. For example, suppose that the first 15° rudder deflection causes the vessel to turn right, but that the yaw rate at zero rudder, on the way negative, is still to the right. The vessel has gotten "stuck" here, and will require a negative rudder action to pull out of the turn. But if the corrective action causes the vessel to turn left at all, the same memory effect may occur. It is easy to see that the rudder in this case has to be used excessively driving the vessel back and forth. We say that the vessel is unstable, and clearly a poor design.

7.2 Zig-Zag Maneuver

1. With zero rudder, achieve steady speed for one minute.
2. Deflect the rudder to 20°, and hold until the vessel turns 20°.
3. Deflect the rudder to -20°, and hold until the vessel turns to -20∘ with respect to the starting heading.
4. Repeat.

This maneuver establishes several important characteristics of the yaw response. These are: the response time (time to reach a given heading), the yaw overshoot (amount the vessel exceeds $\pm 20^\circ$ when the rudder has turned the other way), and the total period for the 20° oscillations. Of course, similar tests can be made with different rudder angles and different threshold vessel headings.

7.3 Circle Maneuver

From a steady speed, zero yaw rate condition, the rudder is moved to a new setting. The vessel responds by turning in a circle. After steady state is reached again, parameters of interest are the turning diameter, the drift angle β, the speed loss, and the angle of heel ψ.

7.3.1 Drift Angle

The drift angle is the equivalent to angle of attack for lifting surfaces, and describes how the vessel "skids" during a turn. If the turning circle has radius R (measured from the vessel origin), then the speed *tangential* to the circle is $U = rR$. The vessel-reference velocity components are thus $u = U\cos\beta$ and $v = -U\sin\beta$. A line along the vessel centerline reaches closest to the true center of the turning circle at a point termed the *turning center*. At this location, which may or may not exist on the physical vessel, there is no apparent lateral velocity, and it appears to an observer there that the vessel turns about this point.

7.3.2 Speed Loss

Speed loss occurs primarily because of drag induced by the drift angle. A vessel which drifts very little may have very little speed loss.

7.3.3 Heel Angle

Heel during turning occurs as a result of the intrinsic coupling of sway, yaw, and roll caused by the center of gravity. In a surface vessel, the fluid forces act below the waterline, but the center of gravity is near the waterline or above. When the rudder is first deflected, inertial terms dominate (Phase 1) and the sway equation is

$$(m - Y_{\dot{v}})\dot{v} - (Y_{\dot{r}} - mx_G)\dot{r} = Y_\delta \delta. \tag{89}$$

The coefficients for $\dot{r}$ are quite small, and thus the vessel first rolls to starboard (positive) for a positive rudder action.
When steady turning conditions are reached (Phase 3), hydrodynamic forces equalize the centrifugal force mUr and the rudder force $Y_\delta \delta$. The sway equation is

$$-Y_v v + (mU - Y_r)r = Y_\delta \delta, \tag{90}$$

with Y_r small, $v < 0$ when $r > 0$ for most vessels, and $|Y_v v| > |Y_\delta \delta|$. Because the centrifugal force acts above the waterline, the vessel ultimately rolls to port (negative) for a positive rudder action.
The transition between the inertially-dominated and steady-turning regimes includes an overshoot: in the above formulas, the vessel overshoots the final port roll angle as the vessel slows. From the sway equation, we see that if the rudder is straightened out at this point, the roll will momentarily be even worse!
In summary, the vessel rolls into the turn initially, but then out of the turn in the steady state.

7.3.4 Heeling in Submarines with Sails

Submarines typically roll into a turn during all phases. Unlike surface vessels, which have the rigid mass center above the center of fluid forcing, submarines have the mass center below the rudder action point, and additionally feel the effects of a large sail above both. The inertial equation

$$(m - Y_{\dot{v}})\dot{v} - (Y_{\dot{r}} - mx_G)\dot{r} = Y_\delta \delta \tag{91}$$

is dominated by $m\dot{v}$ (acting low), $-Y_{\dot{v}}\dot{v}$ (acting high), and $Y_\delta \delta$ (intermediate). Because $|Y_{\dot{v}}| > m$, the vessel rolls under the sail, the keel out of the turn. In the steady state,

$$-Y_v v + (mU - Y_r)r = Y_\delta \delta. \tag{92}$$

The drift angle β keeps the Y_v-force, acting high, toward the center of the turn, and again centrifugal force mUr causes the bottom of the submarine to move out of the turn. Hence, the roll angle of a submarine with a sail is always into

the turn, both initially and in the steady state. The heel angle declines as the speed of the submarine drops.

8 STREAMLINED BODIES

8.1 Nominal Drag Force

A symmetric streamlined body at zero angle of attack experiences only a drag force, which has the form

$$F_A = -\frac{1}{2}\rho C_A A_o U^2. \tag{93}$$

The drag coefficient C_A has both pressure and skin friction components, and hence area A_o is usually that of the wetted surface. Note that the A-subscript will be used to denote zero angle of attack conditions; also, the sign of F_A is negative, because it opposes the vehicle's x-axis.

8.2 Munk Moment

Any shape other than a sphere generates a moment when inclined in an inviscid flow. d'Alembert's paradox predicts zero net *force*, but not necessarily a zero moment. This *Munk moment* arises for a simple reason, the asymmetric location of the stagnation points, where pressure is highest on the front of the body (decelerating flow) and lowest on the back (accelerating flow). The Munk moment is always destabilizing, in the sense that it acts to turn the vehicle perpendicular to the flow.

Consider a symmetric body with added mass components A_{xx} along the vehicle (slender) x-axis (forward), and A_{zz} along the vehicle's z-axis z (up). We will limit the present discussion to the vertical plane, but similar arguments can be used to describe the horizontal plane. Let α represent the angle of attack, taken to be positive with the nose up – this equates to a negative pitch angle ϕ in vehicle coordinates, if it is moving horizontally. The Munk moment is:

$$\begin{aligned} M_m &= -\frac{1}{2}(A_{zz} - A_{xx})U^2 \sin 2\alpha \\ &\simeq -(A_{zz} - A_{xx})U^2\alpha. \end{aligned} \tag{94}$$

$A_{zz} > A_{xx}$ for a slender body, and the negative sign indicates a negative pitch with respect to the vehicle's pitch axis. The added mass terms A_{zz} and A_{xx} can be estimated from analytical expressions (available only for regular shapes such as ellipsoids), from numerical calculation, or from slender body approximation (to follow).

8.3 Separation Moment

In a viscous fluid, flow over a streamlined body is similar to that of potential flow, with the exceptions of the boundary layer, and a small region near the trailing end. In this latter area, a helical vortex may form and convect downstream. Since vortices correlate with low pressure, the effect of such a vortex is stabilizing, but it also induces drag. The formation of the vortex depends on the angle of attack, and it may cover a larger area (increasing the stabilizing moment and drag) for a larger angle of attack. For a small angle of attack, the transverse force F_n can be written in the same form as for control surfaces:

$$\begin{aligned} F_n &= \frac{1}{2}\rho C_n A_o U^2 \\ &\simeq \frac{1}{2}\rho \frac{\partial C_n}{\partial \alpha}\alpha A_o U^2. \end{aligned} \tag{95}$$

With a positive angle of attack, this force is in the positive z-direction. The zero-α drag force F_A is modified by the vortex shedding:

$$\begin{aligned} F_a &= -\frac{1}{2}\rho C_a A_o U^2 \text{ , where} \\ C_a &= C_A \cos^2\phi. \end{aligned} \tag{96}$$

The last relation is based on writing $C_A(U\cos\phi)^2$ as $(C_A\cos^2\phi)U^2$, i.e., a decomposition using apparent velocity.

8.4 Net Effects: Aerodynamic Center

The Munk moment and the moment induced by separation are competing, and their magnitudes determine the stability of a hullform. First we simplify:

$$\begin{aligned} F_a &= -\gamma_a \\ F_n &= \gamma_n \alpha \\ M_m &= -\gamma_m \alpha. \end{aligned}$$

Each constant γ is taken as positive, and the signs reflect orientation in the vehicle reference frame, with a nose-up angle of attack. The Munk moment is a

pure couple which does not depend on a reference point. We pick a temporary origin O for F_n however, and write the total pitch moment about O as:

$$\begin{aligned} M &= M_m + F_n l_n \\ &= (-\gamma_m + \gamma_n l_n)\alpha. \end{aligned} \tag{97}$$

where l_n denotes the (positive) distance between O and the application point of F_n. The net moment about O is zero if we select

$$l_n = \frac{\gamma_m}{\gamma_n}, \tag{98}$$

and the location of O is then called the aerodynamic center or AC.
The point AC has an intuitive explanation: it is the location on the hull where F_n would act to create the total moment. Hence, if the vehicle's origin lies in front of AC, the net moment is stabilizing. If the origin lies behind AC, the moment is destabilizing. For self-propelled vehicles, the mass center must be forward of AC for stability. Similarly, for towed vehicles, the towpoint must be located forward of AC. In many cases with very streamlined bodies, the aerodynamic center is significantly *ahead* of the nose, and in this case, a rigid sting would have to extend at least to AC in order for stable towing. As a final note, since the Munk moment persists even in inviscid flow, AC moves infinitely far forward as viscosity effects diminish.

8.5 Role of Fins in Moving the Aerodynamic Center

Control surfaces or fixed fins are often attached to the stern of a slender vehicle to enhance directional stability. Fixed surfaces induce lift and drag on the body:

$$\begin{aligned} L = \frac{1}{2}\rho A_f U^2 C_l(\alpha) &\simeq \gamma_L \alpha \\ D = -\frac{1}{2}\rho A_f U^2 C_d &\simeq -\gamma_D \text{ (constant)} \end{aligned} \tag{99}$$

These forces act somewhere on the fin, and are signed again to match the vehicle frame, with $\gamma > 0$ and $\alpha > 0$. The summed forces on the body are thus:

$$\begin{aligned} X &= F_a - |D|\cos\alpha + |L|\sin\alpha \\ &\simeq -\gamma_a - \gamma_D + \gamma_L\alpha^2 \\ Z &= F_n + |L|\cos\alpha + |D|\sin\alpha \\ &\simeq \gamma_n\alpha + \gamma_L\alpha + \gamma_D\alpha. \end{aligned} \tag{100}$$

All of the forces are pushing the vehicle up. If we say that the fins act a distance l_f behind the temporary origin O, and that the moment carried by the fins themselves is very small (compared to the moment induced by Ll_f) the total moment is as follows:

$$M = (-\gamma_m + \gamma_n l_n)\alpha + (\gamma_L + \gamma_D)l_f\alpha. \tag{101}$$

The moment about O vanishes if

$$\gamma_m = \gamma_n l_n + l_f(\gamma_L + \gamma_D). \tag{102}$$

The Munk moment γ_m opposes the aggregate effects of vorticity lift γ_n and the fins' lift and drag $\gamma_L + \gamma_D$. With very large fins, this latter term is large, so that l_f might be very small; this is the case of AC moving aft toward the fins. A vehicle with excessively large fins will be difficult to turn and maneuver.
Equation 102 contains two length measurements, referenced to an arbitrary body point O. To solve it explicitly, let l_{fn} denote the (positive) distance that the fins are located behind F_n; this is likely a small number, since both effects usually act near the stern. We solve for l_f:

$$l_f = \frac{\gamma_m + \gamma_n l_{fn}}{\gamma_n + \gamma_L + \gamma_D}. \tag{103}$$

This is the distance that AC is located forward of the fins, and thus AC can be referenced to any other fixed point easily. Without fins, it can be recalled that

$$l_n = \frac{\gamma_m}{\gamma_n}.$$

Hence, the fins act directly in the denominator to shorten l_f. Note that if the fins are located forward of the vortex shedding force F_n, i.e., $l_{fn} < 0$, l_f is reduced, but since AC is referenced to the fins, there is no net gain in stability.

8.6 Aggregate Effects of Body and Fins

Since all of the terms discussed so far have the same dependence on α, it is possible to group them into a condensed form. Setting $\hat{F}_a$ and $\hat{F}_n$ to account for the fuselage and fins, we have

$$\begin{aligned} X &= \hat{F}_a \simeq -\frac{1}{2}\rho \hat{C}_a \hat{A}_o U^2 \\ Z &= \hat{F}_n \simeq \frac{1}{2}\rho \hat{C}'_n \hat{A}_o U^2 \alpha \\ M &= -\hat{F}_n x_{AC} \simeq -\frac{1}{2}\hat{C}'_n \hat{A}_o U^2 x_{AC} \alpha. \end{aligned} \tag{104}$$

8.7 Coefficients Z_w, M_w, Z_q, and M_q for a Slender Body

The angle of attack α is related to the cross-body velocity w as follows:

$$\begin{aligned} \alpha &= -\tan^{-1}\left(\frac{w}{u}\right) \\ &\simeq -\frac{w}{U} \text{ for } U >> w. \end{aligned} \tag{105}$$

We can then write several linear hydrodynamic coefficients easily:

$$\begin{aligned} Z_w &= -\frac{1}{2}\rho \hat{C}'_n \hat{A}_o U \\ M_w &= \frac{1}{2}\rho \hat{C}'_n \hat{A}_o U x_{AC}. \end{aligned} \tag{106}$$

The rotation of the vessel involves complex flow, which depends on both w and q, as well as their derivatives. To start, we consider the contribution of the fins only – slender body theory, introduced shortly, provides good results for the hull. The fin center of pressure is located a distance l_f aft of the body origin, and we assume that the vehicle is moving horizontally, with an instantaneous pitch angle of θ. The angle of attack seen by the fin is a combination of a part due to θ and a part linear with q:

$$\alpha_f \simeq -\theta + \frac{l_f q}{U} \tag{107}$$

and so lateral force and moment derivatives (for the fin alone) emerge as

$$\begin{aligned} Z_q &= -\frac{1}{2}\rho C_l' A_f U l_f \\ M_q &= -\frac{1}{2}\rho C_l' A_f U l_f^2. \end{aligned} \tag{108}$$

9 SLENDER-BODY THEORY

9.1 Introduction

Consider a slender body with $d << L$, that is mostly straight. The body could be asymmetric in cross-section, or even flexible, but we require that the lateral variations are small and smooth along the length. The idea of the slender-body theory, under these assumptions, is to think of the body as a longitudinal stack of thin sections, each having an easily-computed added mass. The effects are integrated along the length to approximate lift force and moment. Slender-body theory is accurate for small ratios d/L, except near the ends of the body.

As one example, if the diameter of a body of revolution is $d(s)$, then we can compute $\delta m_a(x)$, where the nominal added mass value for a cylinder is

$$\delta m_a = \rho \frac{\pi}{4} d^2 \delta x. \tag{109}$$

The added mass is equal to the mass of the water displaced by the cylinder. The equation above turns out to be a good approximation for a number of two-dimensional shapes, including flat plates and ellipses, if d is taken as the width dimension presented to the flow. Many formulas for added mass of two-dimensional sections, as well as for simple three-dimensional bodies, can be found in the books by Newman and Blevins.

9.2 Kinematics Following the Fluid

The added mass forces and moments derive from accelerations that a fluid particles experience when they encounter the body. We use the notion of a fluid derivative for this purpose: the operator d/dt indicates a derivative taken in the frame of the passing particle, not the vehicle. Hence, this usage has an indirect connection with the derivative described in our previous discussion of rigid-body dynamics.

For the purposes of explaining the theory, we will consider the two-dimensional heave/surge problem only. The local geometry is described by the location of the centerline; it has vertical location (in body coordinates) of $z_b(x,t)$, and local angle $\alpha(x,t)$. The time-dependence indicates that the configuration is free to change with time, i.e., the body is flexible. Note that the curvilinear coordinate s is nearly equal to the body-reference (linear) coordinate x.

The velocity of a fluid particle *normal* to the body at x is $w_n(t,x)$:

$$w_n = \frac{\partial z_b}{\partial t}\cos\alpha - U\sin\alpha. \tag{110}$$

The first component is the time derivative in the body frame, and the second due to the deflection of the particle by the inclined body. If the body reference frame is rotated to the flow, that is, if $w \neq 0$, then $\partial z_b/\partial t$ will contain w. For small angles, $\sin\alpha \simeq \tan\alpha = \partial z_b/\partial x$, and we can write

$$w_n \simeq \frac{\partial z_b}{\partial t} - U\frac{\partial z_b}{\partial x}.$$

The fluid derivative operator in action is as follows:

$$w_n = \frac{dz_b}{dt} = \left(\frac{\partial}{\partial t} - U\frac{\partial}{\partial x}\right) z_b.$$

9.3 Derivative Following the Fluid

A more formal derivation for the fluid derivative operator is quite simple. Let $\mu(x,t)$ represent some property of a fluid particle.

$$\begin{aligned}\frac{d}{dt}\left[\mu(x,t)\right] &= \lim_{\delta t\to 0}\frac{1}{\delta t}\left[\mu(x+\delta x, t+\delta t) - \mu(x,t)\right] \\ &= \left[\frac{\partial\mu}{\partial t} - U\frac{\partial\mu}{\partial x}\right].\end{aligned}$$

The second equality can be verified using a Taylor series expansion of $\mu(x+\delta x, t+\delta t)$:

$$\mu(x+\delta x, t+\delta t) = \mu(x,t) + \frac{\partial\mu}{\partial t}\delta t + \frac{\partial\mu}{\partial x}\delta x + h.o.t.,$$

and noting that $\delta x = -U\delta t$. The fluid is convected downstream with respect to the body.

9.4 Differential Force on the Body

If the local transverse velocity is $w_n(x,t)$, then the differential inertial force on the body here is the derivative (following the fluid) of the momentum:

$$\delta F = -\frac{d}{dt}\left[m_a(x,t)w_n(x,t)\right]\delta x. \tag{111}$$

Note that we could here let the added mass vary with time also – this is the case of a changing cross-section! The lateral velocity of the point $z_b(x)$ in the body-reference frame is

$$\frac{\partial z_b}{\partial t} = w - xq, \tag{112}$$

such that

$$w_n = w - xq - U\alpha. \tag{113}$$

Taking the derivative, we have

$$\frac{\delta F}{\delta x} = -\left(\frac{\partial}{\partial t} - U\frac{\partial}{\partial x}\right)\left[m_a(x,t)(w(t) - xq(t) - U\alpha(x,t))\right].$$

We now restrict ourselves to a rigid body, so that neither m_a nor α may change with time.

$$\frac{\delta F}{\delta x} = m_a(x)(-\dot{w} + x\dot{q}) + U\frac{\partial}{\partial x}\left[m_a(x)(w - xq - U\alpha)\right]. \tag{114}$$

9.5 Total Force on a Vessel

The net lift force on the body, computed with strip theory is

$$Z = \int_{x_T}^{x_N} \delta F dx \tag{115}$$

where x_T represents the coordinate of the tail, and x_N is the coordinate of the nose. Expanding, we have

$$\begin{aligned} Z &= \int_{x_T}^{x_N} m_a(x)\left[-\dot{w} + x\dot{q}\right] dx + U\int_{x_T}^{x_N} \frac{\partial}{\partial x}\left[m_a(x)(w - xq - U\alpha)\right] dx \\ &= -m_{33}\dot{w} - m_{35}\dot{q} + U m_a(x)(w - xq - U\alpha)|_{x=x_T}^{x=x_N}. \end{aligned}$$

We made use here of the added mass definitions

$$\begin{aligned} m_{33} &= \int_{x_T}^{x_N} m_a(x)dx \\ m_{35} &= -\int_{x_T}^{x_N} x m_a(x)dx. \end{aligned}$$

Additionally, for vessels with pointed noses and flat tails, the added mass m_a at the nose is zero, so that a simpler form occurs:

$$Z = -m_{33}\dot{w} - m_{35}\dot{q} - U m_a(x_T)(w - x_T q - U\alpha(x_T)). \tag{116}$$

In terms of the linear hydrodynamic derivatives, the strip theory thus provides

$$\begin{aligned} Z_{\dot{w}} &= -m_{33} \\ Z_{\dot{q}} &= -m_{35} \\ Z_w &= -U m_a(x_T) \\ Z_q &= U x_T m_a(x_T) \\ Z_{\alpha(x_T)} &= U^2 m_a(x_T). \end{aligned}$$

It is interesting to note that both Z_w and $Z_{\alpha(x_T)}$ depend on a nonzero base area. In general, however, potential flow estimates do not create lift (or drag) forces for a smooth body, so this should come as no surprise. The two terms are clearly related, since their difference depends only on how the body coordinate system is oriented to the flow. Another noteworthy fact is that the lift force depends only on α at the tail; α could take any value(s) along the body, with no effect on Z.

9.6 Total Moment on a Vessel

A similar procedure can be applied to the moment predictions from slender body theory (again for small α):

$$\begin{aligned} M &= -\int_{x_T}^{x_N} x\delta F dx \\ &= \int_{x_T}^{x_N} x\left(\frac{\partial}{\partial t} - U\frac{\partial}{\partial x}\right)\left[m_a(x)(w - xq - U\alpha)\right] dx \\ &= \int_{x_T}^{x_N} x m_a(x)(\dot{w} - x\dot{q}) dx - U\int_{x_T}^{x_N} x\frac{\partial}{\partial x}\left[m_a(x)(w - xq + U\alpha)\right] dx. \end{aligned}$$

Then we make the further definition

$$m_{55} = \int_{x_T}^{x_N} x^2 m_a(x) dx,$$

(note that $m_{35} = m_{53}$) and use integration by parts to obtain

$$\begin{aligned} M &= -m_{35}\dot{w} - m_{55}\dot{q} - U x m_a(x)(w - xq - U\alpha)|_{x=x_T}^{x=x_N} + \\ &\quad U\int_{x_T}^{x_N} m_a(x)(w - xq - U\alpha) dx. \end{aligned}$$

The integral above contains the product $m_a(x)\alpha(x)$, which must be calculated if α changes along the length. For simplicity, we now assume that α is in fact constant on the length, leading to

$$\begin{aligned} M &= -m_{35}\dot{w} - m_{55}\dot{q} + U x_T m_a(x_T)(w - x_T q - U\alpha) + \\ &\quad U m_{33} w + U m_{35} q - U^2 m_{33}\alpha. \end{aligned}$$

Finally, the linear hydrodynamic moment derivatives are

$$\begin{aligned} M_{\dot{w}} &= -m_{35} \\ M_{\dot{q}} &= -m_{55} \\ M_w &= U x_T m_a(x_T) + U m_{33} \\ M_q &= -U x_T^2 m_a(x_T) + U m_{35} \\ M_\alpha &= -U^2 x_T m_a(x_T) - U^2 m_{33}. \end{aligned}$$

The derivative M_w is closely-related to the Munk moment, whose linearization would provide $M_w = (m_{33} - m_{11})U$. The Munk moment (an exact result) may therefore be used to make a correction to the second term in the slender-body approximation above of M_w. As with the lift force, M_w and M_α are closely related, depending only on the orientation of the body frame to the flow.

9.7 Relation to Wing Lift

There is an important connection between the slender body theory terms involving added mass at the tail ($m_a(x_T)$), and low aspect-ratio wing theory. The lift force from the latter is of the form $L = -\frac{1}{2}\rho U A C_l' w$, where $A = cs$, the product of chord (long) and span (short).
The lift coefficient slope is approximated by (Hoerner)

$$C_l' \approx \frac{1}{2}\pi(AR), \tag{117}$$

where (AR) is the aspect ratio. Inserting this approximation into the lift formula, we obtain

$$L = -\frac{\pi}{4}\rho s^2 U w. \tag{118}$$

Now we look at a slender body approximation of the same force: The added mass at the tail is $m_a(x_T) = \rho s^2 \pi/4$, and using the slender-body estimate for Z_w, we calculate for lift:

$$\begin{aligned} Z &= -m_a(x_T) U w \\ &= -\frac{\pi}{4}\rho s^2 U w. \end{aligned}$$

Slender-body theory is thus able to recover exactly the lift of a low-aspect ratio wing. Where does the slender-body predict the force will act? Recalling that $M_w = U m_{33} + U x_T m_a(x_T)$, and since $m_{33} = 0$ for a front-back symmetric wing, the estimated lift force acts at the trailing edge. This location will tend to stabilize the wing, in the sense that it acts to orient the wing parallel to the incoming flow.

9.8 Convention: Hydrodynamic Mass Matrix A

Hydrodynamic derivatives that depend on accelerations are often written as components of a mass matrix A. By listing the body-referenced velocities in the order $\vec{s} = [u, v, w, p, q, r]$, we write $(M + A)\dot{\vec{s}} = \vec{F}$, where M is the mass matrix of the *material* vessel and F is a generalized force. Therefore $A_{33} = -Z_{\dot{w}}$, $A_{5,3} = -M_{\dot{w}}$, and so on.

10 PRACTICAL LIFT CALCULATIONS

10.1 Characteristics of Lift-Producing Mechanisms

At a small angle of attack, a slender body experiences transverse force due to: helical body vortices, the blunt trailing end, and fins. The helical body vortices are stable and symmetric in this condition, and are convected continuously into the wake. The low pressure associated with the vortices provides the suction force, usually toward the stern of the vehicle. The blunt trailing end induces lift as a product of added mass effects, and can be accurately modeled with slender body theory. A blunt trailing edge also induces some drag, which itself is stabilizing. The fins can often be properly modeled using experimental data parametrized with aspect ratio and several other geometric quantities.

As the angle of attack becomes larger, the approximations in the fin and slender-body analysis will break down. The helical vortices can become bigger while remaining stable, but eventually will split randomly. Some of it convects downstream, and the rest peels away from the body; this shedding is nonsymmetric, and greatly increases drag by widening the wake. In the limit of a 90° angle of attack, vorticity sheds as if from a bluff-body, and there is little axial convection.

10.2 Jorgensen's Formulas

There are some heuristic and theoretical formulas for predicting transverse force and moment on a body at various angles of attack, and we now present one of them due to Jorgensen. The formulas provide a good systematic procedure for design, and are best suited to vehicles with a blunt trailing edge. We call the area of the stern the *base area.*

Let the body have length L, and reference area A_r. This area could be the frontal projected area, the planform area, or the wetted area. The body travels at speed U, and angle of attack α. The normal force, axial force, and moment coefficients are defined as follows:

$$\begin{aligned} C_N &= \frac{F_N}{\frac{1}{2}\rho U^2 A_r} \\ C_A &= \frac{F_A}{\frac{1}{2}\rho U^2 A_r} \end{aligned} \tag{119}$$

$$C_M = \frac{M_{x_m}}{\frac{1}{2}\rho U^2 A_r L}.$$

The moment M_{x_m} is taken about a point x_m, measured back from the nose; this location is arbitrary, and appears explicitly in the formula for C_m. Jorgensen gives the coefficients as follows:

$$C_N = \frac{A_b}{A_r}\sin 2\alpha \cos\frac{\alpha}{2} + \frac{A_p}{A_r} C_{d_n} \sin^2\alpha \quad (120)$$

$$C_A = C_{A_o}\cos^2\alpha \quad (121)$$

$$C_M = -\frac{\nabla - A_b(L - x_m)}{A_r L}\sin 2\alpha\cos\frac{\alpha}{2} - C_{d_n}\frac{A_p}{A_r}\left(\frac{x_m - x_c}{L}\right)\sin^2\alpha. \quad (122)$$

We have listed only the formulas for the special case of circular cross-section, although the complete equations do account for more complex shapes. Further, we have assumed that $L >> D$, which is also not a constraint in the complete equations. The parameters used here are

- A_b: stern base area. $A_b = 0$ for a body that tapers to a point at the stern.
- C_{d_n}: crossflow drag coefficient; equivalent to that of an infinite circular cylinder. If "normal" Reynolds number $Re_n = U\sin\alpha D/\nu$,
  - $C_d \approx 1.2, Re_n < 3\times 10^5$
  - $C_d \approx 0.3, 3\times 10^5 < Re_n < 7\times 10^5$
  - $C_d \approx 0.6, 7\times 10^5 < Re_n$.
- A_p: planform area.
- C_{A_o}: axial drag at zero angle of attack, both frictional and form. $C_{A_o} \simeq 0.002 - 0.006$ for slender streamlined bodies, based on wetted surface area. It depends on $Re = UL/\nu$.
- ∇: body volume.
- x_c: distance from the nose backwards to the center of the planform area.

In the formula for normal force, we see that if $A_b = 0$, only drag forces act to create lift, through a $\sin^2\alpha$-dependence. Similarly, the axial force is simply the zero-α result, modified by $\cos^2\alpha$. In both cases, scaling of U^2 into the body principle directions is all that is required.
There are several terms that match exactly the slender-body theory approximations for small α. These are the first term in the normal force (C_N), and the entire first term in the moment (C_M), whether or not $A_b = 0$. Finally, we note that the second term in C_M disappears if $x_m = x_c$, i.e., if the moment is referenced to the center of the planform area. The idea here is that the fore and aft components of crossflow drag cancel out.
The aerodynamic center (again referenced toward the stern, from the nose) can be found after the coefficients are computed:

$$x_{AC} = x_m + \frac{C_M}{C_N} L. \tag{123}$$

As written, the moment coefficient is negative if the moment destabilizes the body, while C_N is always positive. Thus, the moment seeks to move the AC forward on the body, but the effect is moderated by the lift force.

10.3 Hoerner's Data: Notation

An excellent reference for experimental data is the two-volume set by S. Hoerner. It contains a large amount of aerodynamic data from many different types of vehicles, wings, and other common engineering shapes. A few notations are used throughout the books, and are described here.
First, dynamic pressure is given as $q = \frac{1}{2}\rho U^2$, such that two typical body lift coefficients are:

$$C_Y = \frac{Y}{DLq}$$
$$C_{Y_d} = \frac{Y}{D^2 q}.$$

The first version uses the *rectangular planform area* as a reference, while the second uses the *square frontal area*. Hence, $C_Y = C_{Y_d} D/L$. Two moment coefficients are:

$$C_N = \frac{N}{LD^2q}$$
$$C_{N_1} = \frac{N_1}{LD^2q},$$

where N is the moment taken about the body mid-point, and N_1 is taken about the nose. Note that the reference area for moment is the *square* frontal projection, and the reference length is body length L. The following relation holds for these definitions

$$C_{N_1} = C_N + \frac{1}{2}C_{Y_d}.$$

The lift and moment coefficients are strongly dependent on angle of attack; Hoerner uses the notation

$$\begin{aligned} C_{nb} &= \frac{\partial C_N}{\partial b} \\ C_{n\cdot b} &= \frac{\partial C_{N_1}}{\partial b} \\ C_{yb} &= \frac{\partial C_y}{\partial b}, \end{aligned}$$

and so on, where b is the angle of attack, usually in degrees. It follows from above that $C_{n\cdot b} = C_{nb} + C_{ydb}/2$.

10.4 Slender-Body Theory vs. Experiment

In an experiment, the net moment is measured, comprising both the destabilizing part due to the potential flow, and the stabilizing part due to vortex shedding or a blunt tail. Comparison of the measurements and the theory allows us to place the action point of the suction force. This section gives the formula for this location in Hoerner's notation, and gives two further examples of how well the slender-body theory matches experiments.

For $L/D > 6$, the slender-body (pure added mass) estimates give $\tilde{C}_{nb} \simeq -0.015/deg$, acting to destabilize the vehicle. The value compares well with $-0.027/deg$ for a long cylinder and $-0.018/deg$ for a long ellipsoid; it also

reduces to -0.009 for $L/D = 4$. Note that the negative sign here is consistent with Hoerner's convention that destabilizing moments have negative sign.
The experimental lift force is typically given by $C_{Yb} \simeq 0.003/deg$; this acts at a point on the latter half of the vehicle, stabilizing the angle. Because this coefficient scales roughly with wetted area, proportional to LD, it changes little with L/D. It can be compared with a low-aspect ratio wing, which achieves an equivalent lift of $\pi(AR)/2 = 0.0027$ for $(AR) = 10 \simeq D/L$.
The point at which the viscous forces act can then be estimated as the following distance aft of the nose:

$$\frac{x}{L} = \frac{C_{n\cdot b} - \tilde{C}_{nb}}{C_{ydb}} \tag{124}$$

The calculation uses experimental values of C_{ydb} and $C_{n\cdot b}$, the moment slope referenced to the nose. In the table following are values from Hoerner (p. 13-2, Figure 2) for a symmetric and a blunt-ended body.

	symmetric	blunt
L/D	6.7	6.7
$\tilde{C}_{nb}$	-0.012	-0.012
C_{yb}	0.0031	0.0037
C_{ydb}	0.021	0.025
$C_{n\cdot b}$	0.0012 (stable)	0.0031 (stable)
C_{nb}	-0.0093 (unstable)	-0.0094 (unstable)
x/L	0.63	0.60

In comparing the two body shapes, we see that the moment at the nose is much more stable (positive) for the body with a blunt trailing edge. At the body midpoint, however, both vehicles are equally unstable. The blunt-tailed geometry has a much larger lift force, but it acts too close to the midpoint to add any stability there.
The lift force dependence on the blunt tail is not difficult to see, using slender-body theory. Consider a body, with trailing edge radius r. The slender-body lift force associated with this end is simply the product of speed U and local added mass $m_a(x_T)$ (in our previous notation). It comes out to be

$$Z = \frac{1}{2}\rho U^2(\pi r^2)(2\alpha), \tag{125}$$

such that the first term in parentheses is an effective area, and the second is a lift coefficient. With respect to the area πr^2, the lift curve slope is therefore

$2/rad$. Expressed in terms of the Hoerner reference area D^2, the equivalent lift coefficient is $C_{ydb} = 0.0044/deg$, where we made the assumption here that $2r/D = 0.4$ for the data in the table. This lift difference, due solely to the blunt end condition, is consistent with measurements.

10.5 Slender-Body Approximation for Fin Lift

Let us now consider two fins of span s each, acting at the tail end of the vehicle. This is the case if the vehicle body tapers to a point where the fins have their trailing edge. The slender-body approximation of lift as a result of blunt-end conditions is

$$Z = \pi s^2 \rho U^2 \alpha. \tag{126}$$

Letting the aspect ratio be $(AR) = (2s)^2/A_f$, where A_f is the total area of the fin pair, substitution will give a lift curve slope of

$$C_l' = \frac{\pi}{2}(AR).$$

This is known as Jones' formula, and is quite accurate for $(AR) \simeq 1$. It is inadequate for higher-aspect ratio wings however, overestimating the lift by about 30% when $(AR) = 2$, and worsening further as (AR) grows.

11 FINS AND LIFTING SURFACES

Vessels traveling at significant speed typically use rudders, elevators, and other streamlined control surfaces to maneuver. Their utility arises mainly from the high lift forces they can develop, with little drag penalty. Lift is always defined to act in a direction perpendicular to the flow, and drag in the same direction as the flow.

11.1 Origin of Lift

A lifting surface is nominally an extrusion of a streamlined cross-section: the cross-section has a rounded leading edge, sharp trailing edge, and a smooth surface. The theory of lifting surfaces centers on the Kutta condition, which requires that fluid particle streamlines do not wrap around the trailing edge of the surface, but instead rejoin with streamlines from the other side of the wing at the trailing edge. This fact is true for a non-stalled surface at any angle of attack.
Since the separation point on the front of the section rotates with the angle of attack, it is clear that the fluid must travel faster over one side of the surface than the other. The reduced Bernoulli pressure this induces can then be thought of as the lift-producing mechanism. More formally, lift arises from circulation Γ:

$$\Gamma = \oint \vec{V} \cdot d\vec{s}. \tag{127}$$

and then $L = -\rho U \Gamma$. Circulation is the integral of velocity around the cross-section, and a lifting surface requires circulation in order to meet the Kutta condition.

11.2 Three-Dimensional Effects: Finite Length

Since all practical lifting surfaces have finite length, the flow near the ends may be three-dimensional. Prandtl's inviscid theory provides some insight. Since bound circulation cannot end abruptly at the wing end, it continues on in the fluid, leading to so-called wing-tip vortices. This continuation causes induced velocities at the tips, and some induced drag. Another description for the wing-tip vortices is that the pressure difference across the surface simply causes flow around the end.

A critical parameter which governs the extent of three-dimensional effects is the aspect ratio:

$$AR = \frac{span}{chord} = \frac{span^2}{area}. \tag{128}$$

The second representation is useful for non-rectangular control surfaces. The effective span is taken to be the length between the free ends of a symmetric wing. If the wing is attached to a wall, the effective span is twice the physical value, by reflection, and in this case the effective aspect ratio is therefore twice the physical value.

The aspect ratio is a strong determinant of wing performance: for a given angle of attack, a larger aspect ratio achieves a higher lift value, but also stalls earlier.

Lift is written as

$$L = \frac{1}{2}\rho U^2 A C_l, \tag{129}$$

where A is the single-side area of the surface. For angles of attack α below stall, the lift coefficient C_l is nearly linear with α: $C_l = C_l'\alpha$, where C_l' is called the lift coefficient slope, and has one empirical description

$$C_l' = \frac{1}{\frac{1}{2\pi\bar{\alpha}} + \frac{1}{\pi(AR)} + \frac{1}{2\pi(AR)^2}}, \tag{130}$$

where α is in radians, $\bar{\alpha} \simeq 0.90$, and AR is the effective aspect ratio. When $AR \to \infty$, the theoretical and maximum value for C_l' is 2π.

The lift generated on a surface is the result of a distributed pressure field; this fact creates both a net force and a net moment. A single equivalent force acts at a so-called center of action x_A, which depends mainly on the aspect ratio. For high AR, $x_A \simeq c/4$, measured back from the front of the wing. For low AR, $x_A \simeq c/2$.

11.3 Ring Fins

Ring fins are useful when space allows, since they are omnidirectional, and structurally more robust than cantilevered plane surfaces. The effective aspect ratio for a ring of diameter d is given as

$$AR = \frac{4d}{\pi c}. \tag{131}$$

The effective area of the ring is taken as

$$A_e = \frac{\pi}{2} dc, \tag{132}$$

and we thus have $L = \frac{1}{2}\rho U^2 A_e C_l' \alpha$, where one formula for C_l' is

$$C_l' = \frac{1}{0.63 + \frac{1}{\pi(AR)}}. \tag{133}$$

12 PROPELLERS AND PROPULSION

12.1 Introduction

We discuss in this section the nature of steady and unsteady propulsion. In many marine vessels and vehicles, an engine (diesel or gas turbine, say) or an electric motor drives the propeller through a linkage of shafts, reducers, and bearings, and the effects of each part are important in the response of the net system. Large, commercial surface vessels spend the vast majority of their time operating in open-water and at constant speed. In this case, steady propulsion conditions are generally optimized for fuel efficiency. An approximation of the transient behavior of a system can be made using the quasi-static assumption. In the second section, we list several low-order models of thrusters, which have recently been used to model and simulate truly unsteady conditions.

12.2 Steady Propulsion of Vessels

The notation we will use is as given in Table 1, and there are two different flow conditions to consider. *Self-propelled* conditions refer to the propeller being installed and its propelling the vessel; there are no additional forces or moments on the vessel, such as would be caused by a towing bar or hawser. Furthermore, the flow around the hull interacts with the flow through the propeller. We use an sp subscript to indicate specifically self-propulsion conditions. Conversely, when the propeller is run in open water, i.e., not behind a hull, we use an o subscript; when the hull is towed with no propeller we use a t subscript. When subscripts are not used, generalization to either condition is implied. Finally, because of similitude (using diameter D in place of L when the propeller is involved), we do not distinguish between the magnitude of forces in model and full-scale vessels.

12.2.1 Basic Characteristics

In the steady state, force balance in self-propulsion requires that

$$R_{sp} = T_{sp}. \tag{134}$$

The gear ratio λ is usually large, indicating that the propeller turns much more slowly than the driving engine or motor. The following relations define the gearbox:

R_{sp}	N	hull resistance under self-propulsion
R_t	N	towed hull resistance (no propeller attached)
T	N	thrust of the propeller
n_e	Hz	rotational speed of the engine
n_m	Hz	maximum value of n_e
n_p	Hz	rotational speed of the propeller
λ		gear ratio
Q_e	Nm	engine torque
Q_p	Nm	propeller torque
η_g		gearbox efficiency
P_e	W	engine power
P_p	W	propeller shaft power
D	m	propeller diameter
U	m/s	vessel speed
U_p	m/s	water speed seen at the propeller
Q_m	Nm	maximum engine torque
f	kg/s	fuel rate (or energy rate in electric motor)
f_m	kg/s	maximum value of f

Table 1: Nomenclature

$$\begin{aligned} n_e &= \lambda n_p \\ Q_p &= \eta_g \lambda Q_e, \end{aligned} \tag{135}$$

and power follows as $P_p = \eta_g P_e$, for any flow condition. We call $J = U_p/n_p D$ the advance ratio of the prop when it is exposed to a water speed U_p; note that in the wake of the vessel, U_p may not be the same as the speed of the vessel U. A propeller operating *in open water* can be characterized by two nondimensional parameters which are both functions of J:

$$K_T = \frac{T_o}{\rho n_p^2 D^4} \text{ (thrust coefficient)} \tag{136}$$

$$K_Q = \frac{Q_{p_o}}{\rho n_p^2 D^5} \text{ (torque coefficient).} \tag{137}$$

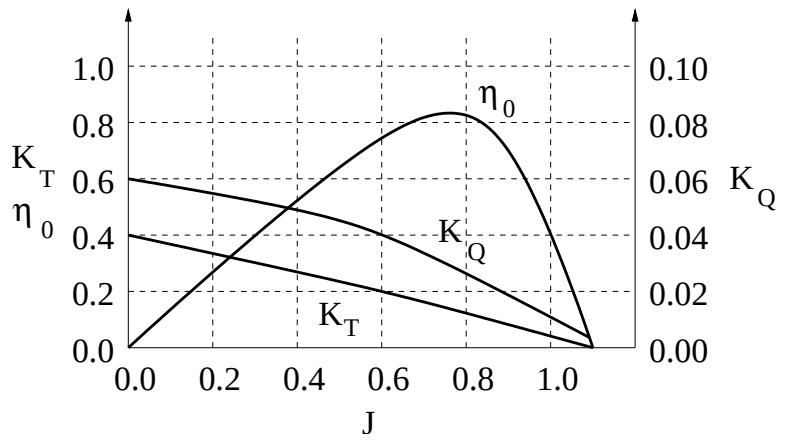

Figure 4: Typical thrust and torque coefficients.

The open propeller efficiency can be written then as

$$\eta_o = \frac{T_o U}{2\pi n_p Q_{p_o}} = \frac{J(U) K_T}{2\pi K_Q}. \tag{138}$$

This efficiency divides the useful thrust power by the shaft power. Thrust and torque coefficients are typically nearly linear over a range of J, and therefore fit the approximate form:

$$\begin{aligned} K_T(J) &= \beta_1 - \beta_2 J \\ K_Q(J) &= \gamma_1 - \gamma_2 J. \end{aligned} \tag{139}$$

As written, the four coefficients $[\beta_1, \beta_2, \gamma_1, \gamma_2]$ are usually positive, as shown in the figure.
We next introduce three factors useful for scaling and parameterizing our mathematical models:

- $U_p = U(1 - w)$; w is referred to as the *wake fraction*. A typical wake fraction of 0.1, for example, indicates that the incoming velocity seen by the propeller is only 90% of the vessel's speed. The propeller is operating in a wake.

  In practical terms, the wake fraction comes about this way: Suppose the open water thrust of a propeller is known at a given U and n_p. Behind

a vessel moving at speed U, and with the propeller spinning at the same n_p, the prop creates some extra thrust. w scales U at the prop and thus J; w is then chosen so that the open water thrust coefficient matches what is observed. The wake fraction can also be estimated by making direct velocity measurements behind the hull, with no propeller.

- $R_t = R_{sp}(1-t)$. Often, a propeller will increase the resistance of the vessel by creating low-pressure on its intake side (near the hull), which makes $R_{sp} > R_t$. In this case, t is a small positive number, with 0.2 as a typical value. t is called the *thrust deduction* even though it is used to model resistance of the hull; it is obviously specific to both the hull and the propeller(s), and how they interact.

  The thrust deduction is particularly useful, and can be estimated from published values, if only the towed resistance of a hull is known.

- $Q_{p_o} = \eta_R Q_{p_{sp}}$. The *rotative efficiency* η_R, which may be greater than one, translates self-propelled torque to open water torque, for the same incident velocity U_p, thrust T, and rotation rate n_p. η_R is meant to account for spatial variations in the wake of the vessel which are not captured by the wake fraction, as well as the turbulence induced by the hull. Note that in comparison with the wake fraction, rotative efficiency equalizes torque instead of thrust.

A common measure of efficiency, the quasi-propulsive efficiency, is based on the towed resistance, and the self-propelled torque.

$$\begin{aligned} \eta_{QP} &= \frac{R_t U}{2\pi n_p Q_{p_{sp}}} \\ &= \frac{T_o(1-t)U_p\eta_R}{2\pi n_p(1-w)Q_{p_o}} \\ &= \eta_o\eta_R\frac{(1-t)}{(1-w)}. \end{aligned} \tag{140}$$

T_o and Q_{p_o} are values for the inflow speed U_p, and thus that η_o is the open propeller efficiency at this speed. It follows that $T_o(U_p) = T_{sp}$, which was used to complete the above equation. The quasi-propulsive efficiency can be greater than one, since it relies on the towed resistance and in general $R_t > R_{sp}$. The ratio $(1-t)/(1-w)$ is often called the hull efficiency, and we see that a

small thrust deduction t and a large wake fraction w are beneficial effects, but which are in competition. A high rotative efficiency and open water propeller efficiency (at U_p) obviously contribute to an efficient overall system.

12.2.2 Solution for Steady Conditions

The linear form of K_T and K_Q (Equation 140) allows a closed-form solution for the steady-operating conditions. Suppose that the towed resistance is of the form

$$R_t = \frac{1}{2}\rho C_r A_w U^2, \tag{141}$$

where C_r is the resistance coefficient (which will generally depend on Re and Fr), and A_w is the wetted area. Equating the self-propelled thrust and resistance then gives

$$\begin{aligned}
T_{sp} &= R_{sp} \\
T_o &= R_t/(1-t) \\
K_T(J(U_p))\rho n_p^2 D^4(1-t) &= \frac{1}{2}\rho C_r A_w U^2 \\
(\beta_1 - \beta_2 J(U_p))\rho n_p^2 D^4(1-t) &= \frac{1}{2}\rho C_r A_w \frac{U_p^2}{(1-w)^2} \\
\beta_1 - \beta_2 J(U_p) &= \underbrace{\frac{C_r A_w}{2D^2(1-t)(1-w)^2}}_{\delta} J(U_p)^2 \\
J(U_p) &= \frac{-\beta_2 + \sqrt{\beta_2^2 + 4\beta_1\delta}}{2\delta}.
\end{aligned} \tag{142}$$

The last equation predicts the steady-state advance ratio of the vessel, depending only on the propeller open characteristics, and on the hull. The vessel speed can be computed by recalling that $J(U) = U/n_p D$ and $U_p = U(1-w)$, but it is clear that we need now to find n_p. This requires a torque equation, which necessitates a model of the drive engine or motor.

12.2.3 Engine/Motor Models

The torque-speed maps of many engines and motors fit the form

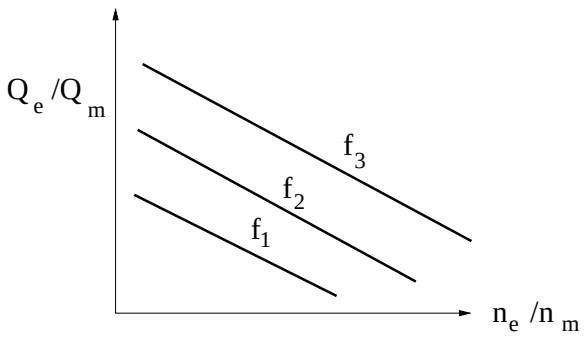

Figure 5: Typical gas turbine engine torque-speed characteristic for increasing fuel rates f_1, f_2, f_3.

$$Q_e = Q_m F(f/f_m, n_e/n_m), \tag{143}$$

where $F()$ is the characteristic function. For example, gas turbines roughly fit the curves shown in the figure (Rubis). More specifically, if $F()$ has the form

$$\begin{aligned} F(f/f_f m, n_e/n_m) &= -\left(a\frac{f}{f_m} + b\right)\frac{n_e}{n_m} + \left(c\frac{f}{f_m} + d\right) \\ &= -\alpha_1 \frac{n_p}{n_m/\lambda} + \alpha_2. \end{aligned} \tag{144}$$

then a closed-form solution for n_e (and thus n_p) can be found. The manipulations begin by equating the engine and propeller torque:

$$\begin{aligned} Q_{p_o}(J(U_p)) &= \eta_R Q_{p_s p}(J(U_p)) \\ \rho n_p^2 D^5 K_Q(J(U_p)) &= \eta_R \eta_g \lambda Q_e \\ \rho n_p^2 D^5(\gamma_1 - \gamma_2 J(U_p)) &= \eta_R \eta_g \lambda Q_m F(f/f_m, n_e/n_m) \\ \frac{n_p^2}{(n_m/\lambda)^2} &= \underbrace{\frac{\eta_R \eta_g \lambda Q_m}{\rho D^5(\gamma_1 - \gamma_2 J(U_p))(n_m/\lambda)^2}}_{\epsilon}\left(-\alpha_1 \frac{n_p}{(n_m/\lambda)} + \alpha_2\right) \\ \frac{n_p}{(n_m/\lambda)} &= \frac{-\epsilon\alpha_1 + \sqrt{\epsilon^2\alpha_1^2 + 4\epsilon\alpha_2}}{2}. \end{aligned} \tag{145}$$

Note that the fuel rate enters through both α_1 and α_2.
The dynamic response of the coupled propulsion and ship systems, under the assumption of quasi-static propeller conditions, is given by

$$\begin{aligned} (m + m_a)\dot{u} &= T_{sp} - R_{sp} \\ 2\pi I_p \dot{n}_p &= \eta_g \lambda Q_e - Q_{p_s p}. \end{aligned} \tag{146}$$

Making the necessary substitutions creates a nonlinear model with f as the input; this is left as a problem for the reader.

12.3 Unsteady Propulsion Models

When accurate positioning of the vehicle is critical, the quasi-static assumption used above does not suffice. Instead, the transient behavior of the propulsion system needs to be considered. The problem of unsteady propulsion is still in development, although there have been some very successful models in recent years. It should be pointed out that the models described below all pertain to open-water conditions and electric motors, since the positioning problem has been central to bluff vehicles with multiple electric thrusters.
We use the subscript m to denote a quantity in the motor, and p for the propeller.

12.3.1 One-State Model: Yoerger *et al.*

The torque equation at the propeller and the thrust relation are

$$I_p \dot{\omega}_p = \lambda Q_m - K_\omega \omega_p |\omega_p| \tag{147}$$

$$T = C_t \omega_p |\omega_p|. \tag{148}$$

where I_p is the total (material plus fluid) inertia reflected to the prop;the propeller spins at ω_p radians per second. The differential equation in ω_p pits the torque delivered by the motor against a quadratic-drag type loss which depends on rotation speed. The thrust is then given as a static map directly from the rotation speed.
This model requires the identification of three parameters: I_p, K_ω, and C_t. It is a first-order, nonlinear, low-pass filter from Q_m to T, whose bandwidth depends directly on Q_m.

12.3.2 Two-State Model: Healey *et al.*

The two-state model includes the velocity of a mass of water moving in the vicinity of the blades. It can accommodate a tunnel around the propeller, which is very common in thrusters for positioning. The torque equation, similarly to the above, is referenced to the motor and given as

$$I_m\dot{\omega}_m = -K_\omega\omega_m + K_vV - Q_p/\lambda. \tag{149}$$

Here, K_ω represents losses in the motor due to spinning (friction and resistive), and K_v is the gain on the input voltage (so that the current amplifier is included in K_v). The second dynamic equation is for the fluid velocity at the propeller:

$$\rho AL\gamma\dot{U}_p = -\rho A\Delta\beta(U_p - U)|U_p - U| + T. \tag{150}$$

Here A is the disc area of the tunnel, or the propeller disk diameter if no tunnel exists. L denotes the length of the tunnel, and γ is the effective added mass ratio. Together, $\rho AL\gamma$ is the added mass that is accelerated by the blades; this mass is always nonzero, even if there is no tunnel. The parameter $\Delta\beta$ is called the differential momentum flux coefficient across the propeller; it may be on the order of 0.2 for propellers with tunnels, and up to 2.0 for open propellers. The thrust and torque of the propeller are approximated using wing theory, which invokes lift and drag coefficients, as well as an effective angle of attack and the propeller pitch. However, these formulae are static maps, and therefore introduce no new dynamics. As with the one-state model of Yoerger *et al.*, this version requires the identification of the various coefficients from experiments. This model has the advantage that it creates a thrust overshoot for a step input, which is in fact observed in experiments.

13 TOWING OF VEHICLES

Vehicles which are towed have some similarities to the vehicles that have been discussed so far. For example, towed vehicles are often streamlined, and usually need good directional stability. Some towed vehicles might have active lifting surfaces or thrusters for attitude control. On the other hand, if they are to be supported by a cable, towed vehicles may be quite heavy in water, and do not have to be self-propelled. The cable itself is an important factor in the behavior of the complete towed system, and in this section, we concentrate on cable mechanics more than vehicle characteristics, which can generally be handled with the same tools as other vehicles, i.e., slender-body theory, wing theory, linearization, etc.. Some basic guidelines for vehicle design are given at the end of this section.

Modern cables can easily exceed $5000m$ in length, even a heavy steel cable with $2cm$ diameter. The cables are generally circular in cross section, and may carry power conductors and multiple communication channels (fiber optic). The extreme L/D ratio for these cables obviates any bending stiffness effects. Cable systems come in a variety of configurations, and one main division may be made simply of the density of the cable. Light-tether systems are characterized by neutrally-buoyant (or nearly so) cables, with either a minimal vehicle at the end, as in a towed array, or a vehicle capable of maneuvering itself, such as a remotely-operated vehicle. The towed array is a relatively high-velocity system that nominally streams out horizontally behind the vessel. An ROV, on the other hand, operates at low speed, and must have large propulsors to control the tether if there are currents. Heavy systems, in contrast, employ a heavy cable and possibly a heavy weight; the rationale is that gravity will tend to keep the cable vertical and make the deployment robust against currents and towing speed. The heavy systems will generally transmit surface motions and tensions to the towed vehicle much more easily than light-tether systems. We will not discuss light systems specifically here, but rather look at heavy systems. Most of the analysis can be adapted to either case, however.

13.1 Statics

13.1.1 Force Balance

For the purposes of deriving the static configuration of a cable in a flow, we assume for the moment that that it is inextensible. Tension and hydrostatic

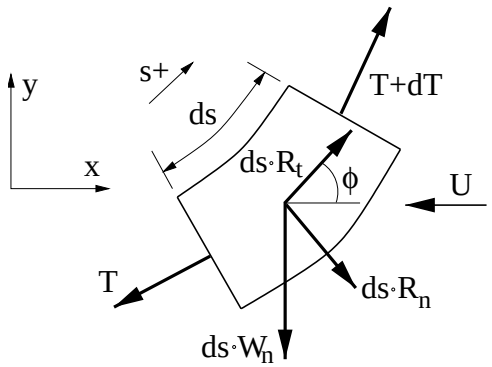

pressure will elongate a cable, but the effect is usually a small percentage of the total length.
We employ the curvilinear axial coordinate s, which we take to be zero at the bottom end of the cable; upwards along the cable is the positive direction. The free-body diagram shown has the following components:

- W_n: net in-water weight of the cable per unit length.
- $R_n(s)$: external normal force, per unit length.
- $R_t(s)$: external tangential force, per unit length.
- $T(s)$: local tension.
- $\phi(s)$: local inclination angle.

Force balance in the tangential and normal coordinates gives two coupled equations for T and ϕ:

$$\frac{dT}{ds} \quad amp;= \quad amp;W_n \sin\phi - R_t \tag{151}$$

$$T\frac{d\phi}{ds} \quad amp;= \quad amp;W_n \cos\phi + R_n. \tag{152}$$

The external forces are primarily fluid drag; the tangential drag is controlled by a frictional drag coefficient C_t, and the normal drag scales with a crossflow drag coefficient C_n. In both cases, the fluid velocity vector, U horizontal toward the left, is to be projected onto the relevant axes, leading to

$$R_t = -\frac{1}{2}\rho C_t d U^2 \cos^2\phi \tag{153}$$

$$R_n = -\frac{1}{2}\rho C_n d U^2 \sin^2\phi. \tag{154}$$

Note that we simplified the drag laws from a usual form $v|v|$ to v^2, since as drawn, $0 \leq \phi \leq \pi/2$.
The equations for T and ϕ can be integrated along the cable coordinate s to find the cable's static configuration. Two boundary conditions are needed, and the common case is that a force balance on the vehicle, dominated by drag, weight, and the cable tension, provides both $T(0)$ and $\phi(0)$. For example, a very heavy but low-drag vehicle will impose $\phi(0) \simeq \pi/2$, with $T(0)$ equal to the in-water weight of the vehicle.
With regard to Cartesian coordinates x, y, the cable configuration follows

$$\frac{dx}{ds} \quad amp;= \quad amp;\cos\phi \tag{155}$$

$$\frac{dy}{ds} \quad amp;= \quad amp;\sin\phi. \tag{156}$$

The simultaneous integration of all four equations (T, ϕ, x, y) defines the cable configuration, and current dependency may be included, say U is a function of y.

13.1.2 Critical Angle

For very deep systems, the total weight of cable will generally exceed that the vehicle. This gives rise to a configuration in which the cable is straight for a majority of its length, but turns as necessary at the vehicle end, to meet the bottom boundary condition. In the straight part of the cable, normal weight and drag components are equalized. The uniform angle is called the critical angle ϕ_c, and can be approximated easily. Let the relative importance of weight be given as

$$\delta = \frac{W_n}{\rho C_n d U^2},$$

85

13 TOWING OF VEHICLES

Vehicles which are towed have some similarities to the vehicles that have been discussed so far. For example, towed vehicles are often streamlined, and usually need good directional stability. Some towed vehicles might have active lifting surfaces or thrusters for attitude control. On the other hand, if they are to be supported by a cable, towed vehicles may be quite heavy in water, and do not have to be self-propelled. The cable itself is an important factor in the behavior of the complete towed system, and in this section, we concentrate on cable mechanics more than vehicle characteristics, which can generally be handled with the same tools as other vehicles, i.e., slender-body theory, wing theory, linearization, etc.. Some basic guidelines for vehicle design are given at the end of this section.

Modern cables can easily exceed $5000m$ in length, even a heavy steel cable with $2cm$ diameter. The cables are generally circular in cross section, and may carry power conductors and multiple communication channels (fiber optic). The extreme L/D ratio for these cables obviates any bending stiffness effects. Cable systems come in a variety of configurations, and one main division may be made simply of the density of the cable. Light-tether systems are characterized by neutrally-buoyant (or nearly so) cables, with either a minimal vehicle at the end, as in a towed array, or a vehicle capable of maneuvering itself, such as a remotely-operated vehicle. The towed array is a relatively high-velocity system that nominally streams out horizontally behind the vessel. An ROV, on the other hand, operates at low speed, and must have large propulsors to control the tether if there are currents. Heavy systems, in contrast, employ a heavy cable and possibly a heavy weight; the rationale is that gravity will tend to keep the cable vertical and make the deployment robust against currents and towing speed. The heavy systems will generally transmit surface motions and tensions to the towed vehicle much more easily than light-tether systems. We will not discuss light systems specifically here, but rather look at heavy systems. Most of the analysis can be adapted to either case, however.

13.1 Statics

13.1.1 Force Balance

For the purposes of deriving the static configuration of a cable in a flow, we assume for the moment that that it is inextensible. Tension and hydrostatic

so that the condition $d\phi/ds = 0$ requires from the force balance

$$\delta \cos\phi_c - \frac{1}{2}\sin^2\phi_c = 0.$$

We are considering the case of $0 < \phi_c < \pi/2$. Substituting $\sin^2\phi_c = 1 - \cos^2\phi_c$, we solve a quadratic equation and keep only the positive solution:

$$\cos\phi_c = \sqrt{\delta^2 + 1} - 1. \tag{157}$$

In the case of a very heavy cable, δ is large, and the linear approximation of the square root $\sqrt{1+\epsilon} \approx 1 + \epsilon/2$ gives

$$\begin{aligned} \cos\phi_c \quad amp;\simeq \quad amp;\frac{1}{2\delta} \longrightarrow \\ \phi_c \quad amp;\simeq \quad amp;\frac{\pi}{2} - \frac{1}{2\delta}. \end{aligned} \tag{158}$$

For a very light cable, δ is small; the same approximation gives

$$\cos\phi_c \simeq 1 - \delta \longrightarrow \phi_c \simeq \sqrt{2\delta}.$$

The table below gives some results of the exact solution, and the approximations.

δ	amp; exact	amp; $\delta >> 1$	amp; $\delta << 1$
0.1	amp; 0.44	amp; -	amp; 0.45
0.2	amp; 0.61	amp; -	amp; 0.63
0.5	amp; 0.91	amp; 0.57	amp; 1.00
1.0	amp; 1.14	amp; 1.07	amp; 1.41
2.0	amp; 1.33	amp; 1.32	amp; -
5.0	amp; 1.47	amp; 1.47	amp; -

13.2 Linearized Dynamics

13.2.1 Derivation

The most direct procedure for deriving useful linear dynamic equations for a planar cable problem is to consider the total tension and angle as made up of static parts summed with dynamic parts:

$$T(s,t) = \bar{T}(s) + \tilde{T}(s,t)$$
$$\phi(s,t) = \bar{\phi}(s) + \tilde{\phi}(s,t).$$

We also write the axial deflection with respect to the static configuration as $p(s,t)$, and the lateral deflection $q(s,t)$. It follows that $\tilde{\phi} = \partial q/\partial s$. Now augment the two static configuration equations with inertial components:

$$\begin{aligned} m\frac{\partial^2 p}{\partial t^2} \quad amp;= \quad amp; \frac{\partial \bar{T}}{\partial s} + \frac{\partial \tilde{T}}{\partial s} - W_n \sin(\bar{\phi}+\tilde{\phi}) - \frac{1}{2}\rho C_t d\left(U\cos\phi + \frac{\partial p}{\partial t}\right)^2 \\ (m+m_a)\frac{\partial^2 q}{\partial t^2} \quad amp;= \quad amp; (\bar{T}+\tilde{T})\left(\frac{\partial \bar{\phi}}{\partial s} + \frac{\partial \tilde{\phi}}{\partial s}\right) - W_n\cos(\bar{\phi}+\tilde{\phi}) + \\ amp; \quad amp; \frac{1}{2}\rho C_n d\left(U\sin\phi - \frac{\partial q}{\partial t}\right)^2. \end{aligned}$$

Here the material mass of the cable per unit length is m, and its transverse added mass is m_a. Note that avoiding the drag law form $v|v|$ again, we have implicitly assumed that $U\cos\phi > |\partial p/\partial t|$ and $U\sin\phi > |\partial q/\partial t|$. If it is not the case, say $U = 0$, then equivalent linearization can be used for the quadratic drag.
Now we perform the trigonometry substitutions in the weight terms, let $\phi \simeq \bar{\phi}$ for the calculation of drag, and substitute the constitutive (Hooke's) law

$$\frac{\partial \tilde{T}}{\partial s} = EA\frac{\partial^2 p}{\partial s^2}.$$

The static solution cancels out of both governing equations, and keeping only linear terms we obtain

$$\begin{aligned} m\frac{\partial^2 p}{\partial t^2} \quad amp;= \quad amp; EA\frac{\partial^2 p}{\partial s^2} - W_n\cos\bar{\phi}\frac{\partial q}{\partial s} - \rho C_t dU\cos\bar{\phi}\frac{\partial p}{\partial t} \\ (m+m_a)\frac{\partial^2 q}{\partial t^2} \quad amp;= \quad amp; \bar{T}\frac{\partial^2 q}{\partial s^2} + EA\frac{\partial p}{\partial s}\frac{\partial \bar{\phi}}{\partial s} + W_n\sin\bar{\phi}\frac{\partial q}{\partial s} - \rho C_n dU\sin\bar{\phi}\frac{\partial q}{\partial t}. \end{aligned}$$

The axial dynamics (p) couples with the lateral equation through the weight term $-W_n\cos\bar{\phi}\tilde{\phi}$. The lateral dynamics ($q$) couples with the axial through the term $\tilde{T}\partial\bar{\phi}/\partial s$. An additional weight term $W_n\sin\bar{\phi}\partial q/\partial s$ also appears. The uncoupled dynamics are both in the form of damped wave equations

$$\begin{aligned} m\frac{\partial^2 p}{\partial t^2} + b_t\frac{\partial p}{\partial t} \quad amp;= \quad amp; EA\frac{\partial^2 p}{\partial s^2} \\ (m+m_a)\frac{\partial^2 q}{\partial t^2} + b_n\frac{\partial q}{\partial t} \quad amp;= \quad amp; \bar{T}\frac{\partial^2 q}{\partial s^2} + W_n\sin\bar{\phi}\frac{\partial q}{\partial s}, \end{aligned}$$

where we made the substitution $b_t = \rho C_t dU\cos\bar{\phi}$ and $b_n = \rho C_n dU\sin\bar{\phi}$. To a linear approximation, the out-of-plane vibrations of a cable are also governed by the second equation above.
Because of light damping in the tangential direction, heavy cables easily transmit motions and tensions along their length, and can develop longitudinal resonant conditions (next section). In contrast, the lateral cable motions are heavily damped, such that disturbances only travel a few tens or hundreds of meters before they dissipate. The nature of the lateral response, in and out

of the towing plane, is a very slow, damped nonlinear filter. High-frequency vessel motions in the horizontal plane are completely missed by the vehicle, while low-frequency motions occur sluggishly, and only after a significant delay time.

	amp; axial	amp; lateral
wave speed	amp; $\sqrt{\frac{EA}{m}}$ amp; FAST	amp; $\sqrt{\frac{\bar{T}(s)}{m+m_a}}$ amp; SLOW
natural frequency	amp; $\frac{n\pi}{L}\sqrt{\frac{EA}{m}}$	amp; $O\left(\frac{n\pi}{L}\sqrt{\frac{\bar{T}(L/2)}{m+m_a}}\right)$
mode shape	amp; sine/cosine	amp; Bessel function
damping	amp; $C_t \simeq O(0.01)$	amp; $C_n \simeq O(1)$
disturbances travel down cable?	amp; amp; YES amp;	amp; amp; NO amp;

13.2.2 Damped Axial Motion

Mode Shape. The axial direction is of particular interest, since it is lightly damped and forced by the heaving of vessels in seas. Consider a long cable governed by the damped wave equation

$$m\ddot{p} + b_t\dot{p} = EAp'' \tag{159}$$

We use over-dots to indicate time derivatives, and primes to indicate spatial derivatives. At the surface, we impose the motion

$$p(L,t) = P\cos\omega t, \tag{160}$$

while the towed vehicle, at the lower end, is an undamped mass responding to the local tension variations:

$$EA\frac{\partial p(0,t)}{\partial s} = M\ddot{p}(0,t). \tag{161}$$

These top and bottom behaviors comprise the boundary conditions for the wave equation. We let $p(s,t) = \tilde{p}(s)\cos\omega t$, so that

$$\tilde{p}'' + \left(\frac{m\omega^2 - i\omega b_t}{EA} \right) \tilde{p} = 0. \tag{162}$$

This admits the solution $\tilde{p}(s) = c_1 \cos ks + c_2 \sin ks$, where

$$k = \sqrt{\frac{m\omega^2 - i\omega b_t}{EA}}. \tag{163}$$

Note that k is complex when $b_t \neq 0$. The top and bottom boundary conditions give, respectively,

$$\begin{array}{rll} P & amp; = & amp; c_1 \cos kL + c_2 \sin kL \\ 0 & amp; = & amp; c_1 + \delta c_2, \end{array}$$

where $\delta = EAk/\omega^2 M$. These can be combined to give the solution

$$\tilde{p} = P \frac{\delta \cos ks - \sin ks}{\delta \cos kL - \sin kL}. \tag{164}$$

In the case that $M \to 0$, the scalar $\delta \to \infty$, simplifying the result to $\tilde{p} = P \cos ks / \cos kL$.

Dynamic Tension. It is possible to compute the dynamic tension via $\tilde{T} = EA\tilde{p}'$. We obtain

$$\tilde{T} = -EAPk \frac{\delta \sin ks + \cos ks}{\delta \cos kL - \sin kL}. \tag{165}$$

There are two dangerous situations:

- The maximum tension is $\bar{T} + |\tilde{T}|$ and must be less than the working load of the cable. This is normally problematic at the top of the cable, where the static tension is highest.
- If $|\tilde{T}| > \bar{T}$, the cable will unload completely and then reload with extremely high impulsive forces. This is known as snap loading; it occurs primarily at the vehicle, where $\bar{T}$ is low.

Natural Frequency. The natural frequency can be found by letting $b_t = 0$, and investigating the singularity of $\tilde{p}$, for which $\delta \cos kL = \sin kL$. In general,

$kL << 1$, but we find that a first-order approximation yields $\omega = \sqrt{EA/LM}$, which is only a correct answer if $M >> mL$, i.e., the system is dominated by the vehicle mass. Some higher order terms need to be kept. We start with better approximations for sin() and cos():

$$\delta \left(1 - \frac{(kL)^2}{2}\right) = kL \left(1 - \frac{(kL)^2}{6}\right).$$

Employing the definition for δ, and recalling that $\omega^2 = k^2 EA/m$, we arrive at

$$\frac{mL}{M} \left(1 - \frac{(kL)^2}{2}\right) = (kL)^2 \left(1 - \frac{(kL)^2}{6}\right).$$

If we match up to second order in kL, then

$$\omega = \sqrt{\frac{EA/L}{M + mL/2}}.$$

This has the familiar form of the square root of a stiffness divided by a mass: the stiffness of the cable is EA/L, and the mass that is oscillating is $M+mL/2$. In very deep water, the effects of $mL/2$ dominate; if $\rho_c = m/A$ is the density of the cable, we have the approximation

$$\omega \simeq \frac{1}{L}\sqrt{\frac{2E}{\rho_c}}.$$

A few examples are given below for a steel cable with $E = 200 \times 10^9 Pa$, and $\rho_c = 7000 kg/m^3$. The natural frequencies near wave excitation at the surface vessel must be taken into account in any design or deployment. Even if a cable can withstand the effects of resonance, it may be undesirable to expose the vehicle to these motions. Some solutions in use today are: stable vessels (e.g., SWATH), heave compensation through an active crane, a clump weight below which a light cable is employed, and an S-shaped length of cable at the bottom formed with flotation balls.

$L = 500m$	amp; $\omega_n = 15.0rad/s$
$1000m$	amp; $7.6rad/s$
$2000m$	amp; $3.7rad/s$
$5000m$	amp; $1.5rad/s$

13.3 Cable Strumming

Cable strumming causes a host of problems, including obvious fatigue when the amplitudes and frequencies are high. The most noteworthy issue with towing is that the vibrations may cause the normal drag coefficient C_n to increase dramatically – from about 1.2 for a non-oscillating cable to as high as 3.5. This drag penalty decreases the critical angle of towing, so that larger lengths of cable are needed to reach a given depth, and the towed system lags further and further behind the surface vessel. The static tension will increase accordingly as well.

Strumming of cables is caused by the proximity of a preferred vortex formation frequency ω_S to the natural frequency of the structure ω_n. This latter frequency can be obtained as a zero of the lightly-damped Bessel function solution of the lateral dynamics equation above. The preferred frequency of vortex formation is given by the empirical relation $\omega_S = 2\pi SU/d$, where S is the Strouhal number, about 0.16-0.20 for a large range of Re. Strumming of amplitude $d/2$ or greater can occur for $0.6 < \omega_S/\omega_n < 2.0$. The book by Blevins is a good general reference.

13.4 Vehicle Design

The physical layout of a towed vehicle is amenable to the analysis tools of self-propelled vehicles, with the main exceptions that the towpoint presents a large mean force as well as some disturbances, and that the vehicle can be quite heavy in water. Here are basic guidelines to be considered:

1. The towpoint must be located above the vehicle center of in-water weight, for basic roll and pitch stability.

2. The towpoint should be forward of the aerodynamic center, for towing stability reasons.

3. The combined center of mass (material and added mass) should be longitudinally *between* the towpoint and the aerodynamic center, and nearer

the towpoint. This will ensure that high-frequency disturbances do not induce excessive pitching.

4. The towpoint should be longitudinally forward of the center of in-air weight, so that the vehicle enters the water fins first, and self-stabilizes with $U > 0$.

5. The center of buoyancy should be behind the in-water center of weight, so that the vehicle pitches downward at small U, and hence the net lift force is downward, away from the surface.

Meeting all of these criteria simultaneously is no small feat, and the performance of the device is very sensitive to small perturbations in the geometry. For this reason, full-scale experiments are commonly used in the design process.

14 TRANSFER FUNCTIONS & STABILITY

The reader is referred to *Laplace Transforms* in the section *MATH FACTS* for preliminary material on the Laplace transform. Partial fractions are presented here, in the context of control systems, as the fundamental link between pole locations and stability.

14.1 Partial Fractions

Solving linear time-invariant systems by the Laplace Transform method will generally create a signal containing the (factored) form

$$Y(s) = \frac{K(s+z_1)(s+z_2)\cdots(s+z_m)}{(s+p_1)(s+p_2)\cdots(s+p_n)}. \tag{166}$$

Although for the moment we are discussing the signal $Y(s)$, later we will see that dynamic systems are described in the same format: in that case we call the impulse response $G(s)$ a transfer function. A system transfer function is identical to its impulse response, since $L(\delta(t)) = 1$.
The constants $-z_i$ are called the zeros of the transfer function or signal, and $-p_i$ are the poles. Viewed in the complex plane, it is clear that the magnitude of $Y(s)$ will go to zero at the zeros, and to infinity at the poles.
Partial fraction expansions alter the form of $Y(s)$ so that the simple transform pairs can be used to find the time-domain output signals. We must have $m < n$; if this is not the case, then we have to divide the numerator by the denominator as necessary to find a simple form.

14.2 Partial Fractions: Unique Poles

Under the condition $m < n$, it is a fact that $Y(s)$ is equivalent to

$$Y(s) = \frac{a_1}{s+p_1} + \frac{a_2}{s+p_2} + \cdots \frac{a_n}{s+p_n}, \tag{167}$$

in the special case that all of the poles are unique and real. The coefficient a_i is termed the *residual* associated with the i'th pole, and once all these are found it is a simple matter to go back to the transform table and look up the time-domain responses.

How to find a_i? A simple rule applies: multiply the right-hand sides of the two equations above by $(s + p_i)$, evaluate them at $s = -p_i$, and solve for a_i, the only one left.

14.3 Example: Partial Fractions with Unique Real Poles

$$G(s) = \frac{s(s+6)}{(s+4)(s-1)} e^{-2s}.$$

Since we have a pure delay and $m = n$, we can initially work with $G(s)/se^{-2s}$. We have

$$\frac{s+6}{(s+4)(s-1)} = \frac{a_1}{s+4} + \frac{a_2}{s-1}, \text{ giving}$$

$$\begin{aligned} a_1 &= \left[\tfrac{(s+6)(s+4)}{(s+4)(s-1)}\right]_{s=-4} = -\frac{2}{5} \\ a_2 &= \left[\tfrac{(s+6)(s-1)}{(s+4)(s-1)}\right]_{s=1} = \frac{7}{5} \end{aligned}$$

Thus

$$\begin{aligned} L^{-1}(G(s)/se^{-2s}) &= -\frac{2}{5}e^{-4t} + \frac{7}{5}e^{t} \longrightarrow \\ g(t) &= \delta(t-2) + \frac{8}{5}e^{-4(t-2)} + \frac{7}{5}e^{t-2}. \end{aligned}$$

The impulse response is needed to account for the step change at $t = 2$. Note that in this example, we were able to apply the derivative operator s *after* expanding the partial fractions. For cases where a second derivative must be taken, i.e., $m \geq n + 1$, special care should be used when accounting for the signal *slope* discontinuity at $t = 0$. The more traditional method, exemplified by Ogata, may prove easier to work through.

The case of repeated real roots may be handled elegantly, but this condition rarely occurs in applications.

14.4 Partial Fractions: Complex-Conjugate Poles

A complex-conjugate pair of poles should be kept together, with the following procedure: employ the form

$$Y(s) = \frac{b_1 s + b_2}{(s+p_1)(s+p_2)} + \frac{a_3}{s+p_3} + \cdots, \tag{168}$$

where $p_1 = p_2^*$ (complex conjugate). As before, multiply through by $(s + p_1)(s + p_2)$, and then evaluate at $s = -p_1$.

14.5 Example: Partial Fractions with Complex Poles

$$G(s) = \frac{s+1}{s(s+j)(s-j)} = \frac{b_1 s + b_2}{(s+j)(s-j)} + \frac{a_3}{s} :$$

$$\begin{aligned} \left[\frac{s+1}{s}\right]_{s=-j} &= [b_1 s + b_2]_{s=-j} \longrightarrow \\ 1 + j &= -b_1 j + b_2 \longrightarrow \\ b_1 &= -1 \\ b_2 &= 1; \text{ also} \\ \left[\frac{s+1}{(s+j)(s-j)}\right]_{s=0} &= a_3 = 1. \end{aligned}$$

Working out the inverse transforms from the table of pairs, we have simply (noting that $\zeta = 0$)

$$g(t) = -\cos t + \sin t + 1(t).$$

14.6 Stability in Linear Systems

In linear systems, *exponential stability* occurs when all the real exponents of e are strictly negative. The signals decay within an exponential envelope. If one exponent is 0, the response never decays or grows in amplitude; this is called *marginal stability*. If at least one real exponent is positive, then one element of the response grows without bound, and the system is *unstable*.

14.7 Stability $\Longleftrightarrow$ Poles in LHP

In the context of partial fraction expansions, the relationship between stability and pole locations is especially clear. The unit step function $1(t)$ has a pole at zero, the exponential e^{-at} has a pole at $-a$, and so on. All of the other pairs exhibit the same property: *A system is stable if and only if all of the poles occur in the left half of the complex plane.* Marginally stable parts correlate with a zero real part, and unstable parts to a positive real part.

14.8 General Stability

There are two definitions, which apply to systems with input $\vec{u}(t)$ and output $\vec{y}(t)$.

1. **Exponential**. If $\vec{u}(t) = \vec{0}$ and $\vec{y}(0) = \vec{y}_o$, then $|y_i(t)| < \alpha e^{-\gamma t}$, for finite α and $\gamma > 0$. The output asymptotically approaches zero, within a decaying exponential envelope.

2. **Bounded-Input Bounded-Output (BIBO)**. If $\vec{y}(0) = \vec{0}$, and $|f_i(t)| < \gamma, \gamma > 0$ and finite, then $|y_i(t)| < \alpha, \alpha > 0$ and finite.

In linear time-invariant systems, the two definitions are identical. Exponential stability is easy to check for linear systems, but for nonlinear systems, BIBO stability is usually easier to achieve.

15 CONTROL FUNDAMENTALS

15.1 Introduction

15.1.1 Plants, Inputs, and Outputs

Controller design is about creating dynamic systems that behave in useful ways. Many target systems are physical; we employ controllers to steer ships, fly jets, position electric motors and hydraulic actuators, and distill alcohol. Controllers are also applied in macro-economics and many other important, non-physical systems. It is the fundamental concept of controller design that a set of input variables acts through a given "plant" to create an output. Feedback control then uses sensed plant outputs to apply corrective inputs:

Plant	Inputs	Outputs	Sensors
Jet aircraft	elevator, rudder, etc.	altitude, hdg	altimeter, GPS
Marine vessel	rudder angle	heading	gyrocompass
Hydraulic robot	valve position	tip position	joint angle
U.S. economy	fed interest rate, etc.	prosperity	inflation, M1
Nuclear reactor	cooling, neutron flux	power level	temp., pressure

15.1.2 The Need for Modeling

Effective control system design usually benefits from an accurate model of the plant, although it must be noted that many industrial controllers can be tuned up satisfactorily with no knowledge of the plant. Ziegler and Nichols, for example, developed a general recipe which we detail later. In any event, plant models simply do not match real-world systems exactly; we can only hope to capture the basic components in the form of differential or integro-differential equations.

Beyond prediction of plant behavior based on physics, the process of *system identification* generates a plant model from data. The process is often problematic, however, since the measured response could be corrupted by sensor noise or physical disturbances in the system which cause it to behave in unpredictable ways. At some frequency high enough, most systems exhibit effects that are difficult to model or reproduce, and this is a limit to controller performance.

15.1.3 Nonlinear Control

The bulk of this subject is taught using the tools of linear systems analysis. The main reason for this restriction is that nonlinear systems are difficult to model, difficult to design controllers for, and difficult overall! Within the paradigm of linear systems, there are many sets of powerful tools available. The reader interested in nonlinear control is referred to the book by Slotine and Li.

15.2 Representing Linear Systems

Except for the most heuristic methods of tuning up simple systems, control system design depends on a model of the plant. The transfer function description of linear systems has already been described in the discussion of the Laplace transform. The state-space form is an entirely equivalent *time-domain* representation that makes a clean extension to systems with multiple inputs and multiple outputs, and opens the way to standard tools from linear algebra.

15.2.1 Standard State-Space Form

We write a linear system in a state-space form as follows

$$\begin{aligned} \dot{x} &= Ax + Bu + Gw \\ y &= Cx + Du + v \end{aligned} \tag{169}$$

where

- x is a state vector, with as many elements as there are orders in the governing differential equations.
- A is a matrix mapping x to its derivative; A captures the natural dynamics of the system without external inputs.
- B is an input gain matrix for the control input u.
- G is a gain matrix for unknown disturbance w; w drives the state just like the control u.
- y is the observation vector, comprised mainly of a linear combination of states Cx (where C is a matrix.

- Du is a direct map from input to output (usually zero for physical systems).
- v is an unknown sensor noise which corrupts the measurement.

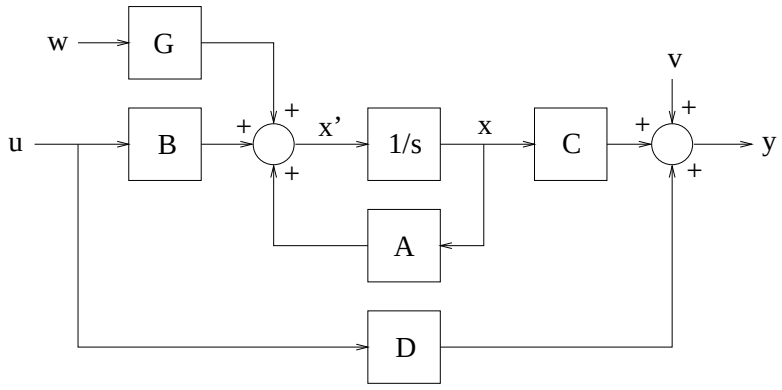

15.2.2 Converting a State-Space Model into a Transfer Function

There are a number of canonical state-space forms available, which can create the same transfer function. In the case of no disturbances or noise, the transfer function (or transfer matrix) can be written as

$$G(s) = \frac{y(s)}{u(s)} = C(sI - A)^{-1}B + D, \tag{170}$$

where I is the identity matrix with the same size as A. A similar equation holds for $y(s)/w(s)$, and clearly $y(s)/v(s) = I$.

15.2.3 Converting a Transfer Function into a State-Space Model

It may be possible to write the corresponding differential equation along one row of the state vector, and then cascade derivatives. For example, consider the following system:

$$\begin{aligned} my''(t) + by'(t) + ky(t) &= u'(t) + u(t) \text{ (mass-spring-dashpot)} \\ G(s) &= \frac{s+1}{ms^2 + bs + k} \end{aligned}$$

Setting $\vec{x} = [y', y]^T$, we obtain the system

$$\begin{aligned} \frac{d\vec{x}}{dt} &= \begin{bmatrix} -b/m & -k/m \\ 1 & 0 \end{bmatrix} \vec{x} + \begin{bmatrix} 1/m \\ 0 \end{bmatrix} u \\ y &= [1 \;\; 1]\, \vec{x} \end{aligned}$$

Note specifically that $dx_2/dt = x_1$, leading to an entry of 1 in the off-diagonal of the second row in A. Entries in the C-matrix are easy to write in this case because of linearity; the system response to u' is the same as the derivative of the system response to u.

15.3 PID Controllers

The most common type of industrial controller is the proportional-integral-derivative (PID) design. If u is the output from the controller, and e is the error signal it receives, this control law has the form

$$\begin{aligned} u(t) &= k_p e(t) + k_i \int_0^t e(\tau) d\tau + k_d e'(t), \\ C(s) = \frac{U(s)}{E(s)} &= k_p + \frac{k_i}{s} + k_d s \\ &= k_p \left[1 + \frac{1}{\tau_i s} + \tau_d s \right], \end{aligned} \tag{171}$$

where the last line is written using the conventions of one overall gain k_p, plus a time characteristic to the integral part (τ_i) and and time characteristic to the derivative part (τ_d).
In words, the proportional part of this control law will create a control action that scales linearly with the error – we often think of this as a spring-like action. The integrator is accumulating the error signal over time, and so the control action from this part will continue to grow as long as an error exists. Finally, the derivative action scales with the derivative of the error. The controller will retard motion toward zero error, which helps to reduce overshoot.
The common variations are: P, PD, PI, PID.

15.4 Example: PID Control

Consider the case of a mass (m) sliding on a frictionless table. It has a perfect thruster that generates force $u(t)$, but is also subject to an unknown

disturbance $d(t)$. If the linear position of the mass is $y(t)$, and it is perfectly measured, we have the plant

$$my''(t) = u(t) + d(t).$$

Suppose that the desired condition is simply $y(t) = 0$, with initial conditions $y(0) = y_o$ and $y'(0) = 0$.

15.4.1 Proportional Only

A proportional controller alone invokes the control law $u(t) = -k_p y(t)$, so that the closed-loop dynamics follow

$$my''(t) = -k_p y(t) + d(t).$$

In the absence of $d(t)$, we see that $y(t) = y_o \cos \sqrt{\frac{k_p}{m}} t$, a marginally stable response that is undesirable.

15.4.2 Proportional-Derivative Only

Let $u(t) = -k_p y(t) - k_d y'(t)$, and it follows that

$$my''(t) = -k_p y(t) - k_d y'(t) + d(t).$$

The system now resembles a second-order mass-spring-dashpot system where k_p plays the part of the spring, and k_d the part of the dashpot. With an excessively large value for k_d, the system would be overdamped and very slow to respond to any command. In most applications, a small amount of overshoot is employed because the response time is shorter. The k_d value for critical damping in this example is $2\sqrt{mk_p}$, and so the rule is $k_d < 2\sqrt{mk_p}$. The result, easily found using the Laplace transform, is

$$y(t) = y_o e^{\frac{-k_d}{2m} t} \left[\cos \omega_d t + \frac{k_d}{2m\omega_d} \sin \omega_d t \right],$$

where $\omega_d = \sqrt{4mk_p - k_d^2}/2m$. This response is exponentially stable as desired. Note that if the mass had a very large amount of natural damping, a *negative* k_d could be used to cancel some of its effect and speed up the system response. Now consider what happens if $d(t)$ has a constant bias d_o: it balances exactly the proportional control part, eventually settling out at $y(t = \infty) = d_o/k_p$. To achieve good rejection of d_o with a PD controller, we would need to set k_p very large. However, very large values of k_p will also drive the resonant frequency ω_d up, which is unacceptable.

15.4.3 Proportional-Integral-Derivative

Now let $u(t) = -k_p y(t) - k_i \int_0^t y(\tau)d\tau - k_d y'(t)$: we have

$$my''(t) = -k_p y(t) - k_i \int_0^t y(\tau)d\tau - k_d y'(t) + d(t).$$

The control system has now created a third-order closed-loop response. If $d(t) = d_o$, a time derivative leads to

$$my'''(t) + k_p y'(t) + k_i y(t) + k_d y''(t) = 0,$$

so that $y(t = \infty) = 0$, as desired, provided the roots are stable.

15.5 Heuristic Tuning

For many practical systems, tuning of a PID controller may proceed without any system model. This is especially pertinent for plants which are open-loop stable, and can be safely tested with varying controllers. One useful approach is due to Ziegler and Nichols (1942), which transforms the basic characteristics of a step response (e.g., the input is $1(t)$) into a reasonable PID design. The idea is to approximate the response curve by a first-order lag (gain k and time constant τ) and a pure delay T:

$$G(s) \simeq \frac{ke^{-Ts}}{\tau s + 1} \tag{172}$$

The following rules apply *only* if the plant contains no dominating, lightly-damped complex poles, and has no poles at the origin:

P	$k_p = 1.0\tau/T$		
PI	$k_p = 0.9\tau/T$	$k_i = 0.27\tau/T^2$	
PID	$k_p = 1.2\tau/T$	$k_i = 0.60\tau/T^2$	$k_d = 0.60\tau$

Note that if no pure time delay exists ($T = 0$), this recipe suggests the proportional gain can become arbitrarily high! Any characteristic other than a true first-order lag would therefore be expected to cause a measurable delay.

15.6 Block Diagrams of Systems

15.6.1 Fundamental Feedback Loop

The topology of a feedback system can be represented graphically by considering each dynamical system element to reside within a box, having an input line and an output line. For example, the plant used above (a simple mass) has transfer function $P(s) = 1/ms^2$, which relates the input, force $u(s)$, into the output, position $y(s)$. In turn, the PD-controller has transfer function $C(s) = k_p + k_d s$; its input is the error signal $E(s) = -y(s)$, and its output is force $u(s)$. The feedback loop in block diagram form is shown below.

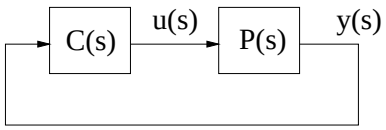

15.6.2 Block Diagrams: General Case

The simple feedback system above is augmented in practice by three external inputs. The first is a process disturbance, which can be taken to act at the input of the physical plant, or at the output. In the former case, it is additive with the control action, and so has some physical meaning. In the second case, the disturbance has the same units as the plant output.

Another external input is the *reference command* or *setpoint*, used to create a more general error signal $e(s) = r(s) - y(s)$. Note that the feedback loop, in trying to force $e(s)$ to zero, will necessarily make $y(s)$ approximate $r(s)$.

The final input is sensor noise, which usually corrupts the feedback signal $y(s)$, causing some error in the evaluation of $e(s)$, and so on. Sensors with very poor

noise properties can ruin the performance of a control system, no matter how perfectly understood are the other components.

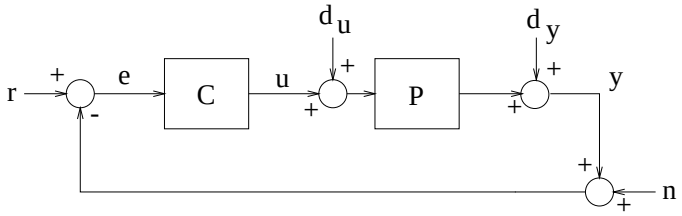

15.6.3 Primary Transfer Functions

Some algebra shows that

$$\begin{aligned} \frac{e}{r} &= \frac{1}{1+PC} = S \\ \frac{y}{r} &= \frac{PC}{1+PC} = T \\ \frac{u}{r} &= \frac{C}{1+CP} = U. \end{aligned}$$

$e/r = S$ relates the reference input and noise to the error, and is known as the *sensitivity function*. We would generally like S to be small at low frequencies, so that the tracking error there is small. $y/r = T$ is called the *complementary sensitivity function*. Note that $S + T = 1$, implying that these two functions must always trade off; they cannot both be small or large at the same time. Other systems we encounter again later are the *(forward) loop transfer function* PC, the loop transfer function broken between C and P: CP, and

$$\begin{aligned} \frac{e}{d_u} &= \frac{-P}{1+PC} \\ \frac{y}{d_u} &= \frac{P}{1+PC} \\ \frac{u}{d_u} &= \frac{-CP}{1+CP} \\ \frac{e}{d_y} &= \frac{-1}{1+PC} = -S \end{aligned}$$

$$\begin{aligned}
\frac{y}{d_y} &= \frac{1}{1+PC} = S \\
\frac{u}{d_y} &= \frac{-C}{1+CP} = -U \\
\frac{e}{n} &= \frac{-1}{1+PC} = -S \\
\frac{y}{n} &= \frac{-PC}{1+PC} = -T \\
\frac{u}{n} &= \frac{-C}{1+CP} = -U.
\end{aligned}$$

If the disturbance is taken at the plant output, then the three functions S, T, and U (control action) completely describe the system. This will in fact be the procedure when we address loopshaping.

16 MODAL ANALYSIS

16.1 Introduction

The evolution of states in a linear system occurs through independent modes, which can be driven by external inputs, and observed through plant output. This section provides the basis for modal analysis of systems. Throughout, we use the state-space description of a system with $D = 0$:

$$\begin{aligned} \dot{\vec{x}} &= A\vec{x} + B\vec{u} \\ \vec{y} &= C\vec{x}. \end{aligned}$$

16.2 Matrix Exponential

16.2.1 Definition

In the instance of an unforced response to initial conditions, consider the system

$$\dot{\vec{x}} = A\vec{x}, \qquad \vec{x}(t=0) = \vec{\chi}.$$

In the scalar case, the response is $x(t) = \chi e^{at}$, giving a decaying exponential if $a < 0$. The same notation holds for the case of a vector $\vec{x}$, and matrix A:

$$\begin{aligned} \vec{x}(t) &= e^{At}\vec{\chi}, \text{ where} \\ e^{At} &= I + At + \frac{(At)^2}{2!} + \cdots \end{aligned}$$

e^{At} is usually called the matrix exponential.

16.2.2 Modal Canonical Form

Introductory material on the eigenvalue problem and modal decomposition can be found in the *MATH FACTS* section. This modal decomposition of A leads to a very useful state-space representation. Namely, since $A = V\Lambda V^{-1}$, a transformation of state variables can be made, $\vec{x} = V\vec{z}$, leading to

$$\begin{aligned} \dot{\vec{z}} &= \Lambda\vec{z} + V^{-1}B\vec{u} \\ \vec{y} &= CV\vec{z}. \end{aligned} \tag{173}$$

This is called the modal canonical form, since the states are simply the modal amplitudes. These states are uncoupled in Λ, but may be coupled through the input ($V^{-1}B$) and output (CV) mappings. The modal form is numerically robust for computations.

16.2.3 Modal Decomposition of Response

Now we are ready to look at the matrix exponential e^{At} in terms of its constituent modes. Employing the above form for A, we find that

$$\begin{aligned} e^{At} &= I + At + \frac{(At)^2}{2!} + \cdots \\ &= V\left(I + \Lambda t + \frac{(\Lambda t)^2}{2!} + \cdots\right)W^T \\ &= Ve^{\Lambda t}W^T \\ &= \sum_{i=1}^{n} e^{\lambda_i t}\vec{v}_i\vec{w}_i^T. \end{aligned}$$

In terms of the response to an initial condition $\vec{\chi}$, we have

$$\vec{x}(t) = \sum_{i=1}^{n} e^{\lambda_i t}\vec{v}_i(\vec{w}_i^T\vec{\chi}).$$

The product $\vec{w}_i^T\vec{\chi}$ is a scalar, the projection of the initial conditions onto the i'th mode. If $\vec{\chi}$ is perpendicular to $\vec{w}_i$, then the product is zero and the i'th mode does not respond. Otherwise, the i'th mode does participate in the response. The projection of the i'th mode onto the *states* $\vec{x}$ is through the right eigenvector $\vec{v}_i$.
For stability of the system, the eigenvalues of A, that is, λ_i, must have negative real parts; they are in fact the poles of the equivalent transfer function description.

16.3 Forced Response and Controllability

Now consider the system with an external input $\vec{u}$:

$$\dot{\vec{x}} = A\vec{x} + B\vec{u}, \qquad \vec{x}(t=0) = \vec{\chi}.$$

Taking the Laplace transform of the system, taking into account the initial condition for the derivative, we have

$$\begin{aligned} s\vec{x}(s) - \vec{\chi} &= A\vec{x}(s) + B\vec{u}(s) \longrightarrow \\ \vec{x}(s) &= (sI - A)^{-1}\vec{\chi} + (sI - A)^{-1}B\vec{u}(s). \end{aligned}$$

Thus $(sI - A)^{-1}$ can be recognized as the Laplace transform of the matrix exponential e^{At}. In the time domain, the second term then has the form of a convolution of the matrix exponential and the net input $B\vec{u}$:

$$\begin{aligned} \vec{x}(t) &= \int_0^t e^{A(t-\tau)}B\vec{u}(\tau)d\tau \\ &= \sum_{i=1}^{n}\int_0^t e^{\lambda_i(t-\tau)}\vec{v}_i\vec{w}_i^T B\vec{u}(\tau)d\tau. \end{aligned}$$

Suppose now that there are m inputs, such that $B = [\vec{b}_1, \vec{b}_2, \cdots, \vec{b}_m]$. Then some rearrangement will give

$$\vec{x}(t) = \sum_{i=1}^{n}\vec{v}_i\sum_{k=1}^{m}(\vec{w}_i^T\vec{b}_k)\int_0^t e^{\lambda_i(t-\tau)}\vec{u}_k(\tau)d\tau.$$

The product $\vec{w}_i^T\vec{b}_k$, a scalar, represents the projection of the k'th control channel onto the i'th mode. We say that the i'th mode is controllable from the k'th input if the product is nonzero. If a given mode i has $\vec{w}_i^T\vec{b}_k = 0$ for all input channels k, then the mode is uncontrollable.
In normal applications, controllability for the entire system is checked using the following test: Construct the so-called controllability matrix:

$$M_c = [B, AB, \cdots, A^{n-1}B]. \tag{174}$$

This matrix has size $n \times (nm)$, where m is the number of input channels. If M_c has rank n, then the system is controllable, i.e., all modes are controllable.

16.4 Plant Output and Observability

We now turn to a related question: can the complete state vector of the system be observed given only the output measurements $\vec{y}$, and the known control $\vec{u}$? The response due to the external input is easy to compute deterministically, through the convolution integral. Consider the part due to initial conditions $\vec{\chi}$. We found above

$$\vec{x}(t) = \sum_{i=1}^{n} e^{\lambda_i t} \vec{v}_i \vec{w}_i^T \vec{\chi}.$$

The observation is $\vec{y} = C\vec{x}$ (r channels of output), and writing

$$C = \begin{bmatrix} \vec{c}_1^T \\ \cdot \\ \vec{c}_r^T \end{bmatrix}.$$

the k'th channel of the output is

$$y_k(t) = \sum_{i=1}^{n} (\vec{c}_k^T \vec{v}_i) e^{\lambda_i t} (\vec{w}_i^T \vec{\chi}).$$

The i'th mode is observable in the k'th output if the product $\vec{c}_k^T \vec{v}_i \neq 0$. We say that a system is observable if every mode can be seen in at least one output channel. The usual test for system observability requires computation of the observability matrix:

$$M_o = \left[C^T, A^T C^T, \cdots, (A^T)^{n-1} C^T \right]. \tag{175}$$

This matrix has size $n \times (rn)$; the system is observable if M_o has rank n.

17 CONTROL SYSTEMS – LOOPSHAPING

17.1 Introduction

This section formalizes the notion of loopshaping for linear control system design. The loopshaping approach is inherently two-fold. First, we shape the open-loop transfer function (or matrix) $P(s)C(s)$, to meet performance and robustness specifications. Once this is done, then the compensator must be computed, from from knowing the nominal product $P(s)C(s)$, and the nominal plant $P(s)$.

Most of the analysis here is given for single-input, single-output systems, but the link to multivariable control is not too difficult. In particular, absolute values of transfer functions are replaced with the maximum singular values of transfer matrices. Design based on singular values is the idea of L_2-control, or LQG/LTR, to be presented in the next lectures.

17.2 Roots of Stability – Nyquist Criterion

We consider the SISO feedback system with reference trajectory $r(s)$ and plant output $y(s)$, as given previously. The tracking error signal is defined as $e(s) = r(s) - y(s)$, thus forming the negative feedback loop. The sensitivity function is written as

$$S(s) = \frac{e(s)}{r(s)} = \frac{1}{1 + P(s)C(s)},$$

where $P(s)$ represents the plant transfer function, and $C(s)$ the compensator. The closed-loop *characteristic equation*, whose roots are the poles of the closed-loop system, is $1 + P(s)C(s) = 0$, equivalent to $\underline{P}(s)\underline{C}(s) + \overline{P}(s)\overline{C}(s) = 0$, where the underline and overline denote the denominator and numerator, respectively. The Nyquist criterion allows us to assess the stability properties of a system based on $P(s)C(s)$ only. This method for design involves plotting the complex loci of $P(s)C(s)$ for the range $\omega = [-\infty, \infty]$. There is no explicit calculation of the closed-loop poles, and in this sense the design approach is quite different from the root-locus method (see Ogata).

17.2.1 Mapping Theorem

We impose a reasonable assumption from the outset: The number of poles in $P(s)C(s)$ exceeds the number of zeros. It is a reasonable constraint because otherwise the loop transfer function could pass signals with infinitely high frequency. In the case of a PID controller (two zeros) and a second-order zeroless plant, this constraint can be easily met by adding a high-frequency rolloff to the compensator, the equivalent of low-pass filtering the error signal.
Let $F(s) = 1 + P(s)C(s)$. The heart of the Nyquist analysis is the mapping theorem, which answers the following question: How do paths in the s-plane map into paths in the F-plane? We limit ourselves to *closed, clockwise*(CW) paths in the s-plane, and the remarkable result of the mapping theorem is
Every zero of $F(s)$ enclosed in the s-plane generates exactly one CW encirclement of the origin in the $F(s)$-plane. Conversely, every pole of $F(s)$ enclosed in the s-plane generates exactly one CCW encirclement of the origin in the $F(s)$-plane. Since CW and CCW encirclements of the origin may cancel, the relation is often written $Z - P = CW$.
The trick now is to make the trajectory in the s-plane enclose all unstable poles, i.e., the path encloses the entire right-half plane, moving up the imaginary axis, and then proceeding to the right at an arbitrarily large radius, back to the negative imaginary axis.
Since the zeros of $F(s)$ are in fact the poles of the closed-loop transfer function, e.g., $S(s)$, stability requires that there are *no* zeros of $F(s)$ in the right-half s-plane. This leads to a slightly shorter form of the above relation:

$$P = CCW. \tag{176}$$

In words, stability requires that the number of unstable poles in $F(s)$ is equal to the number of CCW encirclements of the origin, as s sweeps around the entire right-half s-plane.

17.2.2 Nyquist Criterion

The Nyquist criterion now follows from one translation. Namely, encirclements of the origin by $F(s)$ are equivalent to encirclements of the point $(-1 + 0j)$ by $F(s) - 1$, or $P(s)C(s)$. Then the stability criterion can be cast in terms of the *unstable poles of $P(s)C(s)$, instead of those of $F(s)$*:

$$P = CCW \longleftrightarrow \text{ closed-loop stability} \tag{177}$$

This is in fact the complete Nyquist criterion for stability. It is a necessary and sufficient condition that the number of unstable poles in the loop transfer function $P(s)C(s)$ must be matched by an equal number of CCW encirclements of the critical point $(-1 + 0j)$.
There are several details to keep in mind when making Nyquist plots:

- If neither the plant nor the controller have unstable modes, then the loci of $P(s)C(s)$ must not encircle the critical point at all.
- Because the path taken in the s-plane includes negative frequencies (i.e., the negative imaginary axis), the loci of $P(s)C(s)$ occur as complex conjugates – the plot is symmetric about the real axis.
- The requirement that the number of poles in $P(s)C(s)$ exceeds the number of zeros means that at high frequencies, $P(s)C(s)$ always decays such that the loci go to the origin.
- For the multivariable (MIMO) case, the procedure of looking at individual Nyquist plots for each element of a transfer matrix is unreliable and outdated. Referring to the multivariable definition of $S(s)$, we should count the encirclements for the function $[det(I + P(s)C(s)) - 1]$ instead of $P(s)C(s)$. The use of gain and phase margin in design is similar to the SISO case.

17.2.3 Robustness on the Nyquist Plot

The question of robustness in the presence of modelling errors is central to control system design. There are two natural measures of robustness for the Nyquist plot, each having a very clear graphical representation. The loci need to stay away from the critical point; how close the loci come to it can be expressed in terms of magnitude and angle.

- When the angle of $P(s)C(s)$ is $-180°$, the magnitude $|P(s)C(s)|$ should not be near one.
- When the magnitude $|P(s)C(s)| = 1$, its angle should not be $-180°$.

These notions lead to definition of the *gain margin* k_g and *phase margin* γ for a design. As the figure shows, the definition of k_g is different for stable and unstable $P(s)C(s)$. Rules of thumb are as follows. For a stable plant, $k_g \geq 2$ and $\gamma \geq 30°$; for an unstable plant, $k_g \leq 0.5$ and $\gamma \geq 30°$.

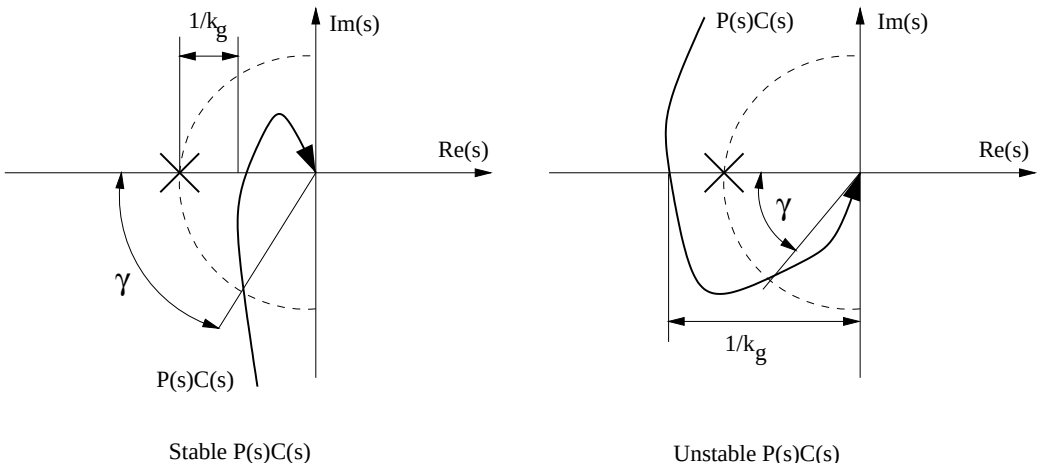

17.3 Design for Nominal Performance

Performance requirements of a feedback controller, using the nominal plant model, can be cast in terms of the Nyquist plot. We restrict the discussion to the scalar case in the following sections.
Since the sensitivity function maps reference input $r(s)$ to tracking error $e(s)$, we know that $|S(s)|$ should be small at low frequencies. For example, if one-percent tracking is to be maintained for all frequencies below $\omega = \lambda$, then $|S(s)| < 0.01, \forall \omega < \lambda$. This can be formalized by writing

$$|W_1(s)S(s)| < 1, \tag{178}$$

where $W_1(s)$ is a stable weighting function of frequency. To force $S(s)$ to be small at low ω, $W_1(s)$ should be large in the same range. The requirement $|W_1(s)S(s)| < 1$ is equivalent to $|W_1(s)| < |1 + P(s)C(s)|$, and this latter condition can be interpreted as: The loci of $P(s)C(s)$ must stay outside the disk of radius $W_1(s)$, which is to be centered on the critical point $(-1 + 0j)$. The disk is to be quite large, possibly infinitely large, at the lower frequencies.

17.4 Design for Robustness

It is a ubiquitous observation that models of plants degrade with increasing frequency. For example, the DC gain and slow, lightly-damped modes or zeros are easy to observe, but higher-frequency components in the response may

be hard to capture or even excite repeatably. Higher-frequency behavior may have more nonlinear properties as well.
The effects of modeling uncertainty can be considered to enter the nominal feedback system as a disturbance at the plant output, d_y. One of the most useful descriptions of model uncertainty is the multiplicative uncertainty:

$$\tilde{P}(s) = (1 + \Delta(s)W_2(s))P(s). \tag{179}$$

Here, $P(s)$ represents the nominal plant model used in the design of the control loop, and $\tilde{P}(s)$ is the actual, perturbed plant. The perturbation is of the multiplicative type, $\Delta(s)W_2(s)P(s)$, where $\Delta(s)$ is an *unknown but stable* function of frequency for which $|\Delta(s)| \leq 1$. The weighting function $W_2(s)$ scales $\Delta(s)$ with frequency; $W_2(s)$ should be growing with increasing frequency, since the uncertainty grows. However, $W_2(s)$ should not grow any faster than necessary, since it will turn out to be at the cost of nominal performance.
In the scalar case, the weight can be estimated as follows: since $\tilde{P}/P - 1 = \Delta W_2$, it will suffice to let $|\tilde{P}/P - 1| < |W_2|$.

Example: Let $\tilde{P} = k/(s-1)$, where k is in the range 2–5. We need to create a nominal model $P = k_0/(s-1)$, with the smallest possible value of W_2, which will not vary with frequency in this case. Two equations can be written using the above estimate, for the two extreme values of k, yielding $k_0 = 7/2$, and $W_2 = 3/7$.

For constructing the Nyquist plot, we observe that
$\tilde{P}(s)C(s) = (1+\Delta(s)W_2(s))P(s)C(s)$. The path of the perturbed plant could be anywhere on a disk of radius $|W_2(s)P(s)C(s)|$, centered on the nominal loci $P(s)C(s)$. The robustness condition is that this disk should not intersect the critical point. This can be written as

$$\begin{aligned} |1 + PC| &> |W_2PC| \longleftrightarrow \\ 1 &> \frac{|W_2PC|}{|1 + PC|} \longleftrightarrow \\ 1 &> |W_2T|, \end{aligned} \tag{180}$$

where T is the complementary sensitivity function. The last inequality is thus a condition for robust stability in the presence of multiplicative uncertainty parametrized with W_2.

17.5 Robust Performance

The condition for good performance with plant uncertainty is a combination of the above two conditions. Graphically, the disk at the critical point, with radius $|W_1|$, should not intersect the disk of radius $|W_2PC|$, centered on the nominal locus PC. This is met if

$$|W_1S| + |W_2T| < 1. \tag{181}$$

The robust performance requirement is related to the magnitude $|PC|$ at different frequencies, as follows:

1. At low frequency, $|W_1S| \simeq |W_1/PC|$, since $|PC|$ is large. This leads directly to the performance condition $|PC| > |W_1|$ in this range.

2. At high frequency, $W_2T| \simeq |W_2PC|$, since $|PC|$ is small. We must therefore have $|PC| < 1/|W_2|$, for robustness.

17.6 Implications of Bode's Integral

The loop transfer function PC cannot roll off too rapidly in the crossover region. The simple reason is that a steep slope induces a large phase loss, which in turn degrades the phase margin. To see this requires a short foray into Bode's integral. For a transfer function $H(s)$, the crucial relation is

$$angle(H(j\omega_0)) = \frac{1}{\pi}\int_{-\infty}^{\infty} \frac{d}{d\nu}(ln|H(j\omega)) \cdot ln(coth(|\nu|/2))d\nu, \tag{182}$$

where $\nu = ln(\omega/\omega_0)$. The integral is hence taken over the log of a frequency normalized with ω_0. It is not hard to see how the integral controls the angle: the function $ln(coth(|\nu|/2))$ is nonzero only near $\nu = 0$, implying that the angle depends only on the local slope $d(ln|H|)/d\nu$. Thus, if the slope is large, the angle is large.

Example: Suppose $H(s) = \omega_0^n/s^n$, i.e., it is a simple function with n poles at the origin, and no zeros; ω_0 is a fixed constant. It follows that $|H| = \omega_0^n/\omega^n$, and $ln|H| = -nln(\omega/\omega_0)$, so that $d(ln|H|)/d\nu = -n$. Then we have just

$$angle(H) = -\frac{n}{\pi}\int_{-\infty}^{\infty} ln(coth(|\nu|/2))d\nu = -\frac{n\pi}{2}. \tag{183}$$

This integral is trivial to look up or compute. Each pole at the origin clearly induces 90° of phase loss. In the general case, each pole not at the origin induces 90° of phase loss for frequencies above the pole. Each zero at the origin adds 90° phase lead, while zeros not at the origin at 90° of phase lead for frequencies above the zero. In the immediate neighborhood of these poles and zeros, the phase may vary significantly with frequency.
The Nyquist loci are clearly susceptible to these variations is phase, and the phase margin can be easily lost if the slope of PC at crossover (where the magnitude is unity) is too steep. The slope can safely be first-order ($-20dB/decade$, equivalent to a single pole), and may be second-order ($-40dB/decade$) if an adequate phase angle can be maintained near crossover.

17.7 The Recipe for Loopshaping

In the above analysis, we have extensively described what the open loop transfer function PC should look like, to meet robustness and performance specifications. We have said very little about how to get the compensator C, the critical component. For clarity, let the designed loop transfer function be renamed, $L = PC$. We will use concepts from optimal linear control for the MIMO case, but in the scalar case, it suffices to just pick

$$C = L/P. \tag{184}$$

This extraordinarily simple step involves a plant inversion.
The overall idea is to first shape L as a stable transfer function meeting the requirements of stability and robustness, and then divide through by the plant.

- When the plant is stable and has stable zeros (minimum-phase), the division can be made directly.
- One caveat for the well-behaved plant is that lightly-damped poles or zeros should not be cancelled verbatim by the compensator, because the closed-loop response will be sensitive to any slight change in the resonant frequency. The usual procedure is to widen the notch or pole in the compensator, through a higher damping ratio.
- Non-minimum phase or unstable behavior in the plant can usually be handled by performing the loopshaping for the closest stable model, and then explicitly considering the effects of adding the unstable parts. In

the case of unstable zeros, we find that they impose an unavoidable frequency limit for the crossover. In general, the troublesome zeros must be *faster* than the closed-loop frequency response.

In the case of unstable poles, the converse is true: The feedback system must be faster than the corresponding frequency of the unstable mode.

When a control system involves multiple inputs and outputs, the ideas from scalar loopshaping can be adapted using the singular value. We list below some basic properties of the singular value decomposition, which is analogous to an eigenvector, or modal, analysis. Useful properties and relations for the singular value are found in the section *MATH FACTS*.
The condition for MIMO robust performance can be written in many ways, including a direct extension of our scalar condition

$$\overline{\sigma}(W_1 S) + \overline{\sigma}(W_2 T) < 1. \tag{185}$$

The open-loop transfer matrix L should be shaped accordingly. In the following sections, we use the properties of optimal state estimation and control to perform the plant inversion for MIMO systems.

18 LINEAR QUADRATIC REGULATOR

18.1 Introduction

The simple form of loopshaping in scalar systems does not extend directly to multivariable (MIMO) plants, which are characterized by transfer matrices instead of transfer functions.
The notion of optimality is closely tied to MIMO control system design. Optimal controllers, i.e., controllers that are the *best* possible, according to some figure of merit, turn out to generate only stabilizing controllers for MIMO plants. In this sense, optimal control solutions provide an automated design procedure – we have only to decide what figure of merit to use. The linear quadratic regulator (LQR) is a well-known design technique that provides practical feedback gains.

18.2 Full-State Feedback

For the derivation of the linear quadratic regulator, we assume the plant to be written in state-space form $\dot{x} = Ax + Bu$, and that *all* of the n states x are available for the controller. The feedback gain is a matrix K, implemented as $u = -K(x - x_{desired})$. The system dynamics are then written as:

$$\dot{x} = (A - BK)x + Kx_{desired}. \tag{186}$$

$x_{desired}$ represents the vector of desired states, and serves as the external input to the closed-loop system. The "A-matrix" of the closed loop system is $(A - BK)$, and the "B-matrix" of the closed-loop system is K. The closed-loop system has exactly as many outputs as inputs: n. The column dimension of B equals the number of channels available in u, and must match the row dimension of K. Pole-placement is the process of placing the poles of $(A-BK)$ in stable, suitably-damped locations in the complex plane.

18.3 Dynamic Programming

There are at least two conventional derivations for the LQR; we present here one based on *dynamic programming*, due to R. Bellman. The key observation is best given through a loose example:
Suppose that we are driving from Point A to Point C, and we ask what is the shortest path in miles. If A and C represent Los Angeles and Boston,

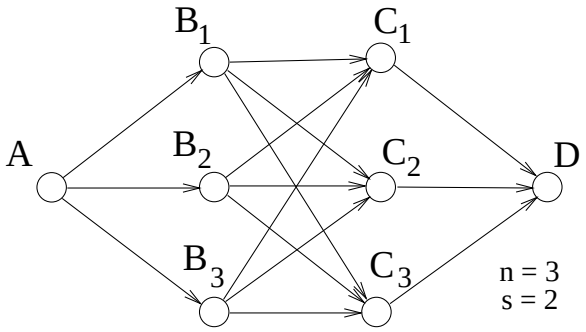

for example, there are *many* paths to choose from! Assume that one way or another we have found the best path, and that a Point B lies along this path, say Las Vegas. Let X be an arbitrary point east of Las Vegas. If we were to now solve the optimization problem for getting from only Las Vegas to Boston, this same arbitrary point X would be along the new optimal path as well.
The point is a subtle one: the optimization problem from Las Vegas to Boston is easier than that from Los Angeles to Boston, and the idea is to use this property *backwards* through time to evolve the optimal path, beginning in Boston.

Example: Nodal Travel. We now add some structure to the above experiment. Consider now traveling from point A (Los Angeles) to Point D (Boston). Suppose there are only three places to cross the Rocky Mountains, B_1, B_2, B_3, and three places to cross the Mississippi River, C_1, C_2, C_3.[3] By way of notation, we say that the path from A to B_1 is AB_1. Suppose that all of the paths (and distances) from A to the B-nodes are known, as are those from the B-nodes to the C-nodes, and the C-nodes to the terminal point D. There are nine unique paths from A to D.
A brute-force approach sums up the total distance for all the possible paths, and picks the shortest one. In terms of computations, we could summarize that this method requires nine additions of three numbers, equivalent to eighteen additions of two numbers. The *comparison* of numbers is relatively cheap.
The dynamic programming approach has two steps. First, from each B-node, pick the best path to D. There are three possible paths from B_1 to D, for example, and nine paths total from the B-level to D. Store the best paths as $B_1D|_{opt}, B_2D|_{opt}, B_3D|_{opt}$. This operation involves nine additions of two

[3]Apologies to readers not familiar with American geography.

numbers.
Second, compute the distance for each of the possible paths from A to D, *constrained to the optimal paths from the B-nodes onward*: $AB_1 + B_1D|_{opt}$, $AB_2 + B_2D|_{opt}$, or $AB_3 + B_3D|_{opt}$. The combined path with the shortest distance is the total solution; this second step involves three sums of two numbers, and total optimization is done in twelve additions of two numbers.
Needless to say, this example gives only a mild advantage to the dynamic programming approach over brute force. The gap widens vastly, however, as one increases the dimensions of the solution space. In general, if there are s layers of nodes (e.g., rivers or mountain ranges), and each has width n (e.g., n river crossing points), the brute force approach will take (sn^s) additions, while the dynamic programming procedure involves only $(n^2(s-1)+n)$ additions. In the case of $n = 5$, $s = 5$, brute force requires 6250 additions; dynamic programming needs only 105.

18.4 Dynamic Programming and Full-State Feedback

We consider here the regulation problem, that is, of keeping $x_{desired} = 0$. The closed-loop system thus is intended to reject disturbances and recover from initial conditions, but not necessarily follow y-trajectories. There are several necessary definitions. First we define an instantaneous *penalty* function $l(x(t), u(t))$, which is to be greater than zero for all nonzero x and u. The *cost* associated with this penalty, along an optimal trajectory, is

$$J = \int_0^\infty l(x(t), u(t))dt, \tag{187}$$

i.e., the integral over time of the instantaneous penalty. Finally, the *optimal return* is the cost of the optimal trajectory remaining after time t:

$$V(x(t), u(t)) = \int_t^\infty l(x(\tau), u(\tau))d\tau. \tag{188}$$

.
We have directly from the dynamic programming principle

$$V(x(t), u(t)) = \min_u \left\{ l(x(t), u(t))\delta t + V(x(t+\delta t), u(t+\delta t)) \right\}. \tag{189}$$

The minimization of $V(x(t), u(t))$ is made by considering all the possible control inputs u in the time interval $(t, t+\delta t)$. As suggested by dynamic programming, the return at time t is constructed from the return at $t+\delta t$, and

the differential component due to $l(x,u)$. If V is smooth and has no explicit dependence on t, as written, then

$$\begin{aligned} V(x(t+\delta t),u(t+\delta t)) &= V(x(t),u(t)) + \frac{\partial V}{\partial x}\frac{dx}{dt}\,\delta t + h.o.t. \longrightarrow \quad (190) \\ &= V(x(t),u(t)) + \frac{\partial V}{\partial x}(Ax(t)+Bu(t))\delta t. \end{aligned}$$

Now control input u in the interval $(t, t+\delta t)$ cannot affect $V(x(t),u(t))$, so inserting the above and making a cancellation gives

$$0 = \min_u \left\{ l(x(t),u(t)) + \frac{\partial V}{\partial x}(Ax(t)+Bu(t)) \right\}. \quad (191)$$

We next make the assumption that $V(x,u)$ has the following form:

$$V(x,u) = \frac{1}{2}x^T P x, \quad (192)$$

where P is a symmetric matrix, and positive definite.[4][5] It follows that

$$\begin{aligned} \frac{\partial V}{\partial x} &= x^T P \longrightarrow \quad (193) \\ 0 &= \min_u \left\{ l(x,u) + x^T P(Ax+Bu) \right\}. \end{aligned}$$

We finally specify the instantaneous penalty function. The LQR employs the special quadratic form

$$l(x,u) = \frac{1}{2}x^T Q x + \frac{1}{2}u^T R u, \quad (194)$$

where Q and R are both symmetric and positive definite. The matrices Q and R are to be set by the user, and represent the main "tuning knobs" for the LQR. Substitution of this form into the above equation, and setting the derivative with respect to u to zero gives

[4]Positive definiteness means that $x^T P x > 0$ for all nonzero x, and $x^T P x = 0$ if $x = 0$.

[5]This suggested form for the optimal return can be confirmed after the optimal controller is derived.

$$\begin{aligned} 0 &= u^T R + x^T PB \\ u^T &= -x^T PBR^{-1} \\ u &= -R^{-1}B^T Px. \end{aligned} \tag{195}$$

The **gain matrix** for the feedback control is thus $K = R^{-1}B^T P$. Inserting this solution back into equation 194, and eliminating u in favor of x, we have

$$0 = \frac{1}{2}x^T Qx - \frac{1}{2}x^T PBR^{-1}B^T P + x^T PAx.$$

All the matrices here are symmetric except for PA; since $x^T PAx = x^T A^T Px$, we can make its effect symmetric by letting

$$x^T PAx = \frac{1}{2}x^T PAx + \frac{1}{2}x^T A^T Px,$$

leading to the final matrix-only result

$$0 = Q + PA + A^T P - PBR^{-1}B^T P. \tag{196}$$

This equation is the *matrix algebraic Riccati equation* (MARE), whose solution P is needed to compute the optimal feedback gain K. The MARE is easily solved by standard numerical tools in linear algebra.

18.5 Properties and Use of the LQR

Static Gain. The LQR generates a static gain matrix K, which is not a dynamical system. Hence, the order of the closed-loop system is the same as that of the plant.

Robustness. The LQR achieves infinite gain margin: $k_g = \infty$, implying that the loci of (PC) (scalar case) or $(det(I + PC) - 1)$ (MIMO case) approach the origin along the imaginary axis. The LQR also guarantees phase margin $\gamma \geq 60$ degrees. This is in good agreement with the practical guidelines for control system design.

Output Variables. In many cases, it is not the states x which are to be minimized, but the output variables y. In this case, we set the weighting matrix $Q = C^T Q' C$, since $y = Cx$, and the auxiliary matrix Q' weights the plant output.

Behavior of Closed-Loop Poles: Expensive Control. When $R >> C^T Q' C$, the cost function is dominated by the control effort u, and so the controller minimizes the control action itself. In the case of a completely stable plant, the gain will indeed go to zero, so that the closed-loop poles approach the open-loop plant poles in a manner consistent with the scalar root locus.
The optimal control *must* always stabilize the closed-loop system, however, so there should be some account made for unstable plant poles. The expensive control solution puts stable closed-loop poles at the *mirror* images of the unstable plant poles.

Behavior of Closed-Loop Poles: Cheap Control. When $R << C^T Q' C$, the cost function is dominated by the output errors y, and there is no penalty for using large u. There are two groups of closed-loop poles. First, poles are placed at stable plant zeros, and at the mirror images of the unstable plant zeros. This part is akin to the high-gain limiting case of the root locus. The remaining poles assume a Butterworth pattern, whose radius increases to infinity as R becomes smaller and smaller.
The Butterworth pattern refers to an arc in the stable left-half plane, as shown in the figure. The angular separation of n closed-loop poles on the arc is constant, and equal to $180°/n$. An angle $90°/n$ separates the most lightly-damped poles from the imaginary axis.

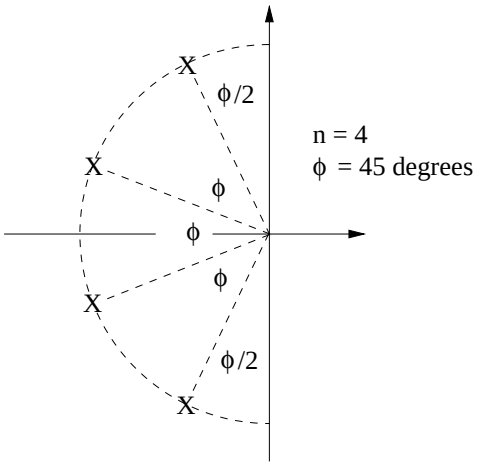
X
X
X
X
ϕ/2
ϕ
ϕ
ϕ
ϕ/2
n = 4
ϕ = 45 degrees

19 KALMAN FILTER

19.1 Introduction

In the previous section, we derived the linear quadratic regulator as an optimal solution for the full-state feedback control problem. The inherent assumption was that each state was known perfectly. In real applications, the measurements are subject to disturbances, and may not allow reconstruction of all the states. This *state estimation* is the task of a model-based estimator having the form:

$$\dot{\hat{x}} = A\hat{x} + Bu + H(y - C\hat{x}) \tag{197}$$

The vector $\hat{x}$ represents the state estimate, whose evolution is governed by the nominal A and B matrices of the plant, and a correction term with the estimator gain matrix H. H operates on the estimation error mapped to the plant output y, since $C\hat{x} = \hat{y}$. Given statistical properties of real plant disturbances and sensor noise, the *Kalman Filter* designs an optimal H.

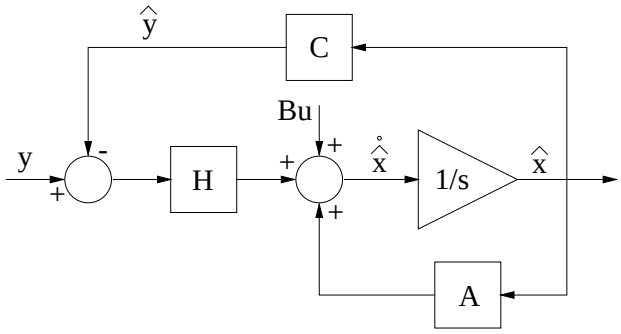

19.2 Problem Statement

We consider the state-space plant model given by:

$$\begin{aligned} \dot{x} &= Ax + Bu + W_1 \\ y &= Cx + W_2. \end{aligned} \tag{198}$$

There are n states, m inputs, and l outputs, so that A has dimension $n \times n$, B is $n \times m$, and C is $l \times n$. The plant subject to two random input signals, W_1

and W_2. W_1 represents disturbances to the plant, since it drives $\dot{x}$ directly; W_2 denotes sensor noise, which corrupts the measurement y.
An important assumption of the Kalman Filter is that W_1 and W_2 are each vectors of unbiased, independent white noise, and that all the $n + l$ channels are uncorrelated. Hence, if $E(\cdot)$ denotes the expected value,

$$\begin{aligned} E(W_1(t_1)W_1(t_2)^T) &= V_1\delta(t_1 - t_2) && (199)\\ E(W_2(t_1)W_2(t_2)^T) &= V_2\delta(t_1 - t_2) && (200)\\ E(W_1(t)W_2(t)^T) &= 0_{n\times l}. && (201) \end{aligned}$$

Here $\delta(t)$ represents the impulse (or delta) function. V_1 is an $n \times n$ diagonal matrix of intensities, and V_2 is an $l \times l$ diagonal matrix of intensities.
The estimation error may be defined as $e = x - \hat{x}$. It can then be verified that

$$\begin{aligned} \dot{e} &= [Ax + Bu + W_1] - [A\hat{x} + Bu + H(y - C\hat{x})] && (202)\\ &= (A - HC)e + (W_1 - HW_2). \end{aligned}$$

The eigenvalues of the matrix $A - HC$ thus determine the stability properties of the estimation error dynamics. The second term above, $W_1 + HW_2$ is considered an external input.
The Kalman filter design provides H that minimizes the scalar cost function

$$J = E(e^T W e), \tag{203}$$

where W is an unspecified symmetric, positive definite weighting matrix. A related matrix, the symmetric *error covariance*, is defined as

$$\Sigma = E(ee^T). \tag{204}$$

There are two main steps for deriving the optimal gain H.

19.3 Step 1: An Equation for $\dot{\Sigma}$

The evolution of Σ follows from some algebra and the convolution form of $e(t)$. We begin with

$$\begin{aligned}\dot{\Sigma} &= E(\dot{e}e^T + e\dot{e}^T) \\ &= E[(A-HC)ee^T + (W_1 - HW_2)e^T + ee^T(A^T - C^TH^T) + \\ &\quad e(W_1^T - W_2^TH^T)].\end{aligned} \tag{205}$$

The last term above can be expanded, using the property that

$$e(t) = e^{(A-HC)t}e(0) + \int_0^t e^{(A-HC)(t-\tau)}(W_1(\tau) - HW_2(\tau))\, d\tau.$$

We have

$$\begin{aligned}E(e(W_1^T - W_2^TH^T)) &= e^{(A-HC)t}E(e(0)(W_1^T - W_2^TH^T)) + \\ &\quad \int_0^t e^{(A-HC)(t-\tau)}E((W_1(\tau) - HW_2(\tau)) \\ &\quad\quad (W_1^T(t) - W_2^T(t)H^T))\, d\tau \\ &= \int_0^t e^{(A-HC)(t-\tau)}E((W_1(\tau) - HW_2(\tau)) \\ &\quad\quad (W_1^T(t) - W_2^T(t)H^T))\, d\tau \\ &= \int_0^t e^{(A-HC)(t-\tau)}(V_1\delta(t-\tau) + HV_2H^T\delta(t-\tau))\, d\tau \\ &= \frac{1}{2}V_1 + \frac{1}{2}HV_2H^T.\end{aligned}$$

To get from the first right-hand side to the second, we note that the initial condition $e(0)$ is uncorrelated with $W_1^T - W_2^TH^T$. The fact that W_1 and HW_2 are uncorrelated leads to the third line, and the final result follows from

$$\int_0^t \delta(t-\tau)d\tau = \frac{1}{2},$$

i.e., the written integral includes only *half* of the impulse.
The final expression for $E(e(W_1^T - W_2^TH^T))$ is symmetric, and therefore appears in Equation 205 twice, leading to

$$\dot{\Sigma} = (A-HC)\Sigma + \Sigma(A^T - C^TH^T) + V_1 + HV_2H^T. \tag{206}$$

This equation governs propagation of the error covariance. It is independent of the initial condition $e(0)$, and depends on the (as yet) unknown estimator gain matrix H.

19.4 Step 2: H as a Function of Σ

We now make the connection between $\Sigma = E(ee^T)$ (a matrix) and $J = E(e^TWe)$ (a scalar). The *trace* of a matrix is the sum of its diagonal elements, and it can be verified that

$$J = E(e^TWe) = trace(\Sigma W). \tag{207}$$

We now introduce an auxiliary cost function defined as

$$J' = trace(\Sigma W + \Lambda F), \tag{208}$$

where F is an $n \times n$ matrix of zeros, and Λ is an $n \times n$ matrix of unknown Lagrange multipliers. Note that since F is zero, $J' = J$, so minimizing J' solves the same problem. Lagrange multipliers provide an ingenious mechanism for drawing constraints into the optimization; the constraint we invoke is the evolution of Σ, Equation 206:

$$J' = trace\left(\Sigma W + \Lambda(-\dot{\Sigma} + A\Sigma - HC\Sigma + \Sigma A^T - \Sigma C^T H^T + V_1 + HV_2H^T)\right) \tag{209}$$

If J' is an optimal cost, it follows that $\partial J'/\partial H = 0$, i.e., the correct choice of H achieves an extremal value. We need the following lemmas, which give the derivative of a trace with respect to a constituent matrix:

$$\begin{aligned} \frac{\partial}{\partial H} trace(-\Lambda HC\Sigma) &= -\Lambda^T\Sigma C^T \\ \frac{\partial}{\partial H} trace(-\Lambda\Sigma C^T H^T) &= -\Lambda\Sigma C^T \\ \frac{\partial}{\partial H} trace(\Lambda HV_2H^T) &= \Lambda^T HV_2 + \Lambda HV_2. \end{aligned}$$

Proofs of the first two are given at the end of this section; the last lemma uses the chain rule, and the previous two lemmas. Next, we enforce $\Lambda = \Lambda^T$, since the values are arbitrary. Then the condition $\partial J'/\partial H = 0$ leads to

$$\begin{aligned} 0 &= 2\Lambda(-\Sigma C^T + HV_2), \text{ satisfied if} \\ H &= \Sigma C^T V_2^{-1}. \end{aligned} \tag{210}$$

Duality of Linear Quadratic Regulator and Kalman Filter

Linear Quadratic Regulator	Kalman Filter
$\dot{x} = Ax + Bu$	$\dot{x} = Ax + Bu + W_1$
	$y = Cx + W_2$
$u = -Kx$	$\dot{\hat{x}} = A\hat{x} + Bu + H(y - C\hat{x})$
$2J = \int_0^\infty (x^T Q x + u^T R u) dt$	$J = E(e^T W e)$
$Q \geq 0, R > 0$	$V_1 \geq 0$, $V_2 > 0$
$K = R^{-1} B^T P$	$H = \Sigma C^T V_2^{-1}$
$PA + A^T P + Q - PBR^{-1}B^T P = 0$	$\Sigma A^T + A\Sigma + V_1 - \Sigma C^T V_2^{-1} C\Sigma = 0$

Hence the estimator gain matrix H can be written as a function of Σ. Inserting this back into Equation 206, we obtain

$$\dot{\Sigma} = A\Sigma + \Sigma A^T + V_1 - \Sigma C^T V_2^{-1} C\Sigma. \tag{211}$$

Equations 210 and 211 represent the practical solution to the Kalman filtering problem, which minimizes the squared-norm of the estimation error. The evolution of Σ is always stable, and depends only on the constant matrices $[A, C, V_1, V_2]$. Notice also that the result is independent of the weighting matrix W, which might as well be the identity.

19.5 Properties of the Solution

The solution involves a matrix Riccati equation, like the LQR, suggesting a duality with the LQR problem. This is in fact the case, and the same analysis and numerical tools can be applied to both methodologies.
The steady-state solution for Σ is valid for time-invariant systems, leading to a more common MARE form of Equation 211:

$$0 = A\Sigma + \Sigma A^T + V_1 - \Sigma C^T V_2^{-1} C\Sigma. \tag{212}$$

The Kalman Filter is guaranteed to create a stable nominal dynamics $A - HC$, as long as the plant is fully state-observable. This is dual to the stability guarantee of the LQR loop, when the plant is state-controllable. Furthermore, like the LQR, the KF loop achieves 60° phase margin, and infinite gain margin, for all the channels together or independently.

The qualitative dependence of the estimator gain $H = \Sigma C^T V_2^{-1}$ on the other parameters can be easily seen. Recall that V_1 is the intensity matrix of the plant disturbance, V_2 is the intensity of the sensor noise, and Σ is the error covariance matrix.

- A large uncertainty Σ creates large H, placing emphasis on the corrective action of the filter.
- A small disturbance V_1, and large sensor noise V_2 creates a small H, weighting the model dynamics $A\hat{x} + Bu$ more.
- A large disturbance V_1, and small sensor noise V_2 creates a large H, so that the filter's correction is dominant.

The limiting closed-loop poles of the Kalman filter are similar, and dual to those of the LQR:

- $V_2 << V_1$: good sensors, large disturbance, $H >> 1$, *dual to cheap-control problem*. Some closed-loop poles go to the stable plant zeros, or the mirror image of unstable plant zeros. The remaining poles follow a Butterworth pattern whose radius increases with increasing V_1/V_2.
- $V_2 >> V_1$: poor sensors, small disturbance, H small, *dual to expensive-control problem*. Closed-loop poles go to the stable plant poles, and the mirror images of the unstable plant poles.

19.6 Combination of LQR and KF

An optimal output feedback controller is created through the use of a Kalman filter coupled with an LQR full-state feedback gain. This combination is usually known as the Linear Quadratic Gaussian design, or LQG. For the plant given as

$$\begin{aligned} \dot{x} &= Ax + Bu + W_1 \\ y &= Cx + W_2, \end{aligned}$$

we put the Kalman Filter and controller gain G together as follows:

$$\dot{\hat{x}} = A\hat{x} + Bu + H(y - C\hat{x}) \quad (213)$$
$$u = -K\hat{x}. \quad (214)$$

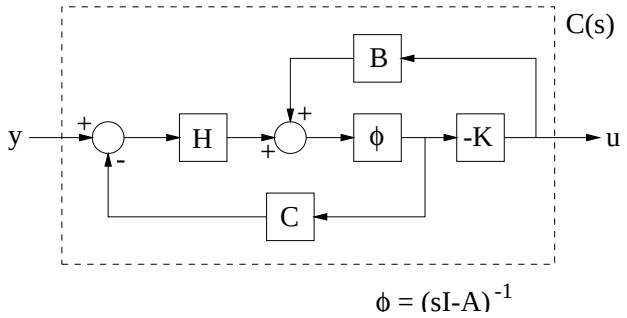

There are two central points to this construction:

1. **Separation Principle**: The eigenvalues of the nominal closed-loop system are made of up the eigenvalues of $(A - HC)$ and the eigenvalues of $(A - BK)$, separately. See proof below.

2. **Output Tracking:** This compensator is a stand-alone system that, as written, tries to drive its input y to zero. It can be hooked up to receive tracking error $e(s) = r(s) - y(s)$ as an input instead, so that it is not limited to the regulation problem alone. In this case, $\hat{x}$ no longer represents an estimated *state*, but rather an estimated state tracking error. We use the output error as a control input in the next section, on loopshaping via loop transfer recovery.

19.7 Proofs of the Intermediate Results

19.7.1 Proof that $E(e^T We) = trace(\Sigma W)$

$$\begin{aligned} E(e^T We) &= E\left(\sum_{i=1}^{n} e_i \left(\sum_{j=1}^{n} W_{ij} e_j\right)\right) \\ &= \sum_{i=1}^{n}\sum_{j=1}^{n} \Sigma_{ij} W_{ji}, \end{aligned}$$

the transpose of W being valid since it is symmetric. Now consider the diagonal elements of the product ΣW:

$$\begin{aligned}
\Sigma W &= \begin{bmatrix} \Sigma_{11}W_{11} + \Sigma_{12}W_{21} + \cdots & \cdot & \cdot \\ \cdot & \Sigma_{21}W_{12} + \Sigma_{22}W_{22} + \cdots & \cdot \\ \cdot & \cdot & \cdots \end{bmatrix} \rightarrow \\
trace(\Sigma W) &= \sum_{i=1}^{n}\sum_{j=1}^{n} \Sigma_{ij}W_{ji}. \quad \square
\end{aligned}$$

19.7.2 Proof that $\frac{\partial}{\partial H} trace(-\Lambda H C \Sigma) = -\Lambda^T \Sigma C^T$

$$\begin{aligned}
trace(AHB) &= trace\left[\sum_{j=1}^{n} A_{ij} \sum_{k=1}^{l} H_{jk}B_{kl}\right], \text{ the } il'\text{th element} \\
&= \sum_{i=1}^{n}\sum_{j=1}^{n} A_{ij} \sum_{k=1}^{l} H_{jk}B_{ki},
\end{aligned}$$

where the second form is a sum over i of the ii'th elements. Now

$$\begin{aligned}
\frac{\partial}{\partial H_{j_o k_o}} trace(AHB) &= \sum_{i=1}^{n} A_{ij_o}B_{k_o i} \\
&= (BA)_{k_o j_o} \\
&= (BA)^T_{j_o k_o} \longrightarrow \\
\frac{\partial}{\partial H} trace(AHB) &= (BA)^T \\
&= A^T B^T. \quad \square
\end{aligned}$$

19.7.3 Proof that $\frac{\partial}{\partial H} trace(-\Lambda \Sigma C^T H^T) = -\Lambda \Sigma C^T$

$$\begin{aligned}
trace(AH^T) &= trace\left[\sum_{j=1}^{n} A_{ij}H^T_{jl}\right], \text{ the } il'\text{th element} \\
&= trace\left[\sum_{j=1}^{n} A_{ij}H_{lj}\right] \\
&= \sum_{i=1}^{n}\sum_{j=1}^{n} A_{ij}H_{ij},
\end{aligned}$$

where the last form is a sum over the ii'th elements. It follows that

$$\begin{aligned} \frac{\partial}{\partial H_{i_o j_o}} trace(AH^T) &= A_{i_o j_o} \longrightarrow \\ \frac{\partial}{\partial H} trace(AH^T) &= A. \quad \square \end{aligned}$$

19.7.4 Proof of the Separation Principle

Without external inputs W_1 and W_2, the closed-loop system evolves according to

$$\frac{d}{dt} \left\{ \begin{array}{c} x \\ \hat{x} \end{array} \right\} = \left[\begin{array}{cc} A & -BK \\ HC & A - BK - HC \end{array} \right] \left\{ \begin{array}{c} x \\ \hat{x} \end{array} \right\}.$$

Using the definition of estimation error $e = x - \hat{x}$, we can write the above in another form:

$$\frac{d}{dt} \left\{ \begin{array}{c} x \\ e \end{array} \right\} = \left[\begin{array}{cc} A - BK & BK \\ 0 & A - HC \end{array} \right] \left\{ \begin{array}{c} x \\ e \end{array} \right\}.$$

If A' represents this compound A-matrix, then its eigenvalues are the roots of $det(sI - A') = 0$. However, the determinant of an upper triangular block matrix is the product of the determinants of each block on the diagonal: $det(sI - A') = det(sI - (A - BK))det(sI - (A - HC))$, and hence the separation of eigenvalues follows.

20 LOOP TRANSFER RECOVERY

20.1 Introduction

The Linear Quadratic Regulator(LQR) and Kalman Filter (KF) provide practical solutions to the full-state feedback and state estimation problems, respectively. If the sensor noise and disturbance properties of the plant are indeed well-known, then an *LQG* design approach, that is, combining the LQR and KF into an output feedback compensator, may yield good results. The LQR tuning matrices Q and R would be picked heuristically to give a reasonable closed-loop response.

There are two reasons to avoid this kind of direct LQG design procedure, however. First, although the LQR and KF each possess good robustness properties, there do exist plants for which there is *no* robustness guarantee for an LQG compensator. Even if one could steer clear of such pathological cases, a second problem is that this design technique has no clear equivalent in frequency space. It cannot be directly mapped to the intuitive ideas of loopshaping and the Nyquist plot, which are at the root of feedback control.

We now reconsider just the feedback loop of the Kalman filter. The KF has open-loop transfer function $L(s) = C\phi(s)H$, where $\phi(s) = (sI - A)^{-1}$. This follows from the estimator evolution equation

$$\dot{\hat{x}} = A\hat{x} + Bu + H(y - C\hat{x})$$

and the figure. Note that we have not included the factor Bu as part of the figure, since it does not affect the error dynamics of the filter.

As noted previously, the KF loop has good robustness properties, specifically to perturbations at the output $\hat{y}$, and further is amenable to output tracking. In short, the KF loop is an ideal candidate for a loopshaping design. Supposing that we have an estimator gain H which creates an attractive loop function $L(s)$, we would like to find the compensator $C(s)$ that establishes

$$\begin{aligned} P(s)C(s) &\approx C\phi(s)H, \text{ or} \\ C\phi(s)BC(s) &\approx C\phi(s)H. \end{aligned} \tag{215}$$

It will turn out that the LQR can be set up so that the an LQG-type compensator achieves exactly this result. The procedure is termed Loop Transfer

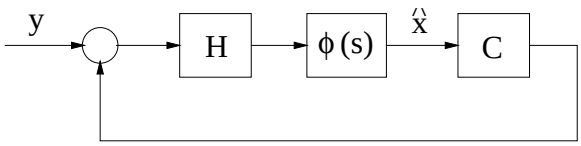

Recovery (LTR), and has two main parts. First, one carries out a KF design for H, so that the Kalman filter loop itself has good performance and robustness properties. In this regard, the KF loop has sensitivity function $S(s) = (I + C\phi(s)H)^{-1}$ and complementary sensitivity $T(s) = (I + C\phi(s)H)^{-1}C\phi(s)H$. The condition $\overline{\sigma}(W_1(s)S(s)) + \overline{\sigma}(W_2(s)T(s)) < 1$ is sufficient for robust performance with multiplicative plant uncertainty at the output. Secondly, we pick suitable parameters of the LQR design, so that the LQG compensator satisfies the approximation of Equation 215.
LTR is useful as a SISO control technique, but has a much larger role in multivariable control.

20.2 A Special Property of the LQR Solution

Letting $Q = C^TC$ and $R = \rho I$, where I is the identity matrix, we will show (roughly) that

$$\lim_{\rho \to 0}(\sqrt{\rho}K) = WC,$$

where K is the LQR gain matrix, and W is an orthonormal matrix, for which $W^TW = I$.
First recall the gain and Riccati equations for the LQR:

$$\begin{aligned} K &= R^{-1}B^TP \\ 0 &= Q + PA + A^TP - PBR^{-1}B^TP. \end{aligned}$$

Now $Q = C^TC = C^TW^TWC = (WC)^TWC$. The Riccati equation becomes

$$0 = \rho(WC)^TWC + \rho PA + \rho A^TP - PBB^TP = 0.$$

In the limit as $\rho \to 0$, it must be the case that $P \to 0$ also, and so in this limit

$$\begin{aligned}
\rho(WC)^T WC &\approx PBB^T P \\
&= (B^T P)^T B^T P \\
&= (R^{-1}B^T P)^T RR(R^{-1}B^T P) \\
&= \rho^2 K^T K \longrightarrow \\
WC &\approx \sqrt{\rho}K. \qquad \square
\end{aligned}$$

Note that another orthonormal matrix W' could be used in separating K^T from K in the last line. This matrix may be absorbed into W through a matrix inverse, however, and so does not need to be written. The result of the last line establishes that the plant must be square: the number of inputs (i.e., rows of K) is equal to the number of outputs (i.e., rows of C).
Finally, we note that the above property is true only for LQR designs with minimum-phase plants, i.e., those with only stable zeros (Kwakernaak and Sivan).

20.3 The Loop Transfer Recovery Result

The theorem is stated as: If $\lim_{\rho\to 0}(\sqrt{\rho}K) = WC$ (the above result), with W an orthonormal matrix, then the limiting LQG controller $C(s)$ satisfies

$$\lim_{\rho\to 0} P(s)C(s) = C\phi(s)H.$$

The LTR method is limited by two conditions:

- The plant has an equal number of inputs and outputs.
- The design plant has no unstable zeros. The LTR method can be in fact be applied in the presence of unstable plant zeros, but the recovery is not to the Kalman filter loop transfer function. Instead, the recovered function will exhibit reasonable limitations inherent to unstable zeros. See Athans for more details and references on this topic.

The proof of the LTR result depends on some easy lemmas, given at the end of this section. First, we develop $C(s)$, with the definitions $\phi(s) = (sI - A)^{-1}$ and $X(s) = (\phi^{-1}(s) + HC)^{-1} = (sI - A + HC)^{-1}$.

$$\begin{aligned}
C(s) &= K(sI - A + BK + HC)^{-1}H \\
&= K(X^{-1}(s) + BK)^{-1}H, \text{ then use Lemma 2} \rightarrow \\
&= K(X(s) - X(s)B(I + KX(s)B)^{-1}KX(s))H \\
&= KX(s)H - KX(s)B(I + KX(s)B)^{-1}KX(s)H \\
&= (I - KX(s)B(I + KX(s)B)^{-1})KX(s)H, \text{ then use Lemma 3} \rightarrow \\
&= (I + KX(s)B)^{-1}KX(s)H \\
&= (\sqrt{\rho}I + \sqrt{\rho}KX(s)B)^{-1}\sqrt{\rho}KX(s)H.
\end{aligned}$$

Next we invoke the result from the LQR design, with $\rho \rightarrow 0$, to eliminate $\sqrt{\rho}K$:

$$\begin{aligned}
\lim_{\rho \rightarrow 0} C(s) &= (WCX(s)B)^{-1}WCX(s)H \\
&= (CX(s)B)^{-1}CX(s)H.
\end{aligned}$$

In the last expression, we used the assumption that W is square and invertible, both properties of orthonormal matrices. Now we look at the product $CX(s)$:

$$\begin{aligned}
CX(s) &= C(SI - A + HC)^{-1} \\
&= C(\phi^{-1}(s) + HC)^{-1}, \text{ then use Lemma 2} \rightarrow \\
&= C(\phi(s) - \phi(s)H(I + C\phi(s)H)^{-1}C\phi(s)) \\
&= (I - C\phi(s)H(I + C\phi(s)H)^{-1})C\phi(s), \text{ then use Lemma 3} \rightarrow \\
&= (I + C\phi(s)H)^{-1}C\phi(s).
\end{aligned}$$

This result, reintroduced into the limiting compensator, gives

$$\begin{aligned}
\lim_{\rho \rightarrow 0} C(s) &= ((I + C\phi(s)H)^{-1}C\phi(s)B)^{-1}(I + C\phi(s)H)^{-1}C\phi(s)H \\
&= (C\phi(s)B)^{-1}C\phi(s)H \\
&= P^{-1}(s)C\phi(s)H.
\end{aligned}$$

Finally it follows that $\lim_{\rho \rightarrow 0} P(s)C(s) = C\phi(s)H$, as desired.

20.4 Usage of the Loop Transfer Recovery

The idea of LTR is to "recover" a Kalman filter loop transfer function $L(s) = C\phi(s)H$, by using the limiting cheap-control LQR design, with $Q = C^TC$ and $R = \rho I$. The LQR design step is thus trivial.
Some specific techniques are useful.

- *Scale the plant outputs* (and references), so that one unit of error in one channel is as undesirable as one unit of error in another channel. For example, in depth and pitch control of a large submarine, one meter of depth error cannot be compared directly with one radian of pitch error.

- *Scale the plant inputs* in the same way. One Newton of propeller thrust cannot be compared with one radian of rudder angle.

- *Design for crossover frequency.* The bandwidth of the controller is roughly equal to the frequency at which the (recovered) loop transfer function crosses over $0dB$. Often, the bandwidth of is a more intuitive design parameter than is, for example, the high-frequency multiplicative weighting W_2. Quantitative uncertainty models are usually at the cost of a lengthy identification effort.

- *Integrators* should be part of the KF loop transfer function, if no steady-state error is to be allowed. Since the Kalman filter loop has only as many poles as the plant, the plant input channels must be augmented with the necessary additional poles (at the origin). Then, once the KF design is completed, and the compensator $C(s)$ is constructed, the integrators are moved from the plant over to the input side of the compensator. The tracking errors will accrue as desired.

20.5 Three Lemmas

Lemma 1: Matrix Inversion

$$(A + BCD)^{-1} = A^{-1} - A^{-1}B(C^{-1} + DA^{-1}B)^{-1}DA^{-1}.$$

Proof:

$$\begin{aligned}
(A+BCD)(A+BCD)^{-1} &= I \\
A(A+BCD)^{-1} &= I - BCD(A+BCD)^{-1} \\
(A+BCD)^{-1} &= A^{-1} - A^{-1}BCD(A+BCD)^{-1} \\
&= A^{-1} - A^{-1}BCD(I+A^{-1}BCD)^{-1}A^{-1} \\
&= A^{-1} - A^{-1}B(D^{-1}C^{-1}+A^{-1}B)^{-1}A^{-1} \\
&= A^{-1} - A^{-1}B(C^{-1}+DA^{-1}B)^{-1}DA^{-1}. \qquad \square
\end{aligned}$$

Lemma 2: Short Form of Lemma 1

$$(X^{-1}+BD)^{-1} = X - XB(I+DXB)^{-1}DX$$

Proof: substitute $A = X^{-1}$ and $C = I$ into Lemma 1.

Lemma 3

$$I - A(I+A)^{-1} = (I+A)^{-1}$$

Proof:

$$\begin{aligned}
I - A(I+A)^{-1} &= (I+A)(I+A)^{-1} - A(I+A)^{-1} \\
&= (I+A-A)(I+A)^{-1} \\
&= (I+A)^{-1}. \qquad \square
\end{aligned}$$

21 SYSTEM IDENTIFICATION

21.1 Introduction

Model-based controller design techniques, such as the LQR and LTR, require a plant model. The process of generating workable models from observed data is the goal of system identification. Good controllers usually have some reasonable robustness guarantees, which motivates identification with simple methods. We discuss in this section four fundamental but useful techniques for approximate system identification of single-input, single-output plants. It should be noted that the area of system identification is a very rich one, and that the methods are only a small subset of what is available.
Except for the last approach, time-domain simulation, the methods are limited to linear models. If different inputs give different linear model coefficients, then it is likely that nonlinear terms are playing a role. The user then has the choice of ignoring the nonlinearity, for example if the operating point is controlled very closely, or developing a controller which takes specific account of the it. In any event, simulations with the nonlinear plant should always be performed to assess the robustness of the control strategy.

21.2 Visual Output from a Simple Input

For low-order plants which can tolerate impulse or step input, a great amount can be learned through step and impulse responses. The basic idea is to express what is observed as a time signal whose Laplace-domain equivalent can be recognized. As an example, consider the plant transfer function $P(s) = k/(\tau s + 1)$, a first-order lag with gain k, and time constant τ. We have $y(s) = k/s(\tau s + 1)$ for the step input $u(s) = 1/s$, and therefore $y(t) = k(1 - e^{-t/\tau})$. The gain k is evident as the maximum value taken by the measured output. The time constant τ is equal to the time required for $y(t)$ to reach the value $k(1 - e^{-1}) = 0.632k$. Similar estimates can be made for second-order systems, especially with the help of step functions parametrized on damping ratio ζ. Systems with order three or higher will usually be more difficult to assess with this visual technique.

Example: Two raw **step responses** in heading were recorded for two different vessels. The first vessel was strongly unstable and had to be powered down abruptly after one second; however, the smoothed data can still be fitted to the curve $y(t) = 0.58(e^t - 1)$. Give estimates of the two plant transfer

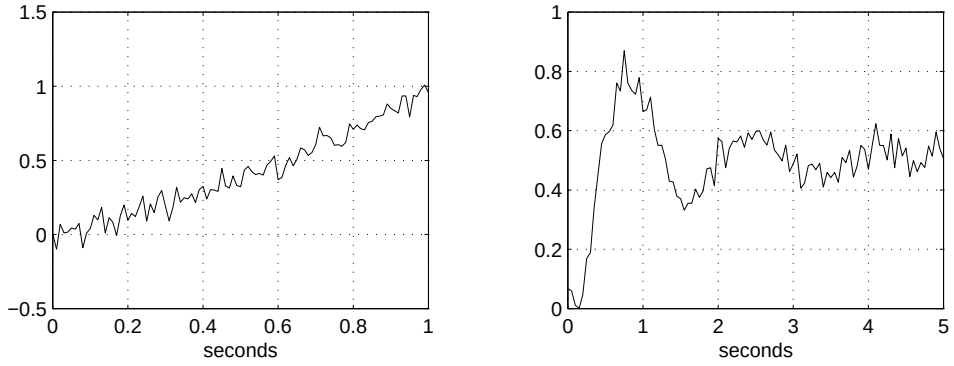

functions $P(s)$, assuming that the step input was of magnitude one.
The time trace of the first system looks like the Laplace transform pair:

$$y(t) = \frac{1}{b-a}(e^{-at} - e^{-bt}) \leftrightarrow y(s) = \frac{1}{(s+a)(s+b)}$$

for the values $b = 0$ and $a = -1$. Thus for the experimental data,

$$y(s) = \frac{0.58}{s(s-1)}.$$

Since $y(s) = \hat{P}(s)u(s)$, where $u(s) = 1/s$, we have $\hat{P}(s) = 0.58/(s-1)$. The second trace looks like a second-order response of the form

$$\frac{y(s)}{u(s)} = \frac{k\omega_n^2}{s^2 + 2\zeta\omega_n s + \omega_n^2},$$

where gain k, undamped frequency ω_n, and ζ are to be determined. First, we note that the steady value of $y(t)$ is about 0.5, so let $k = 0.5$. Next, with respect to the steady value, the first overshoot is about 0.3, and the second overshoot (same side) is about 0.1. The ratio is often written as the logarithmic decrement $\delta = ln(0.3/0.1) \simeq 1.10$, so that the damping ratio is simply $\zeta = \delta/2\pi \simeq 0.175$. Finally, the damped natural period is about $1.7s$, leading to the damped natural frequency $\omega_d = 2\pi/1.7 \simeq 3.70 rad/s$. The undamped natural frequency ω_n is related to ω_d as follows:

$$\omega_n = \frac{\omega_d}{\sqrt{1-\zeta^2}} \simeq 3.75 rad/s.$$

Inserting these into the template above, we have

$$\hat{P}(s) = \frac{7.0}{s^2 + 1.28s + 14.1}.$$

21.3 Transfer Function Estimation – Sinusoidal Input

The main idea of transfer function estimation is that $P(s)$ can be estimated by simply dividing the measured output by the measured input, in the *frequency domain*:

$$\hat{P}(s) = \frac{y(s)}{u(s)}. \tag{216}$$

In applications, the input signal $u(s)$ is known quite accurately because it is generated by a computer. Two sources of error can corrupt the output signal $y(s)$, however: real disturbances and sensor noise. In some cases, disturbances may be band-limited (e.g., water waves), and if these occur in a frequency range far away from the dominant dynamics, the estimated transfer function approach will succeed. A similar argument holds for sensor noise, which in many devices is negligible for low frequencies. A sensor which has noise in the frequency range of the system dynamics is problematic for obvious reasons.
This section discusses the use of periodic inputs to create a Bode plot, while the next section generalizes to broadband input. Bode plots are figures of transfer function magnitude and phase as functions of frequency, which can be either parameterized in terms of poles, zeros, and a gain, or used directly in a loopshaping or Nyquist plot approach.
Certain plants which cannot admit a step or impulsive input will tolerate a sinusoidal input. The idea then is to drive the plant with a narrow-band, i.e., periodic, input signal $u(s)$. For each such test at a specific frequency, compute the magnitude and phase relating the input to the output. Conduct as many tests as are necessary to build a Bode plot of the plant estimate $\hat{P}(s)$.

Example: Sinusoidal rudder angles trajectories, of $10deg$ amplitude ($|u(t)| = 10deg$), were implemented on a vessel operating near its cruising speed. The data are plotted, along with the magnitude and phase of the transfer function

$$\hat{P}(s) = \frac{0.093}{s^2 + 0.83s + 0.21},$$

which holds reasonably well at low frequencies. The phase angle of $y(s)$ is taken with respect to the input signal $u(s)$. Note that the experimental magnitude and phase in this example deteriorate at the higher frequencies. This is a property of almost all physical systems, and an indicator that the plant model cannot be trusted above a certain frequency range.

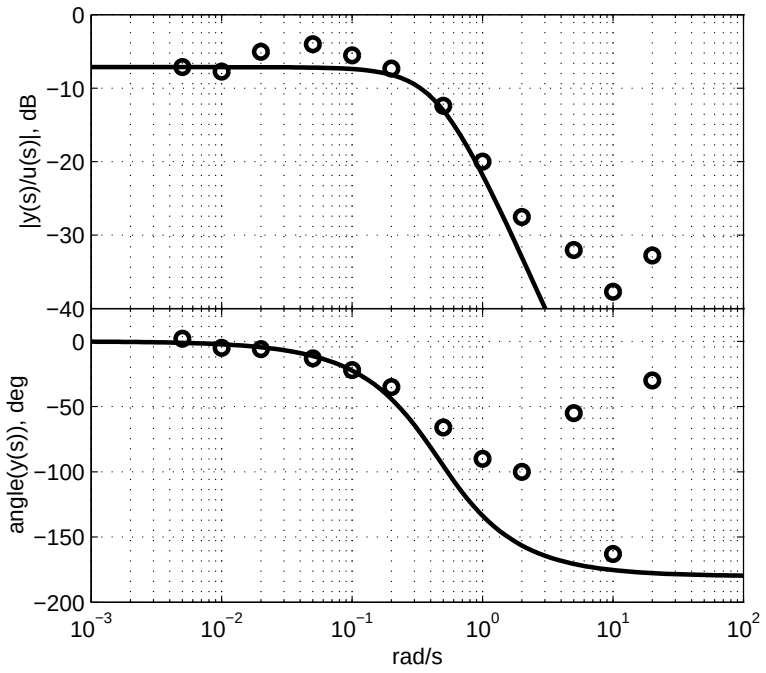

21.4 Transfer Function Estimation – Broadband Input

Many times one needs to deal with experimental data that is broadband, either as the result of a closed-loop run, or of significant disturbances. In this case, frequency-domain analysis can still be used, but elements of spectral analysis are necessary.

21.4.1 Fourier Transform of Sampled Data

For the purpose of analyzing transfer functions, the discrete Fourier transform (DFT) is a standard, optimized tool. It operates on a data vector $x(n)$ of length N:

$$X(m) = \sum_{n=0}^{N-1} x(n) e^{-j2\pi nm/N}, \tag{217}$$

for $m = [1, N]$. We review several points for dealing with the DFT calculation:

- The m'th DFT point is a summation of complex unit-magnitude vectors ($e^{-j2\pi nm/N}$) times the original data ($x(n)$). Dividing the DFT result by N returns the signal to its real magnitude.

- The DFT generates a vector of N complex points as outputs. These correspond to the frequency range

$$\omega_m = \frac{2\pi}{dt} \frac{m-1}{N}, \tag{218}$$

  i.e., the first frequency is 0, and the last frequency is slightly less than the sampling rate.

- The sampling theorem limits our usable frequency range to only one-half of the sampling rate, called the Nyquist rate. The points higher than π/dt correspond to negative frequencies, and a complex-conjugacy holds: $X(2) = X^*(m), X(3) = X^*(m-1)$, and so on. What happens near the Nyquist rate depends on whether N is odd or even.

  An additional multiplication of the DFT result by 2 will give peaks which are of about the right magnitude to be compared with the time-domain signal. With this scaling, the value $X(1)$ is *twice* the true DC value.

- The Nyquist rate depends only on the sampling time step dt, but the frequency vector accompanying the DFT can be made arbitrarily long by increasing the number of data points. To improve the frequency resolution of the DFT, a common approach is to zero-pad the end of the real data,

- The data $x(k)$ should be multiplied by a *smoothing window* $w(k)$, for two reasons. First, if the window goes to a small value near its tails, Gibb's effect (the spectral signature of a discontinuity between $x(1)$ and $x(N)$) can be minimized. The second rationale for windowing is based on the discrete nature of the transform. Because the DFT provides frequency data at only $N/2$ unique frequencies, there is the possibility that a component in the real data lies in between one of these DFT frequencies. The DFT magnitude at a specific $\omega(m)$ is in fact an *average* of continuous frequencies from the neighborhood of the point. Smoothing windows are generally chosen to achieve a tradeoff of two conflicting properties relating to the average: the width of the primary lobe (wide primary lobes bring in frequencies that belong to the adjacent bins $\omega(m-1)$ and $\omega(m+1)$), and the magnitude of the side lobes (tall side lobes bring in frequencies that are far away from $\omega(m)$).

  There are many smoothing windows to choose from; no windowing at all is usually referred to as applying a rectangular window. One of the simplest is the Hann, or cosine, window:

$$w(k) = \frac{1}{2}\left[1 - \cos\left(\frac{2\pi k}{N}\right)\right]$$

- The DFT of a given signal is subject to bias and variance. These can be reduced by taking separate DFT's of sub-sections of data (perhaps zero-padded to maintain frequency resolution), and then averaging them. It is common to use segments which do not overlap, but it is not a necessity. This averaging idea is especially important in transfer function verification; see below.

- If possible, the DFT should be run on a number of samples N which is a multiple of a large power of two. If N is prime, the DFT will take a long time to execute.

The above steps, all of which are available through the Matlab function `spectrum()` for example, will ensure a fair spectral analysis of a time series.

21.4.2 Estimating the Transfer Function

In continuous time, when the plant input $y(t)$ and output $u(t)$ are transformed into frequency space, the estimated transfer function follows from

$$\hat{P}(s) = \frac{y(s)}{u(s)}. \tag{219}$$

As noted above, spectral analysis of a signal benefits by using multiple segments and averaging; we now want to include the same approach in our estimation of $P(s)$. The procedure is:

- For the p'th segment of data, compute the transfer function estimate

$$\hat{P}_p(m) = \frac{Y_p(m)Y_p^*(m)}{U_p(m)U_p^*(m)}.$$

- For the p'th segment of data, compute two covariances and a cross-covariance:

$$\begin{aligned} \Gamma_{uu}^p(m) &= U_p(m)U_p^*(m) \\ \Gamma_{yy}^p(m) &= Y_p(m)Y_p^*(m) \\ \Gamma_{yu}^p(m) &= Y_p(m)U_p^*(m). \end{aligned}$$

- Construct average values of the transfer function estimate and the other quantities:

$$\begin{aligned} \hat{P}(m) &= avg_p(\hat{P}_p(m)) \\ \Gamma_{uu}(m) &= avg_p(\Gamma_{uu}^p(m)) \\ \Gamma_{yy}(m) &= avg_p(\Gamma_{yy}^p(m)) \\ \Gamma_{yu}(m) &= avg_p(\Gamma_{yu}^p(m)) \end{aligned}$$

- Compute the *coherence* function, which assesses the quality of the final estimate $\hat{P}(m)$:

$$Coh(m) = \frac{\Gamma_{yu}(m)\Gamma_{yu}^*(m)}{\Gamma_{yy}(m)\Gamma_{uu}(m)}.$$

If the coherence is near zero, then the segmental cross-covariances $\Gamma^p_{yu}(m)$ are sporadic and have cancelled out; there is no clear relation between the input and the output. This result could be caused by either disturbances or sensor noise, both of which are reasonably assumed to be random processes, and uncoupled to the input signal. Alternatively, if the coherence is near one, then the cross-covariances are in agreement and a real input-output relationship exists. With real data, the coherence will deteriorate at high frequencies and also at any frequency where disturbances or noise occur.

21.5 Time-Domain Simulation

The time-domain simulation approach tweaks the parameters of a simulation so that its output matches the observed output. The method has its main strength in the fact that it applies to *any* model that can be simulated, including those of high order and with significant nonlinearities. On the other hand, the method is computationally expensive and gives no guarantee of a useful solution, or even of convergence.

At the outset, we need to come up with some structure of the plant model. This can be based on physics in many cases. Consider, for example, the case of a mass mounted on a spring and a dashpot, driven by the input force $u(t)$. A fair guess for the *actual* dynamics has the form $my'' + by' + ky = u(t)$, and we plan to look through the three-dimensional parameter space $\vec{\theta} = [m, b, k]$. The simulation operation can be written this way: $\hat{y}(t) = G(\vec{\theta}, u(t))$, and the system identification problem is to minimize $||\hat{y}(t) - y_{obs}(t)||$, say, where $||\cdot||$ here indicates the Euclidean norm. For a given parameter vector $\vec{\theta}$, running the simulation generates a new $\hat{y}$, and computing the norm gives a scalar measure of goodness.

Since the normed error is a complicated function of both $u(t)$ and $\vec{\theta}$, the minimization must proceed iteratively. The Nelder-Meade simplex method is easy to use, and can be invoked with the Matlab function `fmins`. As an example, the three programs listed comprise a working Matlab set for identification of a first-order, nonlinear system. Some notes on use:

- In this example, the same simulation generates the "observed" data and the simulated response. Since the program `simulate` always uses the global variable `theta` as the parameters, we must be careful about setting `theta` in the calling programs.

- After a simulation run is complete, the data is interpolated to the same time scale as the observed data, in order to compute the error.
- The initial guess for `theta` is a random vector; the Simplex method will take over from this point. In many instances, however, `theta` is roughly known, and a better starting value can be given.
- The Simplex method may head into invalid parameter space, e.g., negative mass. The error calculation, however, can be easily augmented by a term which penalizes invalid parameters, e.g.,
  `err = err + 1000*(1-sign(mass))`.
- There is no guarantee that a global minimum will be found or even exists. Starting from different initial guesses for θ may help find better results, but we are still at the mercy of the minimization algorithm, and a very complicated function.

```
%%%%%%%%%%%%%%%%%%%%%%%%%%%%%%%%%%%%%%%%%%%%%%%%%%%%%%%%%%%%%%%%%%%%%%%%

clear all ; clear global ;
global u_obs t_obs y_obs dt theta ;

dt = .3 ; % time step
theta = [1 2] ; % true parameter vector
t_obs = 0:dt:20*dt ; % observed time vector
u_obs = ones(length(t_obs),1) ; % observed input
[t_raw, y_raw] = ode45('simulate', [0 max(t_obs)], 0) ;
y_obs = spline(t_raw, y_raw, t_obs) ; % observed output

[theta_final] = fmins('get_err', randn(2,1)) ;

disp(sprintf('final theta(1):  %g.', theta_final(1))) ;
disp(sprintf('final theta(2):  %g.', theta_final(2))) ;
theta = theta_final ;
[t_raw, y_raw] = ode45('simulate', [0 max(t_obs)], 0) ;
y_sim = spline(t_raw, y_raw, t_obs) ;
figure(1) ; clf ; hold off ;
plot(t_obs, y_obs, t_obs, y_sim, t_obs, u_obs) ;
```

```
%%%%%%%%%%%%%%%%%%%%%%%%%%%%%%%%%%%%%%%%%%%%%%%%%%%%%%%%%%%%%%%%%%%%%%%

function [err] = get_err(theta_arg) ;
global y_obs t_obs theta ;

theta = theta_arg ;
[t_raw, y_raw] = ode45('simulate', [0 max(t_obs)], 0) ;
y_sim = spline(t_raw, y_raw, t_obs) ;
err = norm(y_sim - y_obs) ;
disp(sprintf('error:  %f.', err)) ;

%%%%%%%%%%%%%%%%%%%%%%%%%%%%%%%%%%%%%%%%%%%%%%%%%%%%%%%%%%%%%%%%%%%%%%%

function [ydot] = simulate(t,y) ;

global u_obs dt theta ;

k = theta(1) ;
tau = theta(2) ;

ind = floor(t/dt) + 1 ; % we have to choose which u_obs to use:
% a zero-order hold as implemented.

ydot = ( k*u_obs(ind) - y^3 ) / tau ;

%%%%%%%%%%%%%%%%%%%%%%%%%%%%%%%%%%%%%%%%%%%%%%%%%%%%%%%%%%%%%%%%%%%%%%%
```

22 CARTESIAN NAVIGATION

The bulk of our discussion on maneuvering and control has assumed that the necessary system states can be measured. The marine engineer is in fact faced with choices between many different basic sensor packages, notably compasses, paddle wheels, inertial navigation units, rate gyros, and depth guages, for example. These listed sensors are *self-contained* and rely primarily on the physical properties of the natural environment. There is also a class of *distributed* sensor systems; these generally involve an array of communicating elements, located remotely from the vehicle. We present the fundamental concepts behind two methodologies in this second class: the global positioning system (GPS) and acoustic navigation, both of which can provide high-accuracy absolute Cartesian navigation.

22.1 Acoustic Navigation

Consider a *transponder* A, which can transmit an acoustic signal, and also measure, with microsecond accuracy, the time to receive a reply. Next, place a *responder* B at a distance R away from A; the job of B is just to transmit a signal whenever it receives one, with a (short) predictable response time T_t. Thus, the elapsed time T between a tranmission and consequent reception at A is

$$T = T_t + 2R/c_w,$$

where c_w is the speed of sound in water, about $1450 m/s$. The range R follows by inversion:

$$R = \frac{(T - T_t)c_2}{2}.$$

Suppose that the location of B is known; then a given measurement of R places A on a sphere around B. It is a case of three unknowns (x, y, z) and one equation:

$$(x_A - x_B)^2 + (y_A - y_B)^2 + (z_A - z_B)^2 = R^2.$$

The introduction of a another responder C (typically listening and responding at a different frequency than B) places A on the intersection of two spheres, i.e., a circle. There are two equations, but still three unknowns. When A, B, and C lie in a nearly horizontal plane, then the intersection circle lies in a vertical plane; the addition of a depth sensor to our suite would allow us to pin A's location at one of two points on the circle. Finally, if we know which side A is on, and do not allow for abrupt crossovers, then we have a functional set of measurements for acoustic navigation with just two responders. The *baseline* is the line connecting responders B and C; when A is near this baseline, positional accuracy will be very poor since the two solution spheres are tangent.

Better and better performance can be obtained by increasing the number of responders, and consequently of the baselines and spheres. With three responders, for example, the intersection of a sphere (responder D) and a circle (responders B and C) is two points. Here there are three equations and three unknowns, but the nonlinearity of the equations leads to the non-uniqueness in the solution. A fourth responder or a depth transducer would be needed to completely constrain the solution.

The above discussion is a minimum conceptual explanation of acoustic navigation. There are many other pieces to the approach, including an account of the variation of sound speed c_w with water depth, obtaining the Cartesian locations of the responder network, and handling various geometric configurations that give rise to poor or degenerate solutions.

There are two common configurations used for acoustic navigation, named for the length of the baselines relative to the target (transponder A) range.

(Ultra) Short-Baseline The geometry of SBL or USBL puts very short baselines between the responders compared to the target distance. For instance, the fixed net is often attached to a vessel or other structure, with baseline lengths on the order of 10-100m. Typical frequencies in use are around 100kHz, with a working range of 100-500m to the target. The wavelength of a 100kHz signal is about 1cm and 5cm is a reasonable estimate of the accuracy for these systems.

Long-Baseline Long-baseline systems typically involve a larger responder net, and the target ranges are similar to the baseline lengths. Very large systems utilize frequencies of 10-15kHz (for a placement accuracy around 2-5m), and may have ten-kilometer baselines. Frequent sources of error in long-baseline systems are variations of c_w, and also in multipath. In the latter

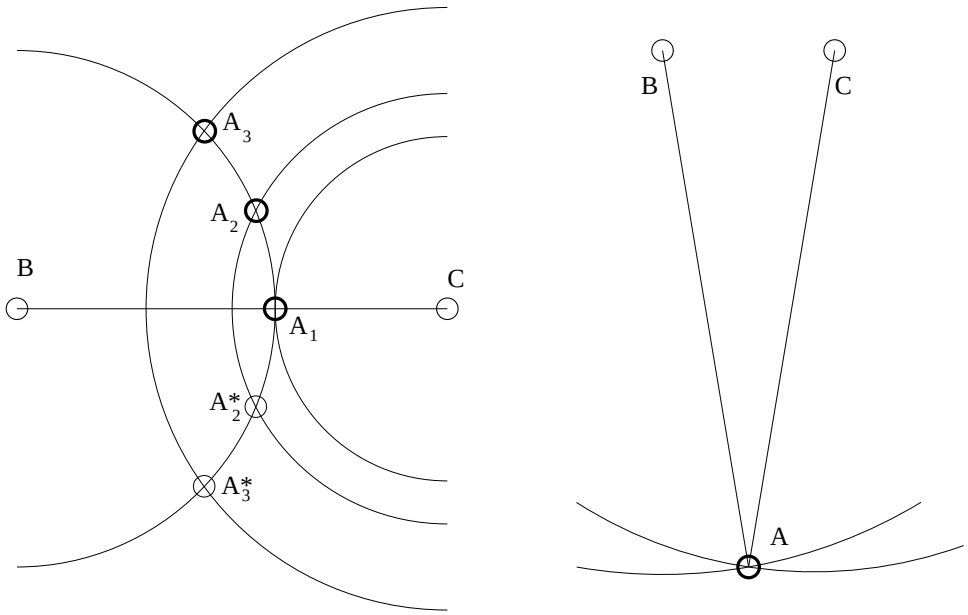

Figure 6: *Left*: General configuration of a long-baseline acoustic system, with target transponder A and fixed responders B and C. The position A_1 is on the baseline and has poor accuracy in the direction normal to the baseline; in contrast, A_3 is well-posed. A_3^* is an additional solution to the two-responder problem. *Right*: General configuration of a short-baseline system.

condition, false signals can be caused by reflections off the seafloor and the surface; these signals are typically eliminated by rejecting those receptions which are outside a very tight and slowly moving window on travel time T. Sometimes, bottom topography can shield a direct acoustic path, and the only receptions available are via multipath!

22.2 Global Positioning System (GPS)

The GPS system is the most powerful system publicly available for absolute position reference above water. It is similar in concept to the acoustic navigation systems described above, but with one fundamental difference: only the one-way travel time from each satellite is measured at the target. The accuracies achieved with GPS are therefore strongly dependent on the accuracy of time-keeping.

The core of the system is a network of 24 satellites arranged in six planes (4 per plane) inclined at 55 degrees from the equatorial plane, at an altitude of about 20,000km. The altitude is chosen carefully to correspond with a 12-hour orbit; geosynchronous orbit is much higher, at around 40,000km. The orbit lines over a *non-rotating* earth are thus near-sinusoids that reach lattitudes of 55°N and 55°S, and the six lines are spaced 60° apart in longitude. With reference to a *rotating* Earth, the spatial frequency is doubled, so that the longitudinal distance between tracks is 30 degrees, or 1800 nautical miles. Each satellite transmits a regular signal which contains, among other items, the time of its transmission, and the three-dimensional location of the satellite (the *ephemeris*). It is from these two pieces of information, from many satellites, that triangulation and navigation are performed at the target.

For the ideal case that the time bases of the target and the satellites are exactly aligned, triangulation of the type described for acoustic navigation is possible. In practical terms, the speed of light $c = 3 \times 10^8 m/s$ implies that a $1ns$ timing error will cause a $0.3m$ range error. For this reason, each of the satellites carries four atomic clocks on board, good to $1ns$ per day. The time base is continually monitored and updated from a ground station, and accurate to within $1ns$. The ephemeris of each satellite is also monitored and updated from the ground station, using a combination of least-squares analysis of past data (1 week), and a Kalman filter to predict the future ephemeris. The accuracy of satellite position is better than $10m$.

We now come to the last thorny issue: how to make target receivers that don't require atomic clocks! The solution is very clever, and illustrated for the case of two-dimensions; the arguments for three dimensions are the same. In two dimensions, the range measurements from two sources locate the target on one of two points (the intersection of two circles). Suppose that the target clock is too slow by an amount $\tilde{t}$, so that the range estimate is

$$r + \tilde{r} = c(t + \tilde{t}).$$

The estimated range circles are too large, and the estimated location of the target too far from the baseline. Introduce a third satellite now so that the intersections of the circle pairs now occur at six points. Three of these are very close, and indicate the approximate true solution. The trick is to find the correction for $\tilde{t}$ that puts the three close solutions onto a single point. This single point is near the centroid of the three approximate points, and represents the best position solution. The target time base can be kept up to date by

performing this check for every set of signals. Hence, the two-dimensional timing problem is solved with three satellites; the three-dimensional timing problem is solved with four satellites.

The position specification for GPS is $25m$, at the 95'th percentile. This is a remarkable feat, given that it is an absolute measure over the entire surface and atmosphere of our $6000km$-radius Earth. Major sources of error include: clock base and satellite navigation ($\approx 2.5m$), ionosphere and troposphere electromagnetic variations ($\approx 2.5m$), and inaccuracies in the receiver and multipath ($\approx 2m$). GPS is also subject to *selective availability* or S/A, the addition of a slow-varying random component in the satellite ephemeris data. Selective availability is controlled by the United States Department of Defense, and degrades the position specification to $100m$ (typical). The advent of *differential GPS* solved most of the S/A concerns of American allies, by providing high-accuracy navigation in local areas. The idea here is that a stationary target can detect the effects of S/A (since it is not moving) and then transmit the corrections over a small geographical area. Many current GPS receivers are capable of decoding these local corrections, which are then applied to their own satellite navigation processing. Differential GPS typically provides 1-2m accuracy.

Finally, as with the acoustic navigation systems described, an independent altitude measurement will enhance the accuracy of GPS, essentially reducing a three-dimensional to a two-dimensional problem.

23 REFERENCES

Short notes indicate how the reference is related to the text.

Dynamics of Mechanical and Electromechanical Systems, S.H. Crandall, D.C. Karnopp, E.F. Kurtz, Jr., and D.C. Pridmore-Brown, Krieger: Malabar, FL, 1985. Coordinate systems and rigid-body dynamics.

Optimal Spacecraft Rotational Maneuvers, J.L. Junkins and J.D. Turner, Elsevier: New York, 1986. Euler angles and quaternions.

Principles of Naval Architecture, 2nd Revision, E.V. Lewis, ed., Society of Naval Architects and Marine Engineers: Jersey City, NJ, 1988. Classical treatment of stability, propulsion, and lifting surfaces.

Marine Hydrodynamics, J.N. Newman, MIT Press: Cambridge, 1997. General reference.

Guidance and Control of Ocean Vehicles, T.I. Fossen, Wiley: New York, 1994. Comprehensive modern treatment of marine dynamics and control.

Formulas for Natural Frequency and Mode Shape, R.D. Blevins, Krieger: Malabar, FL, 1984. Extensive added mass formulas.

A method for estimating static aerodynamic characteristics for slender bodies of circular and noncircular cross section alone and with lifting surfaces at angles of attack from 0° to 90°, L. Jorgensen, NASA Technical Note D-7228, April 1973.

Fluid Dynamic Lift, S.F. Hoerner and H.V. Borst, Hoerner Fluid Dynamics: Bakersfield, CA, 1975. Extensive data on lift of bodies and wings.

Fluid Dynamic Drag, S.F. Hoerner and H.V. Borst, Hoerner Fluid Dynamics: Bakersfield, CA, 1975. Data on drag of bodies and wings.

Marine Propellers and Propulsion, J.S. Carleton, Butterworth-Heinemann: Boston, 1994. Includes a chapter on transverse and azimuthing thrusters.

The influence of thruster dynamics on underwater vehicle behavior and their

incorporation into control system design, D. R. Yoerger, J.G. Cooke, and J.-J. E. Slotine, *IEEE J. Oceanic Engineering*, 15:167-178, 1990. First-order nonlinear thruster model.

Toward an improved understanding of thruster dynamics for underwater vehicles, A.J. Healey, S.M. Rock, S. Cody, D. Miles, and J.P. Brown, *Proc. IEEE Symposium on Autonomous Underwater Vehicle Technology*, pp 340-352. 1994. Second-order nonlinear thruster model.

Accurate four-quadrant nonlinear dynamical model for marine thrusters: Theory and experimental validation, R. Bachmayer, L.L. Whitcomb, and M.A. Grosenbaugh, *IEEE J. Oceanic Engineering*, 25:146-159, 2000. State-of-the-art in thruster modeling.

Acceleration and steady-state propulsion dynamics of a gas turbine ship with controllable-pitch propeller, C.J. Rubis, *Proc. SNAME Annual Meeting*, No. 10, 1972.

Governing ship propulsion gas turbine engines, C.J. Rubis and T.R. Harper, *SNAME Trans.*, 94:283-308, 1986.

Flow-Induced Vibrations, 2nd Edition, R.D. Blevins, Van Nostrand Reinhold, New York, 1990. Cable strumming.

Modern Control Engineering, K. Ogata, Prentice-Hall: Englewood Cliffs, NJ, 1970. SISO linear control.

Circuits, Signals, and Systems, W.M. Siebert, MIT Press: Cambridge, MA, 1986. General reference on transforms.

Applied Nonlinear Control, J.J.-E. Slotine and W. Li, Prentice-Hall: Englewood Cliffs, NJ, 1991.

Feedback Control Theory, J.C. Doyle, B.A. Francis, and A.R. Tannenbaum, Macmillan: New York, 1992. Loopshaping concepts.

Control Engineering: A Modern Approach, P.R. Bélanger, Sauders College Publishing, Philadelphia, 1995. General control reference.

Introduction to Dynamic Systems, D.G. Luenberger, Wiley: New York, 1979.

Dynamic programming and LQR derivation.

Applied Optimal Estimation, A. Gelb, ed., MIT Press: Cambridge, 1988. Kalman filter practical aspects.

Linear Optimal Control Systems, H. Kwakernaak and R. Sivan, Wiley: New York, 1972. Kalman filter derivation and properties.

Multivariable feedback design: concepts for a classical/modern synthesis, J.C. Doyle and G. Stein, *IEEE Trans. Automatic Control*, 26:4-16, 1981. Seminal paper on LTR.

A tutorial on the LQG/LTR method, M. Athans, *Proc. American Control Conference*, pp 1289-1296, 1986.

Multivariable control of a submersible using the LQG/LTR design methodology, R. Martin, L. Valavani, and M. Athans, *Proc. American Control Conference*, pp 1313-1324, 1986. More tutorial LTR.

Optimal Control, F.L. Lewis and V.L. Syrmos, Wiley: New York, 1995. General reference on LTR.

Numerical Recipes in C, 2nd Edition, W.H. Press, S.A. Teukolsky, W.T. Vetterling, and B.P. Flannery, Cambridge University Press: Cambridge, UK, 1992. Function minimization.

Spectral Analysis in Engineering, G.E. Hearn and A.V. Metcalfe, Halsted: New York, 1996. Transfer functions from spectral analysis.

NAVSTAR: Global positioning system – Ten years later, B.W. Parkinson, S.W. Gilbert, *Proc. IEEE*, 71:1177-1186, 1983. The whole issue is in fact dedicated to global positioning systems. There is another such issue: *IEEE Proc.* Vol. 87, No. 1, 1999.

24 PROBLEMS

Many of the following problems use data presented by Fossen and in *Principles of Naval Architecture*.

1. **Inertial dynamics**. The gas generator turbine of a LM-2500 marine engine rotates at $p = 10,000 rpm$ (revolutions per minute), and has a mass of approximately $200 kg$. The following question pertains to the inertial forces experienced by this spinning rigid body, with $I_{xy} = I_{xz} = I_{yz} = x_g = z_g = 0$.

   Because of high rotational speed, the turbine is exceedingly sensitive to lateral balancing. Estimate the net force that the radial bearings would have to support for a $1mm$ mass imbalance, say, $y_g = 1mm$ with respect to the spin axis.

2. **Kinematics.** Although dead-reckoning is not recommended as a method for long-term navigation, it can be quite useful for pre-planning trajectories. For example, consider a surface vessel heading profile as follows:

$t = 0$	$\phi(t) = 0\ rad$
$0 < t <= 60s$	$\phi(t) = t/60 \times \pi/4\ rad$
$60s < t < 240s$	$\phi(t) = \pi/4\ rad$
$240s < t < 300s$	$\phi(t) = (300 - t)/60 \times \pi/4\ rad$
$t = 300s$	$\phi(t) = 0\ rad$

   What is the total distance traveled in the Cartesian x direction during these five minutes? You may assume that the forward speed of the vessel is $u = 1m/s$, and that there is no significant sideslip. *Hint:* Break the trajectory up into three parts, which can be evaluated separately.

3. **Coefficients and system modeling.** Consider a weather vane in a wind of velocity U_o. If θ is the angle of the vane with respect to the wind direction,

   (a) Write the single-degree of freedom (N) linearized equations of motion about the fixed axis **0**.

   (b) Write N_θ, $N_{\dot\theta}$, and $N_{\ddot\theta}$ in terms of N_v, N_r, $N_{\dot r}$, etc..

   (c) If we consider the differential equation

   $$A\ddot{y}(t) + B\dot{y}(t) + Cy(t) = 0,$$

   the condition for stability is that A, B, and C must have the same sign. Express this requirement in terms of the derivatives in the previous question. Give physical interpretations for what would make such a device stable or unstable.

   (d) Create a numerical model of this system, using the MATLAB ODE solver `ode45`. The system equation can be written as two first-order equations:

   $$\frac{d}{dt}\left\{ \begin{array}{c} \dot\theta \\ \theta \end{array} \right\} = \left[\begin{array}{cc} -B/A & -C/A \\ 1 & 0 \end{array} \right] \left\{ \begin{array}{c} \dot\theta \\ \theta \end{array} \right\}.$$

   Simulate the system response to nonzero initial conditions (e.g., $\theta(0) = 1, \dot\theta(0) = 0$). Discuss, using several examples, response sensitivity to B and C, which are related to the aerodynamic coefficients. For example, look at the range $\{A, B, C\} = \{1, \pm 3, \pm 3\}$.

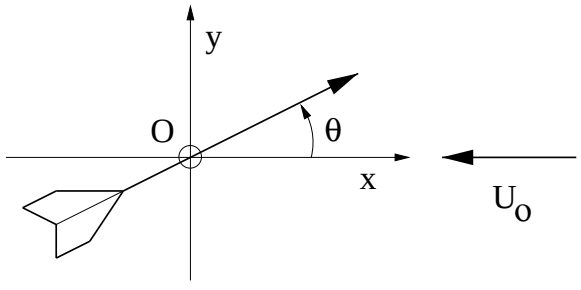

4. **Hydrodynamics.** The figure below shows some characteristic fluid force curves versus a motion parameter. Give the linear hydrodynamic coefficient at two different operating conditions, origin O and A: is it zero, small, finite positive, finite negative?

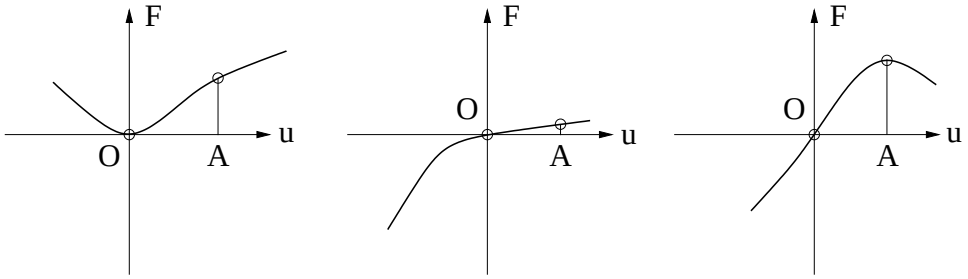

5. **Second-order system.** Consider the vibration of a mass-spring-dashpot system:

$$m\ddot{x} + b\dot{x} + kx = 0,$$

wherein all the coefficients are positive and real (i.e., physical).

(a) Set $x(t) = e^{st}$, and find two solutions for s in terms of m, b, and k, using the quadratic formula. The solution pairs depend on whether b exceeds a critical value: what is the critical value and how do the solutions change?

(b) From the initial condition $x(0) = x_o$, and $\dot{x}(0) = 0$, find the coefficients for the general solution

$$x(t) = c_1 e^{s_1 t} + c_2 e^{s_2}.$$

in terms of x_o, s_1, and s_2. What do you think will happen when $s_1 = s_2$?

(c) Write this $x(t)$ for sub-critical b (that is, complex s) in terms of the standard parameters

$$\begin{aligned}\omega_n &= \sqrt{\frac{k}{m}} \text{ (undamped natural frequency)} \\ \zeta &= \frac{b}{2\sqrt{km}} \text{ (damping ratio)} \\ \omega_d &= \omega_n\sqrt{1-\zeta^2} \text{ (damped natural frequency).}\end{aligned}$$

Give your answer in terms of a real exponential multiplied by a single sine or cosine, and make a sketch.

(d) Sketch the response $x(t)$ for supercritical b, i.e., both s are real, for the same initial conditions. What happens when the roots s_i are far apart vs. when they are close together?

(e) Consider now the case where an input acts to drive the mass from zero initial conditions:

$$m\ddot{x} + b\dot{x} + kx = u.$$

This equation defines a system, with input u, and output x. Using the Laplace transform, write the transfer function for this system, i.e., the impulse response, both in frequency (Laplace) space, and in the time-domain. Make a sketch of the time-domain result. Be sure to cover both the sub-critical and super-critical damping cases.

(f) What is the step response of this system, in both the subcritical and super-critical damping cases? Include sketches.

6. **Submarine roll dynamics and control.** A submarine has weight $1200t$ (tons) and the center of gravity is $0.5m$ above the center of buoyancy (What can you conclude?). The rolling motion can be assumed to be decoupled from the other motions. This submarine has anti-rolling fins to ensure stability. The control hydrodynamic derivative is $K_\delta = -2.8tm$ per degree of fin rotation δ, at a forward speed of $5m/s$.

(a) Write the equation of motion for roll (K).

(b) If the automatic control law $\delta = k_1\psi$ is used, where ψ is the roll angle, what range of k_1 ensures stability?

(c) If the speed suddenly drops to $2.5m/s$, how does the range of stabilizing k_1 change?

7. **Steering**. Draw curves of rudder angle δ vs. yaw rate r for a dynamically stable surface vessel, and then for an unstable vessel. Indicate areas where the vessel turns against the rudder action.

8. **Submarine pitch/heave dynamics.** Consider a submarine moving forward at speed U, and restricted to small motions in the vertical $(x-z)$ plane. Assume that:

   - The submarine is symmetric in the $x-y$ plane and $y_G = 0$. The submarine is not symmetric in the $x-z$ plane due to the sail, etc., but assume it is *nearly* symmetric, so that you can omit certain hydrodynamic terms.
   - At rest, the submarine is neutrally buoyant and stable with the x and y axes horizontal. What does this tell us about the magnitude of the buoyant force and where it acts with respect to the center of weight?

   (a) Derive the equations of motion for the submarine moving at speed U.

   (b) Derive the hydrostatic, restoring pitch moment for small pitch θ.

   (c) Linearize the inertial terms in the equations of motion.

   (d) Expand the fluid forces and moments in terms of the motions. Omit nonlinear and memory effects, and be sure to include the hydrostatic moment. Explain your choices.

   (e) Write out the complete linearized equations of motion. Does surge decouple from pitch and heave? Write out the coupled equations in matrix form.

   (f) Can the submarine be stable in pitch without feedback control? Can the submarine be stable in depth without feedback control?

9. **Submarine stability via slender body theory.**

   (a) An underwater vehicle hull has the shape of a circular cylinder, except at the very ends, where it rapidly tapers down to a point. If

the radius is $0.5m$, length is $17m$, and speed is $2m/s$, use slender-body theory to express the following coefficients: $Z_{\dot{w}}$, $M_{\dot{q}}$, and M_w, all referenced to the body midpoint.

(b) It turns out that in order to match the lift and moment of the hull in experiments, a flat tail of radius $0.4m$ has to be included in the slender-body estimate. Determine the corrected value for M_w, and in addition compute Z_w. Where is the aerodynamic center with respect to the center of the hull, and is this hull stable in pitch? Recall that the aerodynamic center is the equivalent location of the observed lift force that creates the observed moment.

(c) A fin with pre-determined lift slope of $3.6/rad$ is to be applied at the tail to make the device *just* stable in pitch. How big is the required fin area that brings the net M_w to zero, as desired?

10. **Lifting surfaces.** Using the lifting surface formulas, estimate the coefficient K_v of a submarine sail as shown below, for $U = 10m/s$.

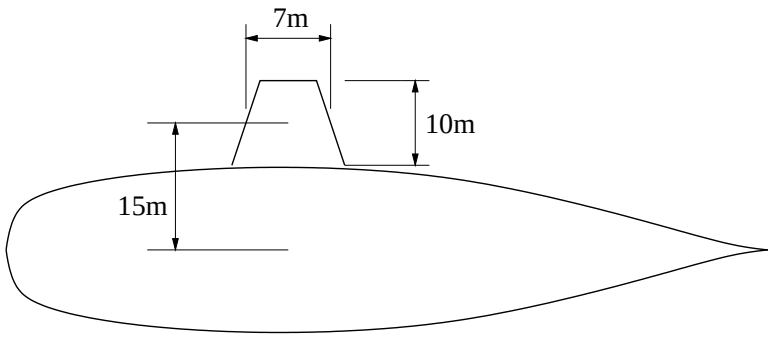

11. **Slender body theory.** Consider a long ellipsoidal body of length l and diameter d.

(a) With $l/d = 7.0$, approximate the cross-body added mass, using slender-body theory, and compare it with the exact results from the table below (Blevins).

(b) Perform the slender body calculation also for a sphere, and compare again to the exact result.

(c) What is the added mass in the in-line direction?

Sphere added mass:	$2\rho\pi a^3/3$
Ellipsoid cross-body added mass:	$4\alpha\rho\pi ab^2/3$
where $a/b = 0.1$:	$\alpha = 0.075$
0.2:	0.143
0.6:	0.355
1.0:	0.500
2.0:	0.704
5.0:	0.894
7.0:	0.933
10.0:	0.960
∞:	1.000
Ellipsoid longitudinal added mass:	$4\alpha\rho\pi ab^2/3$
where $a/b = 0.1$:	$\alpha = 6.148$
0.2:	3.008
0.6:	0.908
1.0:	0.500
2.0:	0.210
5.0:	0.059
7.0:	0.036
10.0:	0.021
∞:	0.000

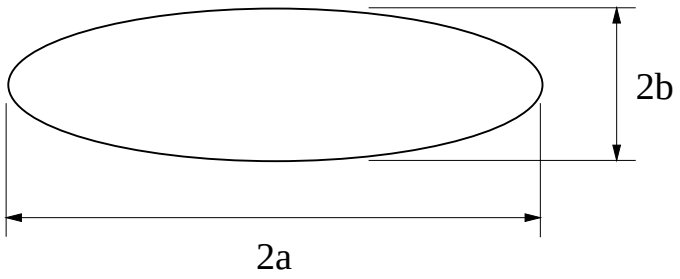

12. **Submarine pitch stability with various methods.** We will calculate the pitch derivative due to an angle of attack, M_w, for a small submarine, using several different methods.

    The submarine is a rotationally symmetric ellipsoid with $L/D = 7$, $L = 35m$. We fix the body origin to the midpoint as shown below. The body

is appended with two fins as shown in the figure: each has an area of $1m^2$, geometric aspect ratio of 3, and has its longitudinal center of action $1m$ forward of the body stern.

(a) Apply wing theory to characterize M_w due to the fins alone.

(b) Apply slender body theory to estimate M_w for the body alone.

(c) Linearize the Munk moment, and give a corrected slender-body value for M_w of the body.

(d) Apply Jorgensen's approximate formulas to estimate M_w for the body; make linearizations where necessary.

(e) Use the experimental data from Hoerner (p. 13.2) below to estimate M_w for the body.

(f) Use the Hoerner result and your result from wing theory to write a net M_w for the body plus fins.

(g) What is the location of the net aerodynamic center? If it has an unstable location forward of the midpoint, what increase in fin area would bring it back to the midpoint?

(h) What is the diameter of a flat stern that will allow the slender body theory to give the same moment as the Hoerner (experimental) data, for the body alone?

(i) What is the diameter of a flat stern that allows the approximate formulas of Jorgensen to give the same moment as the Hoerner data, for the body alone?

Hoerner p. 13.2:
Symmetric body of revolution with $L/D = 6.7$.
Force and moment referenced to body midpoint:
$Z = -0.5\rho U^2 D^2 C_{ydb} \tan(w/u)$. $C_y = 1.20$.
$M = 0.5\rho U^2 D^2 L C_{nb} \tan(w/u)$. $C_m = 0.53$. DESTABILIZING

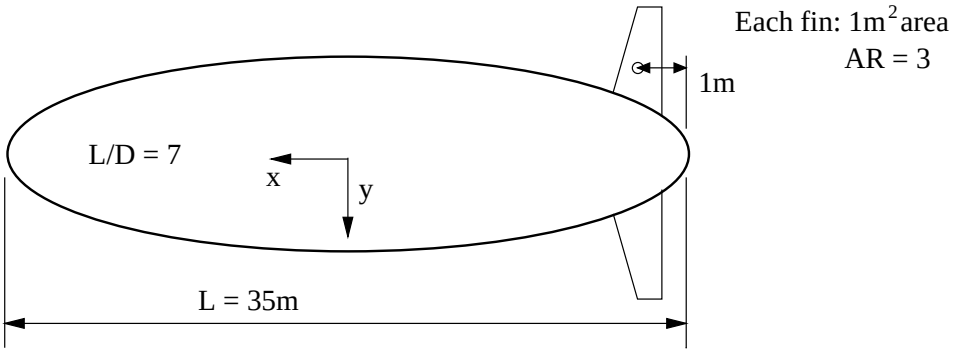

13. **Cable dynamics**. A towing cable is steel-jacketed, with diameter $3cm$, an effective extensibility of $E = 100 \times 10^9 Pa$, and a density of $\rho_c = 5000 kg/m^3$. The vehicle it tows is streamlined, and has negligible mass (M). If we are towing at low speed and $L = 4000m$ depth,

    (a) Calculate ω_1, the first undamped natural frequency in heave, with $mL >> M$.

    (b) If the vessel heaves with a $P = 2m$ amplitude and a 4.5-second period, what is the dynamic tension amplitude at the top ($s = L$) of the cable? The formula for this dynamic tension (with $mL >> M$) is $\tilde{T} = EAPk \sin(ks)/cos(kL)$, where A is the cross-sectional area of the cable, $k = \omega\sqrt{m/EA}$, and m is the cable mass per unit length.

    (c) Taking into account the static tension induced by in-water weight, does the cable unload at the surface, for the heaving conditions above?

14. **Cable mechanics (hard!).** You are asked to assess the operational envelope of a cable/vehicle system which has been installed on a vessel. The cable is steel-jacketed, with diameter $3cm$, an effective extensibility of $100 \times 10^9 Pa$, and a density of $5000 kg/m$. The vehicle is streamlined, and has a mass (material plus added) of $100kg$.

    (a) The towing angle at the vessel cannot exceed $25deg$ from vertical, for reasons of deck and crane geometry. If this angle is considered equal to the critical angle ϕ_c, what is the maximum speed for the system? Assume the normal drag coefficient of the cable is $C_n = 1.2$.

(b) Considering the undamped, uncoupled axial dynamics, express the natural frequency as a function of the vehicle depth, and sketch the curve. If the fastest waves that the surface vessel responds to have period $4s$, what is the "threshold" operating depth?

(c) The undamped, uncoupled lateral dynamics follow the equation

$$(m + m_a)\frac{\partial^2 q}{\partial t^2} = \bar{T}\frac{\partial^2 q}{\partial s} + w_n \sin\bar{\phi}\frac{\partial q}{\partial s},$$

where m_a is the added mass of the cable per unit length, and w_n is the in-water weight of the cable. Separation of variables $q(s,t) = \tilde{q}(s)\cos\omega t$ gives

$$\bar{T}\frac{\partial^2 \tilde{q}}{\partial s^2} + w_n \sin\bar{\phi}\frac{\partial \tilde{q}}{\partial s} + w_n\gamma\tilde{q} = 0,$$

where $\gamma = (m + m_a)\omega^2/w_n$. Simplify this expression by writing $\bar{T} = w_n s$ (the vehicle weight effect is small), $\sin\bar{\phi} \simeq 1$ (the cable is nearly vertical), and then use the substitution $z = 2\sqrt{\gamma s}$ to arrive at the Bessel equation

$$z^2\frac{\partial^2 \tilde{q}}{\partial z^2} + z\frac{\partial \tilde{q}}{\partial z} + z^2\tilde{q} = 0.$$

The derivatives can be transformed from s to z coordinates via the chain rule:

$$\begin{aligned}\frac{\partial \tilde{q}}{ds} &= \frac{\partial \tilde{q}}{\partial z}\cdot\frac{\partial z}{\partial s} \\ \frac{\partial^2 \tilde{q}}{ds^2} &= \frac{\partial^2 \tilde{q}}{\partial z^2}\left(\frac{\partial z}{\partial s}\right)^2 + \frac{\partial \tilde{q}}{\partial z}\cdot\frac{\partial^2 z}{\partial z\partial s}\cdot\frac{\partial z}{\partial s}.\end{aligned}$$

(d) The equation above has a solution of the form $\tilde{q} = cJ_0(z)$, where c is a constant to be found, and $J_0(z)$ is the zero'th order Bessel function of the first kind. If $\tilde{q}(s = L) = Q$, that is, we impose a harmonic input at the top, find c in terms of Q and $z(s = L)$. What condition makes $\tilde{q}$ blow up, indicating a resonance frequency ω_n?

(e) Recalling that strumming occurs when $\omega_n \simeq 0.2U/d$, construct a graph of towing velocities vs. deployment depths for which the strumming would be centered. Include at least the three lowest modes in your sketch, and discuss the trends for the higher modes. $J_0(x) = 0$ for for $x \simeq \pi(n - 0.25), n = 0, 1, 2, \cdots$, especially when x is large. You should find that strumming is hard to avoid in deep towing applications!

15. **Vessel heading control.** We consider the yaw/sway dynamics of a high-speed container ship. All the calculations below are to be made in nondimensional coordinates, so you do not need to perform any transformations in this question.

(a) The nondimensional system with states $\vec{x}' = [v', r']$ evolves according to $d\vec{x}'/dt' = A\vec{x}' + B\delta$, where

$$A = \begin{bmatrix} -0.90 & -0.42 \\ -4.8 & -2.3 \end{bmatrix}, \quad B = \begin{Bmatrix} -0.13 \\ 1.4 \end{Bmatrix}.$$

If the output is yaw rate r', i.e., $C = [0 \quad 1]$, write the transfer function $r'(s)/\delta(s) = C(sI - A)^{-1}B$. Use matrix inversion for the 2×2 matrix $(sI - A)$, perform the matrix multiplications, and then use the quadratic formula if necessary to express your answer as

$$\frac{r'(s)}{\delta(s)} = K\frac{s + z_1}{(s + p_1)(s + p_2)},$$

where K is a constant gain, $-z_1$ is the zero (there is one real zero), and $[-p_1, -p_2]$ are the two poles of the second-order system. Are both poles stable?

(b) For the purposes of autopilot design, the transfer function $\phi(s)/\delta(s)$ is crucial. Fortunately, all you have to do is divide $r'(s)/\delta(s)$ by another factor of s to account for the fact that $d\phi/dt' = r'$. Sketch all the poles and zeros of the plant transfer function $P(s) = \phi(s)/\delta(s)$ on a root locus plot.

(c) A PID controller $C(s)$ will work to stabilize the heading angle, and brings to $P(s)C(s)$ one additional pole at the origin, and two arbitrary zeros. Demonstrate a rough PID design by devising two controller zero locations that will attract the closed-loop poles into the left-half plane. Draw the path that you expect each closed-loop pole to follow, as the control gain increases from zero to very large values.

You do *not* need to calculate the PID gains that go with your proposed zero locations.

16. **Full-state feedback of a submarine.** The coefficients governing the pitch/heave dynamics of a Deep Submergence Rescue Vehicle (DSRV) are given below. They are nondimensionalized as in the lecture notes, using the factors $\rho/2$, U, and L.

$I'_{xx} = 0.000118$	$M'_q = -0.0113$	$Z'_q = -0.0175$
$I'_{zz} = 0.00193$	$M'_{\dot{q}} = -0.00157$	$Z'_{\dot{q}} = -0.000130$
$x'_G = 0$	$M'_w = 0.0112$	$Z'_w = -0.0439$
$m' = 0.0364$	$M'_{\dot{w}} = -0.000146$	$Z'_{\dot{w}} = -0.0315$
$U = 2.0m/s$	$M'_\delta = -0.0128$	$Z'_\delta = -0.0277$
$L = 15.0m$	$M'_\theta = -0.156/U^2$	

(a) Write the linearized (nondimensional) dynamics in the matrix form $\dot{x} = Ax + Bu$, where the input $u = \delta$, and the state vector is $x = [w', q', \theta, Z']$. Z' here is the elevation of the vehicle in inertial coordinates; your approximation for $\dot{Z}'$ should include both w' and θ.

(b) Is the DSRV vehicle open-loop stable, that is, without control action δ? You can assess this either by finding the eigenvalues of your A-matrix above, or by computing the stability parameter C'.

(c) In preparation for controller design, create a simulation using Matlab. Make a graph of the open-loop step response, showing all the dimensional state variables versus dimensional time.

(d) Assuming that all the states can be measured accurately, a full-state controller $\delta = -Kx$ can be used, where K is a 1×4 gain matrix. Under this control, the system dynamics are governed by

$\dot{x} = (A - BK)x$, so that if $A - BK$ has all negative eigenvalues, the system is stable.

Use the Matlab function `place` to put the four closed-loop poles at $g(-0.95 \pm 0.31i)$ and $g(-0.59 \pm 0.81i)$, $g = 1$. Demonstrate that your closed-loop design is stable against nonzero initial conditions. What are the effects of increasing or decreasing g?

Note that the pole locations suggested above are with respect to the *dimensional* system, i.e., using dimensional time.

17. **Nyquist stability.** The inverted pendulum shown below is often used as a simple model for rocket flight, and can also illustrate the dynamic behavior of an unstable ocean vessel which is propelled from the stern, e.g., a barge being pushed by a tugboat.

    For this problem, we assume that *all* of the mass (m) is concentrated at the distal end of an arm of length l; a high-performance positioning system sets the horizontal position of the cart u_o.

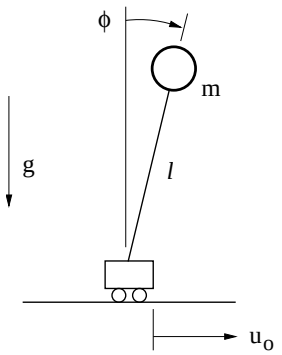

    A Lagrangian derivation of the dynamics gives:

$$\ddot{\phi} = \frac{g}{l}\sin(\phi) - \frac{1}{l}\cos(\phi)\ddot{u}_o.$$

    Note that the *acceleration* of the cart is now considered to be the input to the plant, e.g., $u = \ddot{u}_o$.

    (a) If the observation is taken to be the angle of the bar ϕ, i.e., $y = \phi$, write the state-space representation of the dynamics linearized about the point $\phi = 0$.

(b) Show that this plant is fully state observable and controllable.

(c) Now make the assumption that $l = 1$, and $g = 1$ (it can be achieved through a proper nondimensionalization) What is the transfer function of the plant, $P(s)$? Use this plant model for the rest of this question.

(d) Where are the plant poles and zeros, if any?

(e) A stabilizing controller is not hard to find, and a suggested one is:

$$C(s) = \frac{-4(2s+1)}{s+2}.$$

Create a rough Nyquist plot of the loci of $P(s)C(s)$, for the frequencies $\omega = [0, 2.2, \infty] rad/s$. These three frequencies are all that you need to sketch the overall shape; there are no hidden loops or other features. In the case of $\omega = 2.2$, for which you will need to make explicit calculations, you may find the following identity useful:

$$\frac{a+jb}{c+jd} = \frac{(a+jb)}{(c+jd)}\frac{(c-jd)}{(c-jd)} = \frac{(ac+bd)+j(bc-ad)}{c^2+d^2}.$$

Be sure to include the complex-conjugate points for $-\omega$ on your plot.

(f) Invoke the Nyquist stability criterion to confirm that the closed-loop system is stable.

(g) About how many degrees of phase margin does this design provide? What reduction in low-frequency gain can be tolerated? Is it a reasonable design?

18. **Root locus and loopshaping.** The parameters governing the surface maneuvering of a high-speed container ship are given below for reference:

m'	0.00792	I'_{zz}	0.000456	x'_G	-0.05
L	$175.0m$	U	$8m/s$	Y'_v	-0.00705
$Y'_{\dot{r}}$	0.0000	Y'_v	-0.0116	Y'_r	0.00242
Y'_δ	-0.00258	$N'_{\dot{v}}$	0.0000	$N'_{\dot{r}}$	-0.000419
N'_v	-0.00385	N'_r	-0.00222	N'_δ	0.00126

Note that the center of vessel mass is located *aft* of the origin; for this model, the origin coincides with the center of added mass, so that $Y_{\dot{r}} = N_{\dot{v}} = 0$. The nondimensional system with states $\vec{x}' = [v', r']$ evolves according to $d\vec{x}'/dt' = A\vec{x}' + B\delta$, where

$$A = \begin{bmatrix} -0.90 & -0.42 \\ -4.8 & -2.3 \end{bmatrix}, \quad B = \begin{Bmatrix} -0.13 \\ 1.4 \end{Bmatrix}.$$

The relevant output is yaw rate: $C = [0 \;\; 1]$ and $D = 0$. For the purposes of autopilot design, however, the transfer function $\phi(s)/\delta(s)$ is needed.

The following steps create two heading autopilots, using the root-locus and loopshaping techniques. In addition to the Matlab commands listed below, you will find very useful the convolution function `conv()` which can be used to combine systems, e.g., for numerators,
`numPC = conv(numP,numC);`. Also, be sure that you equalize axis scaling for your plots in the complex-plane, by using `axis('equal');`.

(a) Use the Matlab command `tf()`, or `ss()`, to create a system model of the open-loop transfer function $P(s)C(s)$, using the plant above and a PID-type controller:

$$C(s) = k_p \left(1 + \tau_d s + \frac{1}{\tau_i s}\right).$$

The actual numerical values for k_p, τ_d, and τ_i are to be found in the next step.

(b) Using $\tau_d = 2$ and $\tau_i = 6$ as suggested values, use the Matlab command `rlocus()` and then `rlocfind()` to select a controller gain k_p, that puts the three slow poles in the following sector: 1) minimum undamped frequency (nondimensional) of 0.3, 2) maximum frequency of 0.5, and 3) minimum damping ratio 0.7. Give a root locus plot, with your pole locations clearly marked on top of the trajectories taken as k_p varies. You don't need to show the fourth, fast pole, which will be quite far to the left.

(c) Apply the k_p you selected to $P(s)C(s)$, and then use the Matlab functions `feedback()` to create the resulting feedback system, and

`step()` to plot the closed-loop system response to a step input in desired heading.

(d) Use the Matlab command `nyquist()` to make a Nyquist plot of $P(s)C(s)$ for your design. Make a visual estimate of the gain and phase margins.

(e) An alternate approach for controller design of this stable plant is loopshaping: For the open-loop function $L(s) = \omega_c/s$, where $\omega_c = 2.0$, invert the plant to come up with a compensator: $C(s) = L(s)/P(s)$. This design has infinite gain margin and 90 degrees phase margin.

(f) As above, create the feedback system, and plot the closed-loop step response.

(g) The loopshaping control is *not quite* a PID-controller; how does it differ, and what would $L(s)$ have to contain to make it a PID?

(h) The controllers you just designed are in nondimensional time coordinates; give the P,I, and D gains for use on a real time scale, for the root-locus design.

19. **LQR**. Consider the state-space system and LQR design:

$$\begin{aligned} A &= \begin{bmatrix} 0 & -1 \\ 1 & 0 \end{bmatrix}, \\ B &= [1 \;\; 0]^T \\ C &= [0 \;\; 1] \\ D &= 0 \\ Q &= C^T C \\ R &= \rho. \end{aligned}$$

The plant is an undamped oscillator with undamped poles at $\pm j$. Note that the plant output is *position* for this problem.

(a) What is the control gain K in terms of ρ? **Hints:** There are two solutions for p_{12}; choose the positive one. Also, the expression for p_{22} is messy; luckily, you won't need to use it.

(b) Determine the limiting approximations for K with ρ very small and very large – these are the cheap control and expensive control problems.

(c) Derive the limiting closed-loop pole locations for $\rho \longrightarrow 0$, giving the frequency and damping ratio of the Butterworth pattern in terms of ρ. You can get the characteristic equation for the poles as $det(sI - (A - BK)) = 0$, and then make it fit the form $s^2 + 2\zeta\omega_n + \omega_n^2 = 0$.

20. **LQR.** Consider the first-order, unstable system governed by $\dot{x} = x + u$, for which the output is $y = x$. The state-space matrices are $A = B = C = 1$.

(a) Solve the LQR Riccati equation for P, for the case $Q = C^T C$ and $R = \rho$. Your answer should give a positive P as a function of ρ alone.

(b) Consider the cheap-control problem, with $\rho \to 0$. Write the leading-term approximations for P and then K, and compute the eigenvalue (there is only one) of the closed-loop system. Note that $eig(M) = M$, if M is a scalar instead of a matrix.

(c) Now look at the expensive-control problem, with $\rho \to \infty$. Again, write the approximations for P and K, and find the closed-loop system eigenvalue.

21. **LQG/LTR.** For the inverted pendulum plant (see previous question) with state-space matrices

$$A = \begin{bmatrix} 0 & 1 \\ 1 & 0 \end{bmatrix}, \quad C = [0 \;\; 1]\,,$$

the KF Riccati equation yields $H = [100 \;\; 14]^T$, for the choices $V_1 = [100 \;\; 0 \;;\; 0 \;\; 0]$, and $V_2 = 0.01$.

(a) Compute the open-loop transfer function for the Kalman filter loop: $L(s) = C(sI - A)^{-1}H$.

(b) Even though this $L(s)$ is unstable, its magnitude plot confirms that it is a reasonable loopshaping design. What is the low-frequency gain for this $L(s)$, and what kind of tracking performance should we expect from the associated LTR design?

(c) Now consider the closed-loop transfer function, which you can write as $S(s) = L(s)/(1 + L(s))$ (the sensitivity). What is the characteristic equation for the closed-loop system, and about what damping ratio has the Kalman filter provided?

22. **LQG/LTR design.** The parameters for the linearized sway/yaw motions of a swimmer delivery vehicle are given below.

```
% Parameters, all nondimensional except [U,L]
U =              4.0 ; % m/s
L =              5.3 ; % m
Izz =            0.006326 ;
m =              0.1415 ;
xg =             0. ;
Yv =            -0.1 ;
Yr =             0.03 ;
Nv =            -0.0074 ;
Nr =            -0.016 ;
Ydelta =         0.027 ;
Yvdot =         -0.055 ;
Yrdot =          0. ;
Nvdot =          0. ;
Nrdot =         -0.0034 ;
Ndelta =        -0.013 ;
```

You are asked to develop an LQG/LTR controller for this plant, and it is suggested that you compose a single Matlab script to perform the steps in sequence. Please make sure you answer all the questions, and include a listing of your code. This entire design is made in nondimensional coordinates.

(a) *Plant Modeling and Characteristics*

i. Construct a state-space plant model, to take rudder angle δ as an input and give heading angle ϕ as an output. Please provide the *numerical* values for the A, B, C matrices. There should be three states in your model, with one input channel and one output channel.

ii. Compute and list the controllability and observability matrices; is the plant state-controllable and state-observable?

iii. Where are the poles of your plant model? Is this model stable?

iv. Show a plot of your plant's step response.

(b) *LQR and KF Designs*

i. Using the Matlab command `lqr()`, you can compute the LQR feedback gain K, for given A, B, Q, and R matrices. With the choices $Q = C^T C$, and $R = \rho$, list K and plot the closed-loop step responses for the choices $\rho = [0.1, 0.001, 0.00001]$. How do the gains and step responses change as you make ρ smaller and smaller?
Note that the fundamental closed-loop LQR system is

$$\begin{aligned} \dot{\vec{x}} &= (A - BK)\vec{x} + BK\vec{x}_{desired} \\ y &= \vec{x}, \end{aligned}$$

i.e., the input to the closed-loop system is $\vec{x}_{desired}$ and the output is $\vec{x}$. Your plot should show specifically the output ϕ, for an input of $\vec{x}_{desired} = [v_{desired} = 0, r_{desired} = 0, \phi_{desired} = 1]$. This compression can be achieved in one step by premultiplying the system by C^T, and post-multiplying it by C:

$$\begin{aligned} \dot{\vec{x}} &= (A - BK)\vec{x} + BKC^T y_{desired} \\ y &= C\vec{x}, \end{aligned}$$

ii. The Matlab command `lqe()` can be used to generate the Kalman filter gain H, given design matrices A, C, V_1, and V_2. For the choices $V_1 = I_{3\times 3}$ and $V_2 = 0.01$, compute H, and make a plot of the closed-loop step response. Be sure to give the numerical values of H.

Note that the `lqe()` command asks for a disturbance gain matrix G; you should set this to $I_{3\times 3}$. The closed-loop KF system is as follows:

$$\begin{aligned} \dot{\hat{x}} &= (A - HC)\hat{x} + Hy \\ \hat{y} &= C\hat{x}, \end{aligned}$$

i.e., the input is the measurement y and the output is an estimated version of it, $\hat{y}$.

(c) *Loop Transfer Recovery*

The LQG compensator is a combination of the KF and LQR designs above. With normal negative feedback, the compensator $C(s)$ has the following state space representation:

$$\begin{aligned} \dot{\vec{z}} &= (A - BK - HC)\vec{z} + He \\ u &= K\vec{z}, \end{aligned}$$

so that the input to the compensator is the tracking error $e = r - y$, and its output u is the control action to be applied as input to the plant. The total open-loop transfer function is the $P(s)C(s)$; in Matlab, you may simply multiply the systems, e.g., `sysPC = sysP * sysC ;`.

i. Make a log(magnitude) plot of the KF open-loop transfer function $L(s) = C(sI - A)^{-1}H$, versus log(frequency). You may find the Matlab command `freqresp()` helpful. $|L(s)|$ should be large at low frequencies, and small at high frequencies, consistent with the rules of loopshaping.

ii. As $\rho \to 0$, the product $P(s)C(s) \to L(s)$. Demonstrate this by computing $P(s)C(s)$ for the three different values of ρ above, and overlaying the respective $|P(s)C(s)|$ over the plot of part 3a).

iii. Make a closed-loop step response plot for the smallest value of ρ. How does it compare with the KF step response of part 2b)?

In real LTR applications, the particular values of V_1 and V_2 can be picked to control the low-frequency gain, and crossover frequency of the open-loop KF system $L(s) = C(sI - A)^{-1}H$.

23. **Inertial navigation.** A triaxial accelerometer package is aligned with the [x,y,z] (fwd, port, up) axes of an underwater vehicle. At a particular instant in time, the three raw accelerations from the strain guages are $[\ddot{x} = -0.96, \ddot{y} = 0.80, \ddot{z} = 9.73]$ meters/second. Note that under the influence of gravity alone, this sensor will always report that the vehicle is accelerating *upwards*.

    (a) Ignoring the coupling of Euler small angles, what estimates can you give for the roll and pitch angles? I suggest that you draw the measurement vector in the coordinates of the vehicle frame, and then consider the orientation of the body which would lead to it.

    (b) Given that the acceleration due to gravity is $9.81 m/s$, how do we know that these are *reasonable* (but not foolproof!) angle calculations to make?

24. **LQG/LTR design: term project**. You are asked to carry out modeling and control system design for the surge dynamics of an oceanic cable-laying vessel. This vessel needs to have very good speed control so that the cable, which is being paid out constantly and sinks slowly under its own weight, lies properly on the seafloor. The bathymetry for the path is well-known but variable, so the vessel will need to slow down and speed up frequently. *Unexpected* deviations in speed from the calculated trajectory are likely to create loops or kinks in the cable, or induce large tensions.

vessel	length	L	$145m$
	draft	h	$9m$
	beam	b	$22m$
	displacement	∇	$17750m^3$
	surge added mass	m_a	$0.07\rho\nabla$
	thrust reduction factor	t	0.19
	wetted surface area	A_w	$5585m^3$
	towed resistance coefficient	C_r	0.0025
	wake fraction at propeller	w	0.22
propeller	diameter	D	$7.21m$
	pitch/diameter ratio	P/D	1.1
	rotative efficiency	η_r	1.025
	zero-speed thrust coefficient	$k_t(J=0)$	0.6
	slope of k_t with J		-0.522
	zero-speed torque coefficient	$k_q(J=0)$	0.1
	slope of k_q with J		-0.0833
	rotational moment of inertia	I_p	$2.03 \times 10^5 kgm^2$
engine	parameter	a	0.876
		b	0.208
		c	2.173
		d	-.0939
	maximum fuel rate	f_m	$1.5kg/s$
	maximum torque	Q_m	$70000Nm$
	maximum speed	n_m	$60Hz$
gearbox	reduction ratio	λ	32
	efficiency	η_g	0.97

It is desired to create a linear controller for the nominal surge motion, and then demonstrate that it will work with a simulation of the real nonlinear system, within a neighborhood of the nominal speed.

The vessel is powered by a single gas turbine engine, driving one propeller. The parameters for the vessel, propeller, and engine system are as given in the table.

The gas turbine torque-speed characteristic fits the relation:

$$\frac{Q_e}{Q_m} = -\left(a\frac{f}{f_m} + b\right)\frac{n_e}{n_m} + \left(c\frac{f}{f_m} + d\right),$$

where Q_e represents the engine torque in Nm, f the fuel rate in kg/s, and n_e the rotation rate of the engine in Hz.

(a) Make a map of the gas turbine characteristics. For instance, make a contour plot which gives Q_e/Q_m (the fraction of maximum torque developed) as a function of f/f_m (the fraction of the maximum fuel rate) and n_e/n_m (the fraction of the maximum rotation rate of the engine).

Be sure to include clipping on your contours, where the calculated torque exceeds Q_m. Similarly, the engine cannot develop negative torque.

(b) Make a table of some steady operating conditions for f_o/f_m in the range of 0.05–0.95, in which you show: advance ratio seen by the propeller, engine torque, propeller rotational speed, engine rotational speed, and vessel linear speed.

Plot the pairs $[f_o/f_m,\ n_{eo}/n_m]$ on the characteristic plot from Part 1, and assess whether the vessel, engine, and propeller are well matched to operate over a range of f_o.

(c) Construct a linear approximation for the plant dynamics around the operating condition $f_o/f_m = 0.8$. If the plant input is δf, and the output is δu, list the A, B, C matrices for your plant, and the eigenvalues. δ here indicates the perturbed value from the steady state, e.g., $f = f_o + \delta f$.

(d) Create an LTR-type controller for the plant. First, choose the filter gains V_1 and V_2 to make the crossover frequency (where the magnitude of $L(s) = C(sI-A)^{-1}H$ passes through unity) about $0.6 rad/s$. This choice corresponds with the closed-loop system being able to overcome waves with period $10 seconds$ or longer. Note that for this scalar design, you will be able to move the curve $|L(s)|$ up or down on the Bode plot, but you cannot easily change its shape, or move it side-to-side.

Secondly, recover this loop shape with an LQG-type controller, using a small control penalty.

You should prepare for this part: a plot of $log(|L(s)|)$ versus $log(\omega)$, a listing of your V_1 and V_2 choices, and the A, B, C matrices of your LQG compensator.

(e) In the event of a current or wind disturbance, the actual vessel speed will vary from the nominal value. This is not acceptable in the long term, given that the vessel is laying out a cable.

An integral action can be added quite easily in the LTR design technique. First, add an integrator to the input of the plant, so that an "augmented plant" is created. This augmented plant has one more state than the original plant:

$$\begin{aligned} A_{aug} &= \begin{bmatrix} \mathrm{A} & \mathrm{B} \\ 0 & 0 \end{bmatrix} \\ B_{aug} &= [0 \;\; 1]^T \\ C_{aug} &= [C \;\; 0] \end{aligned}$$

The idea is to then carry out the KF design and LTR as before, with the augmented plant model. When this is done, move the integrator from the augmented plant into the compensator. The addition of an integrator channel to the plant or compensator can be accomplished with the command `sysPaug = sysP * tf([0 1],[1 0]) ;`, for example.

Present a figure of $|L(s)|$ and the other quantities as you gave them in Part 4. This is to be kept as a separate controller design.

(f) For the purpose of demonstrating your controllers, construct a nonlinear simulation of the plant system, with input f. You don't

need to show anything for this task; it is mostly to verify that the steady conditions you calculated above, with $f = 0.8f_m$, are actually steady conditions from the point of view of the whole simulation. You may wish to use `global` variables in Matlab so that you don't have to type everything in more than once.

(g) Augment your simulation above with the compensator dynamics. If the compensator has states z, and your simulation has states $[u, n_p]$, make a new state vector $[u, n_p, z]$. You will propagate the first two states as usual with the nonlinear equations and the fuel rate f as input. The compensator states z are propagated by a set of system matrices $[A_c, B_c, C_c]$, which you just designed. Note that the input to the compensator is an error signal: $e = r - u$, where u is the speed of the vessel and r is a reference speed. The output of the compensator is then fuel rate f.

We are interested mainly in disturbance rejection, for which you will just set $r = u_o$, the steady condition speed. Recall that you are implementing a controller for operation about a nominal condition; whenever your compensator generates f from the error signal, be sure to *then* add on $0.8f_m$, the part needed to keep us near the steady condition.

Demonstrate four properties, showing time-domain simulations for each:

- The first controller, without integral action, does not completely reject steady disturbances. I suggest you implement a disturbance as an acceleration:
  `uprime = uprime + k`. In the absence of a controller, this line would drive the system with an additional acceleration of $k m/s^2$, thus modelling the effects of steady wind or current. This line is to be added after computing the usual parts of `uprime`.
- The first controller does not reject high frequency disturbances. A suggestion is to let
  `uprime = uprime + k*sin(10*omega_c*t)`, where `omega_c` is the crossover frequency. This adds an oscillating acceleration at ten times the crossover frequency.
- The first controller does, however, reject some lower frequency disturbances. For example, try

`uprime = uprime + k*sin(omega_c/10*t)/100`. Note the extra factor of 100 is included so that the result can be compared directly with the high-frequency disturbance case above. The effect of an acceleration disturbance onto the observed output, velocity u, scales with the inverse of the frequency.

- The second controller, with integral action, rejects steady disturbances. Use the same approach as above for steady disturbances

(h) What is the propeller response during the high-frequency disturbances? Is it reasonable or do we need to slow down the controller bandwidth?